Order Number 9021780

Influences of biological structural features on the acoustic nonlinearity parameter B/A

Zhang, Jian, Ph.D.

University of Illinois at Urbana-Champaign, 1990

U·M·I
300 N. Zeeb Rd.
Ann Arbor, MI 48106

INFLUENCES OF BIOLOGICAL STRUCTURAL FEATURES ON THE ACOUSTIC NONLINEARITY PARAMETER B/A

BY

JIAN ZHANG

B.S., Xiamen University, 1982
M.S., University of Illinois, 1987

THESIS

Submitted in partial fulfillment of the requirements
for the degree of Doctor of Philosophy in Electrical Engineering
in the Graduate College of the
University of Illinois at Urbana-Champaign, 1990

Urbana, Illinois

UNIVERSITY OF ILLINOIS AT URBANA-CHAMPAIGN

THE GRADUATE COLLEGE

JANUARY 1990

WE HEREBY RECOMMEND THAT THE THESIS BY

JIAN ZHANG

ENTITLED INFLUENCES OF BIOLOGICAL STRUCTURAL FEATURES ON THE ACOUSTIC NONLINEARITY PARAMETER B/A

BE ACCEPTED IN PARTIAL FULFILLMENT OF THE REQUIREMENTS FOR THE DEGREE OF DOCTOR OF PHILOSOPHY

Director of Thesis Research

Head of Department

Committee on Final Examination†

Chairperson

† Required for doctor's degree but not for master's

O-517

INFLUENCES OF BIOLOGICAL STRUCTURAL FEATURES ON THE ACOUSTIC NONLINEARITY PARAMETER B/A

Jian Zhang, Ph.D.
Department of Electrical and Computer Engineering
University of Illinois at Urbana-Champaign, 1990
Floyd Dunn, Advisor

The influences of structural factors of biological media on the acoustic nonlinearity parameter B/A were studied at tissue, cellular and molecular levels, using both the thermodynamic method and the finite amplitude method. Experiments were designed to measure the B/A changes by altering structural factors of media physically and biochemically, while keeping chemical compositions unchanged. Evidences were found to support significant structural dependences of the B/A at all three levels. Further analysis suggests that about 26% of dry weight contribution to the total B/A, the B/A value with water contribution subtracted, is due to cell-cell adhesive force in liver tissues, 20% to the hepatocyte cellular structure, and 15% to the molecular structure of protein. No significant B/A changes were observed between the *in vivo* and *in vitro* B/A values in cat livers and during the digestion of protein. In addition, it is found that B/A exhibits an unusually large value near the phase transition regions of liposomes, suggesting the effect of relaxational processes on the B/A value. Finally, implications of the above findings are discussed in the light of the previous studies on the compositional dependence of B/A, and a possible rationale by which the B/A depends on both the chemical composition and structural factors is suggested.

This dissertation is dedicated to those who died innocently in the tragic event of Tiananmen Square in the Spring of 1989.

ACKNOWLEDGEMENTS

I am indebted to my advisor, Professor Floyd Dunn, for providing continuous guidance, support and encouragement throughout this project. I would like to express my deepest thanks to Professor Mark Kuhlenschmidt for his enthusiasm, fruitful discussions and helpful advice. I would also like to thank Professor Richard Magin and Professor Leon Frizzell for their many helpful discussions. Thanks are also due to Ms. Kay Carnes for her advice on animal surgery, Mr. Robert Cicone for his assistance in animal cares and Mr. Billy McNeill for his machining expertise.

Finally, my deep gratitude goes to my parents who have invested much in my education.

This work was supported in part by a grants from the National Science Foundation and a grant from the National Institutes of Health.

TABLE OF CONTENTS

CHAPTER 1

INTRODUCTION

This dissertation is a study of the dependence of the acoustic nonlinearity parameter, B/A, on the structural features of biological media. The evidence for and the magnitude of such dependency is examined. Following the background material from which this study was developed, the study's objective is described in this chapter. A review of the nonlinear acoustics theory and an outline of B/A measurement methods are presented in Chapter 2. The B/A measurement systems implementing both the thermodynamic method and the finite amplitude method, and the experimental procedures employed in the study, are described in Chapter 3. The results and the discussions are presented in Chapter 4. The principal conclusions reached and suggestions for future work in the investigation of the nonlinearity parameter B/A are discussed in Chapter 5.

1.1 Earlier Studies of Nonlinear Bioultrasonics

Ultrasonic energy has been used extensively in medicine. Ultrasound is used in diagnostic applications to obtain anatomical and pathological information about the human body [Shoup and Hart, 1988; Evans et al., 1989; Wade, 1976]. In therapeutic applications, ultrasound is used to deposit energy selectively at certain sites in the body to bring about desired biological effects [Hynynen, 1988; Flachenecker, 1987; Corry et al., 1984]. Until the works of Carstensen, Muir, and collaborators [Carstensen et al., 1980; Muir and Carstensen, 1980; Carstensen et al., 1981], little attention was given to the nonlinear effects attending these applications. The propagation of ultrasonic waves in biological media is often modeled by linearized wave and state equations, partly due to the simplicity of the resulting theory, partly to the validity in describing a large number of acoustic phenomena [Kinsler et al., 1982; Beyer, 1974], and partly to the unavailability until recently of wide-band hydrophone receivers necessary for direct

detection of the nonlinear waveform distortion [Lewin, 1981]. However, it is well known that the wave equation and the state equation are nonlinear in nature, and that linear approximation does not adequately describe all acoustic phenomena [Beyer and Letcher, 1969]. In fact, various nonlinear effects in the frequency and intensity ranges used in medical ultrasound have been reported. At medical diagnostic intensity levels, the nonlinear effects on the beam width were reported for both continuous wave (cw) [Carstensen et al., 1980] and pulsed modes [Bjorno and Lewin, 1982] of operation; and nonlinear waveform distortion and, in some cases, shock wave development in water were observed for pulses generated by the transducers used in commercial imaging systems [Bacon, 1984a, 1984b; Duck, 1984; Duck and Starritt, 1984; Parker, 1985; Starritt et al., 1985]. At medical therapeutic intensity levels, effects on the power transfer efficiency [Carstensen et al., 1980], the intensity-dependent absorption coefficient [Goss and Fry, 1981], and the threshold for lesion production in excised liver [Carstensen et al., 1981] have been reported. With recent development and increasing clinical applications of extracorporeal acoustic techniques for urinary calculi destruction, the propagation of the shock wave generated by the lithotripter has been studied [Parker and Friets, 1987; Flachenecker, 1987; Corry et al., 1984]. As a potentially new diagnostic tool, several methods have been proposed to image the B/A parameter [Ichida et al., 1983, 1984; Cain, 1986; Nakagawa et al., 1985; Houshmand et al., 1988].

With the advent of these nonlinear phenomena in medical applications of ultrasound, a number of investigators have studied the nonlinear propagation of acoustic waves in biological media [Bacon, 1986; Dunn et al., 1981; Law, 1984; Cobb, 1982; Sehgal et al., 1986a]. An essential aspect of these studies has been the measurement and analysis of the nonlinearity parameter, B/A, of biological media, because it relates the diverse nonlinearities of biological media to the general wave propagation theory. Much work has been done on the measurement and the investigation of the B/A parameter (reviewed in Section 1.3, also see [Bjorno, 1986]). This dissertation comprises a portion of the effort to investigate the origin of the B/A parameter of biological media.

The importance in studying the nonlinearity parameter B/A is twofold: (1) to provide more accurate modeling of the propagation of the finite amplitude acoustic wave in biological media, which may allow a more effective administration of therapeutic ultrasound dosage [Swindell, 1985] and the production of higher quality imaging [Bjorno and Lewin, 1982; Rugar, 1984], and (2) to improve the applicability of the B/A parameter to characterize the normal and diseased tissues.

1.2. Physical Origin of Acoustic Nonlinearity

The concept of acoustic nonlinearity and the nonlinearity parameter B/A are introduced in this section.

One of the direct consequences of linear acoustic theory is that the velocity of wave propagation is a constant, viz., for a planar acoustic wave,

$$\frac{dz}{dt} = c \tag{1.1}$$

where z is the propagation displacement along the direction of propagation, t is time, and c is the propagation velocity. As a result, every component of the wave travels at the same velocity, and the waveform remains unchanged as it propagates through the medium. In reality, however, the speed of propagation is not a constant. Two second order phenomena are neglected as a consequence of the linearization of the wave and the state equations. One is due to the finite particle velocity and the other is due to the inherent nonlinearity of the medium.

It is well-known that, for a wave traveling in a moving medium, the effective wave velocity for the wave is the vector sum of the velocity of wave propagation when the medium is stationary and the velocity of the moving medium. An acoustic wave is a manifestation of propagation of the medium particle oscillation energy. For the longitudinal, planar acoustic wave, the particle oscillation is either the same or the opposite to the direction of wave propagation. For instance, for the positive half cycle of a wave whose particle velocities, **u**, are in

the same direction as the propagation velocity, c, the effective propagation velocities are c+|u|; and for the negative half cycle, whose particles move in the opposite direction to the wave propagation, the effective propagation velocities are c-|u|. In general, the propagation velocity can be expressed as

$$\frac{dz}{dt} = c + u \tag{1.2}$$

It can be seen that for small acoustic perturbations, u<<c and thus dz/dt can be approximated by c.

The other phenomenon contributing to the nonlinearity of wave propagation is the fact that the propagation velocity, c, as defined in the linear theory, is not a constant, but also a function of the particle velocity, u. To see this, it is first necessary to examine the state equation for liquid media, which describes the relationship between pressure, p, and density, ρ, of a medium, and can be written as

$$p = p(\rho) \tag{1.3}$$

In general, this relationship is complicated and cannot, except in a few cases, be expressed analytically in closed form. A common method is to expand the equation in a Taylor's series about the ambient density, as

$$p = p_o + \left(\frac{\partial p}{\partial \rho}\right)_{s,\rho=\rho_o} (\rho-\rho_o) + \frac{1}{2!}\left(\frac{\partial^2 p}{\partial \rho^2}\right)_{s,\rho=\rho_o} (\rho-\rho_o)^2 + \frac{1}{3!}\left(\frac{\partial^3 p}{\partial \rho^3}\right)_{s,\rho=\rho_o} (\rho-\rho_o)^3 + \ldots \tag{1.4}$$

where p_o and ρ_o are the ambient pressure and ambient density of the medium, respectively, and s denotes the isentropic process. Defining the coefficients of the series A, B, C, etc., as

$$A \equiv \rho_o \left(\frac{\partial p}{\partial \rho}\right)_{s,\rho=\rho_o} = \rho_o c_o^2 \tag{1.5}$$

$$B \equiv \rho_o^2 \left(\frac{\partial^2 p}{\partial \rho^2} \right)_{s,\rho=\rho_o} \tag{1.6}$$

$$C \equiv \rho_o^3 \left(\frac{\partial^3 p}{\partial \rho^3} \right)_{s,\rho=\rho_o} \tag{1.7}$$

gives

$$p = p_o + A\left(\frac{\rho-\rho_o}{\rho_o}\right) + \frac{B}{2!}\left(\frac{\rho-\rho_o}{\rho_o}\right)^2 + \frac{C}{3!}\left(\frac{\rho-\rho_o}{\rho_o}\right)^3 + \ldots \tag{1.8}$$

The constant B/A is known as the nonlinearity parameter and can be used as a measure of the deviation of a medium from the linearized state equation. For water at 20°C and excess pressure, $p-p_o$, of 6 atmospheres, the B term is about 10^{-4} times and the C term is about 10^{-7} times that of the A term, respectively [Beyer, 1974]. For all practical purposes, terms higher than the B term are usually neglected and the approximation of the equation of state is

$$p = p_o + A\left(\frac{\rho-\rho_o}{\rho_o}\right) + \frac{B}{2!}\left(\frac{\rho-\rho_o}{\rho_o}\right)^2 \tag{1.9}$$

The velocity

$$c^2 = \left(\frac{\partial p}{\partial \rho}\right)_s$$

$$= \frac{A}{\rho_o} + B\frac{(\rho-\rho_o)}{\rho_o^2}$$

$$= c_o^2\left(1 + \frac{B}{A}\frac{\rho-\rho_o}{\rho_o}\right) \tag{1.10}$$

It is clear that the velocity c is not a constant, and that its true value depends upon B/A and the magnitude of an acoustic wave. More rigorous derivation [Blackstock, 1972] shows that

$$c = c_o + \frac{B}{A} u \tag{1.11}$$

Combining Eqs. (1.2) and (1.11), we have

$$\begin{aligned} \frac{dz}{dt} &= c + u \\ &= c_o + (\frac{B}{A} + 1)u \end{aligned} \tag{1.12}$$

It can be seen that the propagation velocity (dz/dt) is a function of the acoustic wave amplitude u. One direct consequence of the amplitude dependent propagation velocity is distortion of the waveform with propagation distance. Different parts of the wave have different particle oscillation amplitudes and, according to Eq. (1.12), propagate at different velocities. For instance, if a cycle of the wave is followed, it is seen that because the positive half cycle has a greater amplitude, it propagates faster than the negative half cycle, and consequently, the wave is distorted from its original form. As the wave propagates, the distortion progresses. At distance z=L, the positive peak catches up with the negative peak, a pressure discontinuity occurs, and the shock wave is formed, as shown in Fig. 1.1. The distance L at which the shock wave is formed is called the discontinuity distance, and is given by [Beyer,1974] as

$$L = \frac{c_o^2}{(1 + \frac{B}{2A})\,\omega\, u_o} \tag{1.13}$$

and the distance measured by L is the shock parameter, σ,

$$\sigma = \frac{z}{L} \tag{1.14}$$

Figure 1.1, calculated using Blackstock's plane wave solution [Blackstock, 1966], demonstrates the progressive wave distortion as a function of the shock parameter in the time domain, and the harmonic growth in the frequency domain. If the waveform distortion can be seen as the primary nonlinear effect, it can explain many secondary effects such as harmonic generation (see Fig. 1.1) and additional absorption. For instance, the additional absorption observed in high amplitude ultrasound, especially as σ approaches unity, can be attributed to a significant amount of the energy at the fundamental frequency being transferred to its higher harmonics. Since absorption at the higher harmonics is greater than that at the fundamental, the effective absorption for a higher amplitude acoustic wave is greater than that of lower amplitude waves [Blackstock, 1964; Goss and Fry, 1981; Carstensen et al., 1982].

The nonlinear state equation is a reflection of the nonquadratic intermolecular potential; that is, if the interaction among molecules was that of simple harmonic oscillation, the state equation would be linear and the nonlinearity parameter zero (see Eq. (1.15)). In reality, molecular interaction is a highly asymmetrically nonquadratic potential which only can be approximated by the quadratic potential in the immediate vicinity of their equilibrium positions. The B/A parameter, together with the velocity, has been related to the Mie potential parameters [Hartmann, 1979] and the adiabatic compressibility has been used to determine the intermolecular energy constants [Moelwyn-Hughes, 1961]. If the Mie potential is expanded as a Taylor's series about the equilibrium position, and Hartmann and Moelwyn-Hughes results are applied, one arrives at

$$U = -U_o + \frac{9}{\gamma} c_o^2 \left(\frac{r-r_o}{r_o}\right)^2 - \frac{27}{2\gamma} c_o^2 \left(\frac{B}{A}\right)\left(\frac{r-r_o}{r_o}\right)^3 + \ldots \qquad (1.15)$$

Figure 1.1 Nonlinear distortion as a finite amplitude wave propagates at different distances, represented by σ. The graphs in the left-hand side are the time domain representations, and those in the right-hand side are the frequency domain representation of the first five harmonics. The fundamental frequency f_o is 3 MHz. The pressure discontinuity can be seen at the σ=1.0, and the N-wave-like waveform, at the σ=2.0. The ringing at the peaks are due to the insufficient harmonics being incorporated in the numerical evaluation.

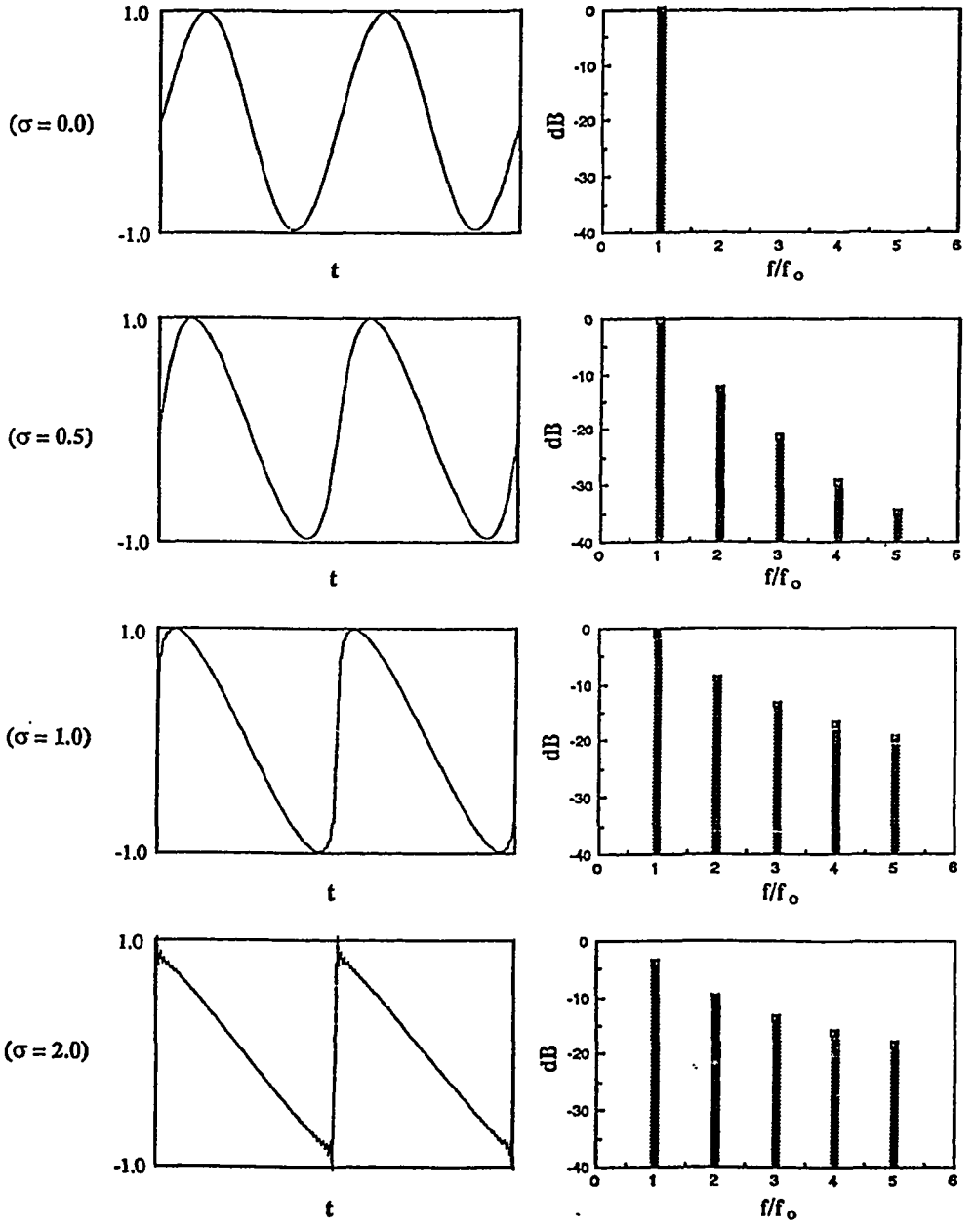
(σ = 0.0)
(σ = 0.5)
(σ = 1.0)
(σ = 2.0)
1.0
-1.0
t
dB
0
-10
-20
-30
-40
0 1 2 3 4 5 6
f/f o

where $r=r_o$ is the equilibrium position, $\gamma=C_p/C_v$ is the ratio of the heat capacities at constant pressure to constant volume, respectively, and the equilibrium potential, $U_o = U(r_o)$, can be measured by heat of vaporization of the liquid. The force between molecules can be written as

$$\begin{aligned} \mathbf{F} &= -\nabla U \\ &= -\frac{\partial U}{\partial r}\mathbf{r} \\ &= -\frac{18}{\gamma}c_o^2\frac{1}{r_o}\left(\frac{r-r_o}{r_o}\right)+\frac{71}{2\gamma}c_o^2\left(\frac{B}{A}\right)\frac{1}{r_o}\left(\frac{r-r_o}{r_o}\right)^2 + \cdots \end{aligned} \tag{1.16}$$

where $\mathbf{r}$ is the unit vector in the same direction as the force $\mathbf{F}$. It can be seen that the velocity c_o appears in the quadratic and cubic terms and B/A appears in the cubic term.

1.3. Nonlinearity Parameter B/A of Biological Media --- A Review

B/A data for various liquids and biological media are shown in Tables 1.1 and 1.2. Similar compilation of the data has been prepared by Everbach [1989]. Table 1.1 collects those B/A values reported for pure liquids (single component liquids) in the temperature range of 20°C to 30°C, whereas Table 1.2 collects those for various aqueous solutions and tissues. It can be seen that the B/A parameter of these media ranges from 5 to 12.

Table 1.1 B/A Data of One-Component Liquids

Liquids	Temp(°C)	B/A	References
D_2O	30	5.01	This study
H_2O	20	5.0	[Beyer, 1974]
	25	5.11	[Zhu et al., 1983]
	30	5.31	[Law et al., 1985]
Carbon Bisulfide	25	6.2	[Beyer, 1960]
Methanol	20	9.61	[Coppens et al., 1966]
	30	9.64	[Coppens et al., 1966]
Ethanol	20	10.52	[Coppens et al., 1966]
	30	10.57	[Coppens et al., 1966]
n-Propanol	20	10.69	[Coppens et al., 1966]
	30	10.71	[Coppens et al., 1966]
n-Butanol	20	10.69	[Coppens et al., 1966]
	30	10.72	[Coppens et al., 1966]
Benzyl Alcohol	30	10.19	[Coppens et al., 1966]
Ethylene Glycol	25	9.88	[Zhu et al., 1983]
	30	9.7	[Beyer, 1974]
		9.93	[Law et al., 1985]
Acetone	20	9.23	[Coppens et al., 1966]
Benzene	20	9.0	[Beyer, 1974]
	25	6.5	[Beyer, 1960]
Chlorobenzene	30	9.33	[Coppens et al., 1966]
Diethylamine	30	10.30	[Coppens et al., 1966]
Ethyl Formate	30	9.8	[Beyer, 1974]
Heptane	30	10.0	[Beyer, 1974]
Hexane	25	9.81	[Zhu et al., 1983]
	30	9.9	[Beyer, 1974]
Methyl Acetate	30	9.7	[Beyer, 1974]
Cyclohexane	30	10.1	[Beyer, 1974]
Nitrobenzene	30	9.9	[Beyer, 1974]
1,2-DHCP	30	11.8	[Beyer, 1974]
Chloroform	25	8.2	[Beyer, 1960]
Carbon Tetrachloride	25	8.7	[Beyer, 1960]
		7.85	[Zhu et al., 1983]
Toluene	20	5.6	[Beyer, 1960]
	25	7.9	[Beyer, 1960]
	30	9.87	[Narayana & Swamy, 1981]
Glycerol	20	8.77	[Sehgal et al., 1984]
(4% H_2O)	25	8.58	[Zhu et al., 1983]
		8.84	[Sehgal et al., 1984]
	30	9.0	[Beyer, 1974]
		9.4	[Law et al., 1985]
		9.08	[Sehgal et al., 1984]

Table 1.2 B/A Values of Biologically Associated Media

Materials	T(ºC)	B/A	References
Sucrose	25	5.50	[Zhu et al., 1987]
D-glucose, anhydrous	25	5.85	[Zhu et al., 1987]
Dextrose (25%)	30	5.96	[Law et al., 1985]
Dextran T150 (24%)	30	6.05	[Law et al., 1985]
Dextran T2000 (26%)	30	6.03	[Law et al., 1985]
BSA (20g/100cc)	25	6.23	[Zhu et al., 1983]
BSA (38.8g/100cc)	30	6.68	[Law et al., 1985]
BSA (20g/100cc)	30	5.46	[Cobb, 1982]
Egg White	30	5.81	[Sehgal et al., 1986c]
Egg Yolk	30	9.76	[Sehgal et al., 1986c]
Milk, Bovine	26	5.1	[Gong et al., 1984]
Bile, Pig	24	6.00	[Sun et al., 1985]
Whole Blood, Porcine	26	5.8	[Gong et al., 1984]
	30	6.22, 6.4	[Law, 1984]
Dog	30	5.43	[Cobb, 1982]
Bovine	26	5.5	[Gong et al., 1984]
Blood Plasma, Human, (Unclotted)	20	5.73	[Everbach, 1989]
	30	5.74	[Everbach, 1989]
Blood Plasma, Human, (Clotted)	20	5.29	[Everbach, 1989]
	30	5.67	[Everbach, 1989]
Gall Bladder, Human	20	6.22	[Dong et al., 1987]
Liver, Pig	24	7.14	[Sun et al., 1985]
	26	6.7-7.0	[Zhu et al., 1987]
Dog	30	7.6-7.9	[Cobb, 1982]
Beef	20	6.74	[Everbach, 1989]
	23	7.5-8.0	[Law et al., 1985]
	30	7.23-8.9	[Law et al., 1985]
	30	6.88	[Law et al., 1983]
	30	6.561-7.11	[Everbach, 1989]
Human, Fetus	17	8.72	[Dong et al., 1987]
Human, Adult (Normal)	20	6.26-6.44	[Sehgal et al., 1986a]
	26	5.51-5.53	[Dong et al., 1987]
	30	6.54	[Sehgal et al., 1984]
	30	6.54-7.13	[Sehgal et al., 1986a]
	30	6.72	[Sehgal et al., 1986c]
	30	6.54	[Dong et al., 1987]
	30	7.6	[Cobb, 1982]
	37	6.60-6.93	[Sehgal et al., 1986a]
Human, (Congestive)	30	6.50	[Sehgal et al., 1986c]
	30	7.2-7.8	[Cobb, 1982]

Table 1.2 (cont.) B/A Values of Biologically Associated Media

Materials		T(°C)	B/A	References
	Human, (Chronic congestion)	20	5.73	[Sehgal et al., 1986a]
		30	5.94	[Sehgal et al., 1986a]
		37	6.12	[Sehgal et al., 1986a]
	Human, (Central congestion)	20	6.36, 6.89	[Sehgal et al., 1986a]
		30	6.46, 7.10	[Sehgal et al., 1986a]
		37	6.81, 7.70	[Sehgal et al., 1986a]
	Human, (Lymphoma leukemia)	20	5.97	[Sehgal et al., 1986a]
		30	6.29	[Sehgal et al., 1986c]
		37	6.37	[Sehgal et al., 1986a]
	Human, (Carcinoma)	30	6.15	[Sehgal et al., 1986c]
	Human, (Small cell bronchogenic carcinoma)	20	5.92	[Sehgal et al., 1986a]
		30	5.77	[Sehgal et al., 1986a]
		37	6.10	[Sehgal et al., 1986a]
	Human, (Cirrhosis)	20	6.16	[Sehgal et al., 1986a]
		30	6.01	[Sehgal et al., 1986c]
		37	6.07	[Sehgal et al., 1986a]
	Human, (Slight fatty)	20	6.87	[Sehgal et al., 1986a]
		30	7.11	[Sehgal et al., 1986c]
		37	7.46	[Sehgal et al., 1986a]
	Human, (Marked fatty)	30	8.83	[Sehgal et al., 1986c]
	Human, (Multiple myeloma)	22	5.603	[Sehgal et al., 1984]
		30	5.796	[Sehgal et al., 1984]
		37	6.178	[Sehgal et al., 1984]
Kidney,	Pig	24	7.10	[Sun et al., 1985]
		26	6.2-6.5	[Zhu et al., 1987]
	Dog	30	7.2	[Cobb, 1982]
	Bovine	25	5.83	[Everbach, 1989]
	Human fetus	17	8.98	[Dong et al., 1987]
Spleen,	Pig	24	7.32	[Sun et al., 1985]
		24	7.1	[Dong et al., 1987]
		26	6.2-6.4	[Zhu et al., 1987]
		26	6.9	[Dong et al., 1987]
	Dog	30	6.8	[Cobb, 1982]
	Bovine	25	6.59	[Everbach, 1989]
Brain,	Pig	26	6.7-7.0	[Zhu et al., 1987]
		26	5.9	[Dong et al., 1987]
	Beef	30	7.6	[Law et al., 1985]
	Human Fetus	18.5	6.55	[Dong et al., 1987]

Table 1.2 (cont.) B/A Values of Biologically Associated Media

Materials		T(°C)	B/A	References
Breast,	Human, (Adenocarcinoma metastatic)	20	6.41	[Sehgal et al., 1986a]
		30	6.52	[Sehgal et al., 1986a]
		37	6.58	[Sehgal et al., 1986a]
Heart,	Pig	24	6.83	[Sun et al., 1985]
		24	7.1	[Dong et al., 1987]
		26	5.9-6.8	[Zhu et al., 1987]
		26	6.83	[Dong et al., 1987]
	Beef	30	6.8-7.4	[Law et al., 1985]
	Human fetus	18	5.8	[Dong et al., 1987]
Muscle,	Pig	24	7.55	[Sun et al., 1985]
		26	6.5-6.6	[Zhu et al., 1987]
		30	7.5-8.1	[Law et al., 1985]
	Human fetus	18	7.43	[Dong et al., 1987]
Tongue,	Pig	26	6.6-7.0	[Zhu et al., 1987]
Fat,	Pig	24	9.90	[Sun et al., 1985]
		26	10.8	[Dong et al., 1987]
		26	9.5-10.9	[Zhu et al., 1987]
		30	10.9-11.3	[Law et al., 1985]
	Human, (Not specified)	22	9.21	[Dong et al., 1987]
		24	9.60	[Dong et al., 1987]
		25	9.90	[Dong et al., 1987]
		37	9.63	[Dong et al., 1987]
	Human, Breast	20	9.3	[Errabolu et al., 1987]
		22	9.206	[Sehgal et al., 1984]
		30	9.909	[Sehgal et al., 1984]
		30	9.5	[Errabolu et al., 1987]
		37	9.633	[Sehgal et al., 1984]
	Human, Subcutaneous	20	10.83	[Errabolu et al., 1987]
		30	10.83	[Errabolu et al., 1987]
		37	9.93	[Errabolu et al., 1987]
	Human, Omentum	20	9.9	[Errabolu et al., 1987]
		30	10.01	[Errabolu et al., 1987]
		37	10.15	[Errabolu et al., 1987]
	Human, Mesenteric	20	10.94	[Errabolu et al., 1987]
		30	11.14	[Errabolu et al., 1987]
		37	11.15	[Errabolu et al., 1987]
Fatty Acid,	Human, Linoleic	20	9.88	[Errabolu et al., 1987]
	Human Oleic	20	10.00	[Errabolu et al., 1987]

Linear dependence of the B/A parameter on concentration has been reported in aqueous solutions of bovine serum albumin, hemoglobin, dextran T2000, dextrose, sucrose and polyethylene glycols [Law, 1984; Law et al., 1985; Cobb, 1982; Gong et al., 1984]. Two mixture laws, which predict a mixture's B/A value by calculating relative contributions from each constituent in the mixture, or inversely, predict volume fractions of constituents by determining the mixture's B/A value, have been proposed independently [Apfel, 1983, 1986; Sehgal et al., 1986a]. Both mixture laws assume the ideal mixture property, viz.,

$$\sum_{i=1}^{n} x_i = 1 \tag{1.17}$$

Apfel's mixture law employs the density ρ, the compressibility β, and the nonlinearity parameter B/A, as independent variables as

$$\begin{aligned} \rho &= \sum_{i=1}^{n} \rho_i x_i \\ \beta &= \sum_{i=1}^{n} \beta_i x_i \\ \left(\frac{B}{A}\right) &= \frac{1}{\beta^2} \sum_{i=1}^{n} \beta_i^2 \left(\frac{B}{A}\right)_i x_i \end{aligned} \tag{1.18}$$

where the x_i are the volume fractions of the i^{th} components. The mixture law proposed by Sehgal et al. employs the density ρ, the speed of sound c, and the phase shift parameter N as

$$\rho = \sum_{i=1}^{n} \rho_i x_i$$

$$\frac{1}{c} = \sum_{i=1}^{n} \frac{x_i}{c_i} \qquad (1.19)$$

$$N = \sum_{i=1}^{n} N_i x_i$$

where the x_i are the volume fractions of the i^{th} component, and the phase shift parameter

$$N = \frac{B/A}{\rho c^3}$$

The above mixture laws have been used to model tissues as mixtures of the three components, water, fat and protein, from which the chemical composition of tissues can be determined from measurements of density, velocity and B/A [Apfel, 1986; Sehgal et al., 1986a; Dong et al., 1987]. It has been found that Apfel's law applies to mixtures which are homogeneous on the scale of a wavelength of the sound, and that Sehgal's law applies to mixtures which are inhomogeneous on the same scale [Everbach, 1989].

Analysis of data presented in Tables 1.1 and 1.2 seems to suggest a binary property of the B/A parameter in biological media. The histogram of Fig. 1.2 is constructed from these data of Table 1.1, with the number of the B/A measurements reported in the interval of 0.2 B/A units along the ordinate and the B/A values of different liquids along the abscissa. If the liquids in Table 1.1 are grouped into two categories, inorganic and organic liquids, then data in Fig. 1.2 show that the inorganic liquids occupy the low end of the spectrum and the organic liquids occupy the high end. Thus, it appears that the B/A parameter of single-component liquid takes values either close to 5 or to 10.

The B/A value for pure fat has been determined to be between 9.9 and 11.5 [Everbach, 1989; Errabolu et al., 1987; Apfel, 1983]; also see discussion in Section 4.2.2. The B/A for protein and carbohydrate, as they are in solid state, can only be estimated from the B/A data of their aqueous solutions of known composition using the mixture laws. Their B/A values calculated using Sehgal's mixture law are shown in Table 1.3, together with those for water and fat, for comparison. The uncertainties of calculated values are derived from the measurement uncertainties reported in the cited references, and are also shown. It can be seen that fat, protein and carbohydrate have essentially very similar B/A values, and that binary property can also be observed among those pure substances commonly known as the constituents of tissues, with water being in one end of the spectrum and fat, protein and carbohydrate being the other end. The preparations in Table 1.2, the mixtures of these components, take the intermediate B/A values, filling the gap between inorganic and organic groups in Fig. 1.2.

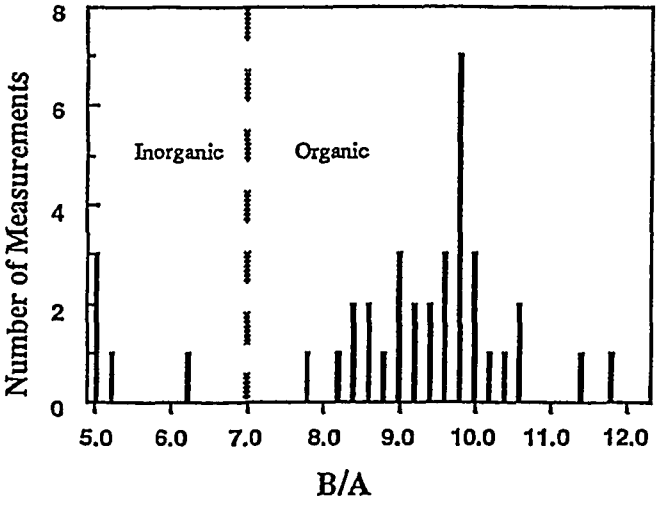

Figure 1.2 Histogram generated from data compiled in Table 1.1.

Investigation of the B/A parameter of tissues also suggested that the B/A parameter not only depends upon the chemical composition of tissues, but also upon their structural features. Law et al. [1985]

reported the decrease of B/A value from 7.7 of intact beef liver to 6.8 of the same beef liver homogenized. This represents about a 40% difference, after subtraction of the water baseline contribution.

Table 1.3 B/A Values for Water, Fat, Protein and Carbohydrate

	ρ(gm/cm^3)	c(m/sec)	B/A	$(B/A)_{cal}$
Water [a]	0.999	1501	5.20	
Corn Oil [b]	0.913	1437	10.57	
Peanut Oil [b]	0.908	1436	10.68	
BSA (38.8%) [c]	1.094	1615	6.68	11.95 ± 2.1
BSA (40g/100cc) [d]	1.076	1574	6.05	8.63 ± 2.7
Dextran T150 (24%) [c]	1.088	1567	6.05	12.63 ± 3.3
Dextran T2000 (26%) [c]	1.090	1574	6.03	11.47 ± 3.1

(a) [Beyer, 1974]
(b) [Everbach, 1989]
(c) [Law et al., 1985]
(d) [Cobb, 1982]

1.4. Purpose and Scope

It is a purpose of this study to examine systematically the influence of the structure of the biological medium on the B/A parameter. Three structural levels are considered, viz., the tissue level, the cellular level, and the molecular level. For each level of structure, experiments were designed to measure the B/A change when the structure of the medium is altered, but the molecular composition is kept the same. The information obtained is expected to clarify whether the B/A parameter depends on the structure of the medium and, if so, the extent of the dependence. Both the finite amplitude method and the thermodynamic method were used to measure the B/A parameter.

The term "structure of the medium," herein refers to the heterogeneous spatial distribution of chemical constituents. Biological tissues are generally not homogeneous mixtures of constituent protein, fat and water molecules, but their constituents are organized into various levels of organization [Vander et al., 1980]. For instance, at the molecular level, amino acid chains are folded to form the secondary structure of proteins; at cellular level, phospholipid molecules are

organized into lipid bilayers and cells; at tissue level, cells are arranged to form tissues. It is a common feature of these examples that the constituent molecules are not arranged randomly and homogeneously, but orderly. The effects of rearrangements of such constituent molecules, with their compositions unchanged, on the B/A of the media they form, will be examined in the remainder of this dissertation. These rearrangements are brought about by perturbing the media physically, by sonication and changing temperature, and biochemically, by denaturation and enzyme digestion.

CHAPTER 2

THEORY AND MEASUREMENT METHODS

Models for finite amplitude acoustic wave propagation, both plane-wave and diffraction theories, are presented in this chapter. The B/A parameter measurement principles, based on these models, are discussed.

2.1. Plane Wave Theory

2.1.1. Wave equation

Acoustic wave motion, as a special case of mechanical motion in continuous media, is generally governed by two basic physical laws, the law of mass conservation and the law of momentum conservation. These laws, together with the description of the mechanical properties of the medium, comprise the Euler equations, which describe the wave motion completely [Rudenko and Soluyan, 1977]. Mathematically, the Euler equations can be written as

$$\frac{\partial \rho}{\partial t} + \nabla\bullet(\rho v) = 0 \tag{2.1}$$

$$\rho[\frac{\partial v}{\partial t} + (v\bullet\nabla)v\,] = -\Delta p \tag{2.2}$$

$$p = p(\rho) \tag{2.3}$$

where ρ is density, v is particle velocity, and p is pressure. Equation (2.1) describes conservation of mass, Eq. (2.2) conservation of momentum, and Eq. (2.3) the mechanical properties of the medium. As discussed in Chapter 1, Eq. (2.3) can be expressed in a Taylor's series

$$p = p_o + A\left(\frac{\rho-\rho_o}{\rho_o}\right) + \frac{B}{2!}\left(\frac{\rho-\rho_o}{\rho_o}\right)^2 + \ldots\ldots \tag{2.4}$$

The equation of motion is obtained by combining the Euler equations to an expression of a single dependent variable (for detailed derivation see [Beyer, 1974]) as

$$\frac{\partial^2 \xi}{\partial t^2} = \frac{c_o^2}{\left(1+\frac{\partial \xi}{\partial z}\right)^{2+\frac{B}{A}}} \frac{\partial^2 \xi}{\partial z^2} \tag{2.5}$$

where ξ is the particle displacement and c_o the infinitesimal velocity of the medium. It is clear that Eq. (2.5) is a nonlinear differential equation; it describes the nonlinear propagation of the acoustic wave in a continuous, nondissipative and nonlinear medium. Generally, attempts to solve Eq. (2.5) for plane-wave solutions can be grouped into either the Fubini-Fay-Blackstock solutions or the solution to Burgers' equation [Beyer, 1974]. Fubini's solution is valid in the region of $\sigma<1$; the so-called weak nonlinearity region. Fay's solution describes a fully developed shock wave (also known as the sawtooth wave or N-wave) propagation and is valid for the region of approximately $\sigma>3.5$. The bridging function, developed by Blackstock using weak shock theory, connects the Fubini and Fay solutions and is valid in a transition region where neither is valid, viz., $1<\sigma<3.5$ [Blackstock, 1966]. The solution to Burgers' equation was obtained by transforming the equation of motion into a Burgers' equation-like format. While lacking in generality, Fubini-Fay-Blackstock descriptions of nonlinear plane-wave propagation are relatively simple, and their physical significances are easy to comprehend. Burgers' solution, taking into account one of the dissipative mechanisms, viz., viscosity, is valid throughout the regions, but is mathematically very complicated. The nonlinearities encountered in most biomedical applications of ultrasonic energy are in the weak nonlinearity region and in the weak shock region. The measurement of the nonlinearity parameter is almost exclusively carried out in the weak nonlinearity region. For these reasons, only the Fubini solution and Burgers' solution in the weak nonlinearity region will be considered.

2.1.2. Fubini solution

Equation (2.5) was first solved in implicit form by Earnshaw [Beyer, 1974]. Assume the boundary condition on the particle velocity at the origin z=0 to be

$$u(0,t) = u_o \sin \omega t \tag{2.6}$$

where u_o is the magnitude of the particle velocity at the z=0, ω is the angular frequency, and t denotes time. Earnshaw's implicit solution can be expressed as

$$u(z,t) = u_o \sin\left[\omega t - \frac{\omega z}{c_o}\left(1 + \frac{B}{2A}\frac{u}{c_o}\right)^{-\frac{2A}{B}-1}\right] \tag{2.7}$$

where c_o is the infinitesimal velocity, B/A is the nonlinearity parameter, and u/c_o is the Mach number. For a low Mach number, Eq. (2.7) can be rewritten by binomial expansion of the inner parenthesis as

$$u(z,t) = u_o \sin\left[\omega t - \frac{\omega z}{c_o}\left(1 - (1 + \frac{B}{2A}) \frac{u}{c_o}\right)\right] \tag{2.8}$$

Note that the particle velocity u(z,t) exists in the phase term, and thus, the phase of the planar wave is modulated by its own amplitude. The Fubini solution is obtained by expanding Eq. (2.8) in a Fourier series as

$$\frac{u}{u_o} = 2\sum_{n=1}^{\infty} \frac{J_n(\frac{n z}{L})}{\frac{n z}{L}} \sin n(\omega t - kz) \tag{2.9}$$

where J_n is the nth order Bessel function. It shows that nonlinear distortion can be expressed equivalently by the harmonic generation. This harmonic generation is the basis of the finite amplitude method for

the measurement of the B/A parameter, which is discussed in Section 2.3.2.

2.1.3 Burgers' equation

Taking into account the viscosity of a dissipative medium, the wave propagation can be described by the Navier-Stokes equation [Kinsler et al., 1982] as

$$\rho_o \frac{\partial^2 \xi}{\partial t^2} = -\frac{\partial p}{\partial z} + \left(\frac{4}{3}\eta + \eta_B\right)\frac{\partial^3 \xi}{\partial z^2 \partial t} \tag{2.10}$$

where η and η_B are the shear and bulk viscosities, respectively. The quadratic equation of state,

$$\frac{\partial p}{\partial z} = -A\frac{\partial^2 \xi}{\partial z^2} + 2A\left(1+\frac{B}{2A}\right)\frac{\partial \xi}{\partial z}\frac{\partial^2 \xi}{\partial z^2} \tag{2.11}$$

can be used in place of the $(\partial p/\partial z)$ term in Eq. (2.10), yielding

$$\rho_o \frac{\partial^2 \xi}{\partial t^2} = A\frac{\partial^2 \xi}{\partial z^2} - 2A\left(1+\frac{B}{2A}\right)\frac{\partial \xi}{\partial z}\frac{\partial^2 \xi}{\partial z^2} + \left(\frac{4}{3}\eta + \eta_B\right)\frac{\partial^3 \xi}{\partial z^2 \partial t} \tag{2.12}$$

With the coordinate transformation, $x = z - c_o t$ and $\tau = t$, and neglecting terms higher than second order, Eq. (2.12) can be written in Burgers' equation form as

$$c_o^3 \frac{\partial u}{\partial x} - \left(1+\frac{B}{2A}\right)c_o u \frac{\partial u}{\partial \tau} = \frac{c_o^3 \alpha}{\omega^2}\frac{\partial^2 u}{\partial \tau^2} \tag{2.13}$$

where α is the absorption coefficient. Equation (2.13) has an exact solution, viz.,

$$\frac{u}{u_o} = \frac{\sum_{n=1}^{\infty} (-1)^{n+1} n I_n(\frac{\Gamma}{2}) e^{-n^2\alpha z} \sin n(\omega t - kz)}{I_o(\frac{\Gamma}{2}) + 2\sum_{n=1}^{\infty} (-1)^n I_n(\frac{\Gamma}{2}) e^{-n^2\alpha z} \cos n(\omega t - kz)} \tag{2.14}$$

where I_n is the Bessel function of order n of the imaginary argument, i.e.,

$$I_n(z) = (i)^{-n} J_n(iz) \tag{2.15}$$

and $\Gamma = (1+B/2A)(u_o/c_o\alpha)(2\pi/\lambda)$. Equation (2.14) is known as Burgers' solution.

2.2. Diffraction Theory

Though it is simple, plane-wave theory is only an approximate description of nonlinear wave propagation. More realistically, since transducers have finite apertures, the acoustic beam "spreads," i.e., diffracts on propagating away from the source. In order to account for this phenomenon, the diffraction theory is needed to be included in the description.

Kuznetsov [1971] has pointed out that, instead of solving the wave Equation (2.5), almost every paper on diffraction theory of nonlinear acoustics begins with the derivation of an ad hoc approximate equation of motion. Heaps [1962] started with the Euler equation described in Section 2.1.1 and derived a set of equations involving the acoustic pressures of different frequency components. Westervelt [1963] and Tjotta and Tjotta [1981] employed the Lighthill exact equation for fluid motion to investigate parametric acoustic arrays. Kuznetsov derived a nonlinear acoustics equation, similar in form to the linear wave equation, from a set of equations of motion which take into account viscosity and heat dissipation.

The common feature in these methodologies is described as follows. First, a set of equations governing the motion in fluid media is constructed. Taking into account different absorption mechanisms and

the nonlinearity of the medium, a differential equation is derived from the equations of motion. Then, by assuming time harmonic motion and Fourier series representation of the nonlinear acoustic field, a set of equations governing different frequency components is derived. And lastly, the set of equations is solved for the harmonic components of the nonlinear field.

Instead of describing each methodology in detail, the formulation by Ingenito and Williams [1971] will be followed and its application to the finite amplitude method will be discussed. Ingenito and Williams used an approach similar to that of Heaps. The derivation begins with Euler's Eqs. (2.1)-(2.3). It assumes that the fundamental and the second harmonic are the only two significant frequency components, i.e.,

$$\Phi(x,y,z,t) = \sum_{i=1}^{\infty} \Phi_i(x,y,z,t)$$
$$\cong \Phi_1(x,y,z,t) + \Phi_2(x,y,z,t) \tag{2.16}$$

and Φ_1 is the solution of the linear wave equation. Φ_1 and Φ_2 are the fundamental and second harmonic components of velocity potential, respectively. A differential equation that governs Φ_2 can be obtained as

$$\left(\nabla^2 - \frac{1}{c^2}\frac{\partial^2}{\partial t^2}\right)\Phi_2 = -\frac{1}{2c_o^2}\frac{\partial}{\partial t}\left[\left(\nabla^2 - \frac{1}{c^2}\frac{\partial^2}{\partial t^2}\right)\Phi_1^2 + \frac{\gamma+1}{c^2}\left(\frac{\partial \Phi_1}{\partial t}\right)^2\right] \tag{2.17}$$

Let Φ_1 and Φ_2 be harmonic in time, or

$$\Phi_1 = \varphi_1(x,y,z)e^{-j\omega t}$$
$$\Phi_2 = \varphi_2(x,y,z)e^{-j\omega t} \tag{2.18}$$

Equation (2.17) can be solved, in cylindrical coordinates (r,θ,z), for the second harmonic acoustic field generated by a circular disc centered at

r=0 and on the z=0 plane. The $\varphi_2(r,z)$ can be expressed in terms of $\varphi_1(r,z)$,

$$\varphi_2(r,z) = -\frac{k^2(\gamma+1)}{8c}\int_{\sigma=0}^{z} e^{jk\sigma}\varphi_1^2(r,\, z-\frac{\sigma}{2})\, d\sigma \tag{2.19}$$

where γ = (B/A+1) and c is the speed of sound. For a circular disc receiver of radius a, the output voltage is assumed to be proportional to the average of φ_2 over its surface, viz.,

$$<\varphi_2(r,z)> = -\left[\frac{k^2(\gamma+1)}{8c}\right]\int_{\sigma=0}^{z} e^{jk\sigma}\left(<\varphi_1(r,z-\frac{\sigma}{2})>\right)^2 d\sigma \tag{2.20}$$

where <*> denotes the average over a transducer surface. The $<\varphi_1>$ has been given by Bass [1958] as

$$<\varphi_1> = -\frac{u_o^2}{k^2} e^{2jkz}\left[1-2\left(1-\frac{\xi^2}{2k^2a^2}\right)\sqrt{\frac{2}{\pi\xi}}\, e^{-j\frac{\pi}{4}}\right] \tag{2.21}$$

where u_o is the velocity amplitude of the vibrating disc, and

$$\xi = (\frac{k}{2})\left[\sqrt{(z^2+4a^2)} - z\right].$$

Substituting Eq. (2.21) into (2.20) gives

$$<\varphi_2(r,z)> = \frac{u_o^2(\gamma+1)}{4c_o} e^{2jkz}\left(\frac{z}{2}+I\right) \tag{2.22}$$

where

$$I = \frac{4}{\sqrt{\pi k}} e^{-j\frac{\pi}{4}} \int_{\frac{z}{2}}^{z} \left[\left(\sqrt{\theta^2+4a^2} - \theta \right)^{\frac{1}{2}} - \frac{1}{8a^2} \left(\sqrt{\theta^2+4a^2} - \theta \right)^{\frac{3}{2}} \right] d\theta$$

Converting the velocity potential into the acoustic pressure using the planar small signal dissipationless relationship,

$$p_2 = -j\omega\rho_o \varphi_2$$

gives

$$|\langle p_2 \rangle| = \omega\rho_o |\langle \varphi_2 \rangle|$$

$$= \frac{\omega p_o^2 (B/A + 2)}{4\rho_o c^3} \left| \frac{z}{2} + I \right|$$

$$= \frac{\pi f p_o^2 (\frac{B}{A} + 2)}{2\rho_o c_o^3} z \left| 1 + \frac{2I}{z} \right| \qquad (2.23)$$

where |*| denotes the magnitude, and the relationship of $p_o = \rho_o c_o u_o$ has been used. Equation (2.23) is very similar to the result from the plane-wave theory, viz.,

$$p_2 = \frac{\pi f p_o^2 (\frac{B}{A} + 2)}{2\rho_o c_o^3} z \qquad (2.24)$$

except for the |1+2I/z| factor. This factor,

$$DIFF = \left| 1 + \frac{2I}{z} \right| \qquad (2.25)$$

is due to the diffraction effect of the acoustic beam and can be calculated as a function of z in order to correct for this effect in B/A parameter measurement.

2.3. Measurement Methods of Nonlinearity Parameter B/A

In this section the nonlinear acoustic theories are applied to the measurement of the nonlinearity parameter B/A. Two methods, finite amplitude and thermodynamic, are discussed. The finite amplitude method, so called for its employment of finite amplitude acoustic wave instead of infinitesimal approximation, has the advantage of no need to subject samples to high pressure, but suffers from low accuracy. The thermodynamic method, while employing high pressure, has the advantage of high accuracy.

2.3.1 Finite amplitude method

As discussed in Section 2.2, the second harmonic acoustic pressure is proportional to the nonlinearity parameter B/A. Equation (2.23) can be rewritten as

$$\frac{B}{A}+2=\frac{2\rho_o c_o^3}{\pi f}\,\frac{p_2(z)}{p_o^2 z}\,(\mathrm{DIFF}(z))^{-1} \tag{2.26}$$

This relation is the basis for the finite amplitude method. However, Eq. (2.26), in this form, cannot be applied directly to B/A measurement because it does not take into account absorption of acoustic energy by the medium. Cobb [1983] proposed an ad hoc approach to correct for absorption of the fundamental and second harmonic frequency components. This approach views Eq. (2.19) as a summation of all the second harmonic pressure components generated locally and propagating toward the receiver (in the positive z direction), since both frequency components are well collimated. The integrand can be seen as the differential amount of the second harmonic component, generated within the region from $z=\sigma$ to $z=\sigma+\Delta\sigma$, known as the generation plane. Thus, taking into account the effect of absorption of the fundamental frequency component propagating from the source (z=0) to the generation plane ($z=\sigma$), φ_1, becomes $\varphi_1\exp(-\alpha_1(z-\sigma))$ with α_1 being the absorption coefficient of the fundamental frequency. Further,

considering the attenuation of the second harmonic frequency component propagating from the generative plane to the receiver, the second harmonic should have been attenuated by a factor of $\exp(-\alpha_2\sigma)$ with α_2 being the attenuation coefficient of the second harmonic component. Equation (2.19) so corrected becomes

$$\langle\varphi_2(r,z)\rangle = -\left[\frac{k^2(\gamma+1)}{8c_o}\right]\int_{\sigma=0}^{z} e^{jk\sigma}\, e^{-\alpha_2\sigma}\, \langle\varphi_1(r,z-\frac{\sigma}{2})\rangle^2\, e^{-2\alpha_1(z-\sigma)}\, d\sigma \tag{2.27}$$

Considering a medium to have a near linear frequency dependence of absorption, i.e., $\alpha_1 \simeq 2\alpha_2$, Eq. (2.27) can be approximated and expressed in terms of acoustic pressure [Law, 1984], as

$$p_2(z) = \frac{\pi f(2+B/A)}{2\rho_o c_o^3} p_o^2\, z\, e^{-(\alpha_1+\alpha_2/2)z}\, DIFF(z) \tag{2.28}$$

Equation (2.28) was used by Law [1984] to measure the B/A parameter.

2.3.2 Thermodynamic method

As seen in Section 1.2, the nonlinear effect comes about because the speed of sound is a function of pressure amplitude. Thus, pressure variation of the finite amplitude acoustic wave reveals the nonlinearity of media. However, an acoustic wave is not the only means of producing an adiabatic pressure variation. Very fast pressure changes, such as the so-called pressure jump [Heremans et al., 1980; Knoche and Wiese, 1974], although not periodic, can also reveal the nonlinearity of media. This is the rationale underlying the thermodynamic method for B/A measurement.

From the definition of A and B in Section 1.2, B/A can be expressed in terms of velocity change with respect to pressure [Beyer, 1974],

$$\frac{B}{A} = 2\rho_o c_o \left(\frac{\partial c}{\partial p}\right)_{s,\rho=\rho_o} \tag{2.29}$$

This relationship was first used by Sehgal et al. [1984] to measure the B/A parameter. Further derivation arrives at the relationship that expresses B/A in terms of velocity variations with respect to the pressure at constant temperature and the temperature with respect to the pressure [Beyer, 1974; Law, 1984]

$$\frac{B}{A} = 2\rho_o c_o \left(\frac{\partial c}{\partial p}\right)_T + \frac{2\beta T c_o}{C_p}\left(\frac{\partial c}{\partial T}\right)_p \tag{2.30}$$

which is the method Beyer and Law used to measure the B/A parameter. The measurement method employed in the present study is based on Eq. (2.29).

CHAPTER 3

INSTRUMENTATION AND PROCEDURES

3.1 Thermodynamic Method

The thermodynamic method of measurement of the nonlinear parameter B/A is based on the thermodynamic expression [Beyer, 1974].

$$B/A = 2\rho_o c_o \left(\frac{\partial c}{\partial p}\right)_s \tag{3.1}$$

where ρ_o is the ambient density of the medium, c_o is the infinitesimal speed of sound and $(\partial c/\partial p)_s$ is the derivative of speed of sound with respect to the pressure for an isentropic process. The pressure jump method [Endoh and Dunn, 1986; Sehgal et al., 1984; Zhu et al., 1983; Heremans et al., 1980; Knoche et al., 1974] was used to create the isentropic change of pressure. The measurement requires the measurements of velocity change during the isentropic pressure jump, velocity at thermal equilibrium, and the density of the media.

3.1.1 Overall description

Two systems were built for measurements of velocity change during a pressure jump. The major difference between the two was the volume of the sample required for measurement. The first system required 25 ml of sample. The second one required about 4 ml, which enables studies involving either expensive commercially available materials or minutely yielded biochemical samples.

Figure 3.1 is a block diagram of the 25 ml system. A 20-cycle gated cw burst at 3 MHz was generated by a Wavetek 271 pulse generator, which was then divided by a power splitter into two equal amplitude pulses. One pulse provided a reference, after being delayed

acoustically. The other pulse was amplified by an RF amplifier (Amplifier Research, model 10LA) to drive one of the transducers of the velocimeter. The velocimeter was composed of two transducers arranged parallel and coaxial to each other and spaced 7.6 cm apart [Law, 1984]. The specimen to be measured was contained between the transducers. The unit was pressurized and depressurized hydraulically. The pulses, after passing through the acoustic delay and the sample in the velocimeter, respectively, were captured by a Tektronix 2430A digital storage oscilloscope. The waveforms were transferred via an IEEE 488 interface to the AT&T PC for signal processing. A cross-correlation method was used to calculate the relative time delay, Δt, between two pulses. The total time delay, t, between the transmitted pulse and the received pulse was the sum of the time delays created by the acoustic delay, t_o, and the relative delay measured by the digital oscilloscope, Δt, i.e.,

$$t = t_o + \Delta t \tag{3.2}$$

Figure 3.2 shows the timing diagram of the pulses. The total time delay was calibrated against known velocity values for degassed and distilled water and was used to calculate the propagation speed in the unknown sample, as

$$c = \frac{1}{t_o + \Delta t} \tag{3.3}$$

Thus, each pair of waveforms provided a velocity value. By using the fast transmit mode of the Tektronix 2430A oscilloscope and the direct memory access (DMA) to the computer, 45 pairs of waveforms were acquired and transmitted at the rate of 17 pairs per second. The waveforms were stored in an array for further processing. After the pressure jump, the temperature inside the sample was slightly lower than its water bath environment. In order to measure the velocity at thermal equilibrium, a period of time was needed for the system to return to the equilibrium state. It was estimated that, after 10 minutes, the velocity of the sample reaches 0.02% of the thermal equilibrium

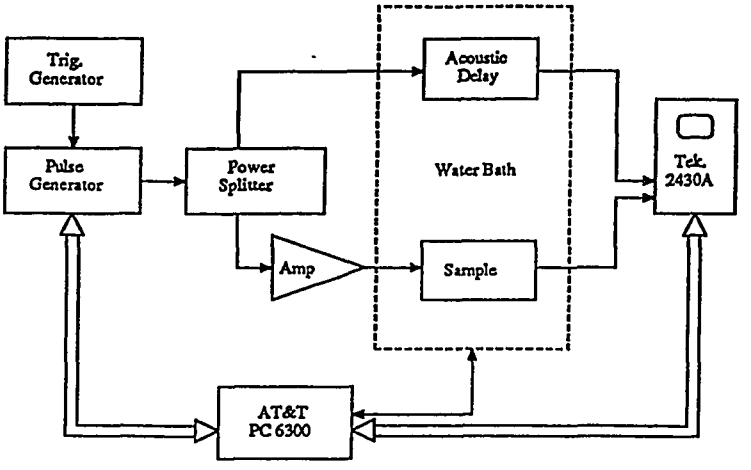

Figure 3.1 Block diagram of the 25 ml B/A measurement system.

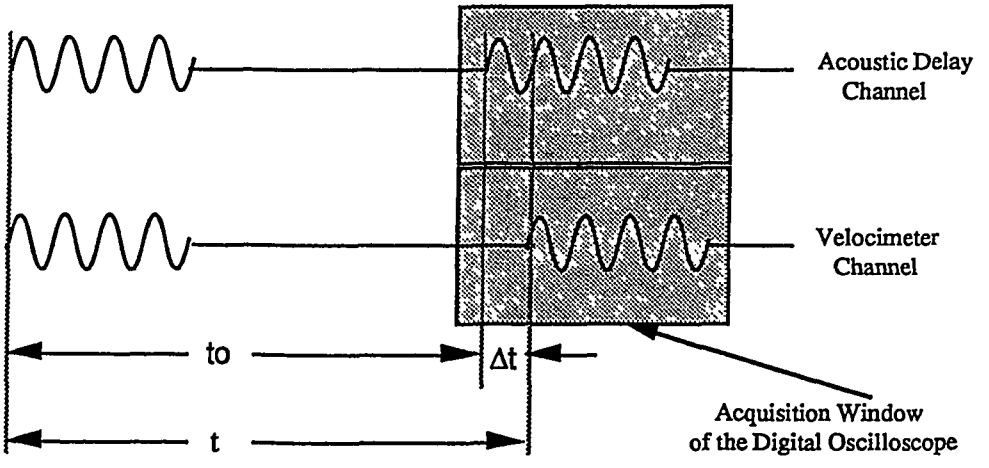

Figure 3.2 Timing diagram of the pulses used in the 25 ml measurement system. The two pulses are acquired by the digital storage oscilloscope, and the highlighted region represents the beginning and the end of the waveform acquisition.

value. During this period, the 45 pairs of waveforms were processed for the velocity profile, which is shown in Fig. 3.3, and the $\Delta c/\Delta p$ value was calculated from the profile. Densities of the samples were measured using picnometers. The density, the velocity at thermal equilibrium, and the velocity change with respect to pressure were then used to determine B/A according to the thermodynamic expression given for B/A, above. The system was tested and found to provide results in good agreement with B/A values reported in the literature, as shown in Fig. 3.4. The standard deviation of the B/A measurement was estimated to be less than ± 0.01 B/A units in degassed and distilled water [Zhang et al., 1988].

The 4 ml system, shown in Fig. 3.5, is similar to the 25 ml system, discussed above, except for its velocimeter construction. Due to the smaller propagation distance, and thus the shorter time of flight, the transmitted pulse and the received pulse were acquired within 1 kilobyte of the record length of the oscilloscope and the acoustic delay was eliminated. The gated pulse, after being amplified, was fed directly to the transmitting transducer and, as a reference, into one of the digital oscilloscope channels. The other channel was used for the received pulse. Both pulses were digitized and transferred to the computer where the time delay was calculated. A similar procedure to that used in the 25 ml system was employed to determine the B/A value. The results in three preparations are compared with those reported in the literature and found to be in good agreement, as shown in Table 3.1. It is also seen that the standard deviations of the measurements by the 4 ml system are about 3 to 4 times greater than those of the 25 ml system.

Velocimeters

The velocimeter was the major component of the measurement system. It was composed of two crystal transducers arranged parallel and coaxial to each other and spaced a distance apart. One of the transducers was used as the transmitter and the other as the receiver. Two velocimeters have been used. One has a 25 ml sample volume [Law et al., 1984] and the other has a 4 ml sample volume.

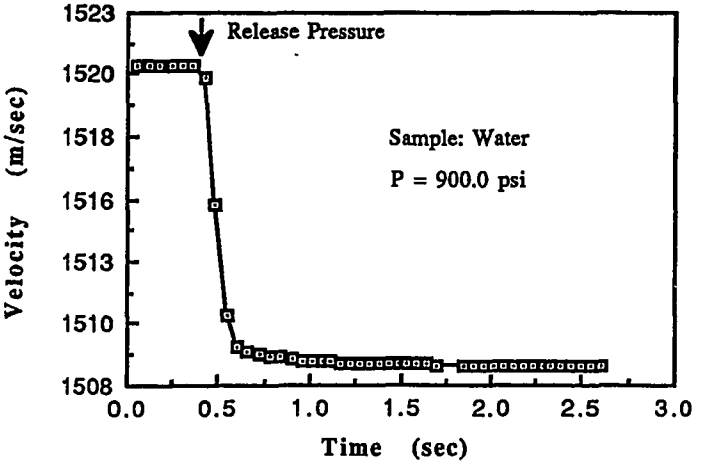

Figure 3.3 Velocity profile during the pressure jump.

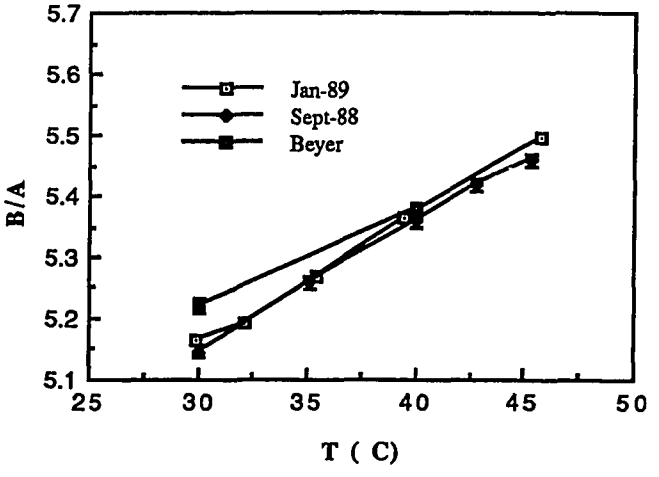

Figure 3.4 Comparison of B/A of water determined by the thermodynamic method with values reported in the literature.

Table 3.1 Comparison of Measured B/A Values with the Literature Values*

Preparations	B/A ± S.D. 4 ml system (30°C)	B/A (T) Literature		
Degassed & Distilled Water	5.18 ± 0.033	5.14 ± 0.001	(30°C)	(a)
		5.22	(30°C)	(b)
		5.11	(25°C)	(c)
		5.31	(30°C)	(d)
25% Dextrose	6.11 ± 0.04	6.13 ± 0.007	(30oC)	(a)
		5.96	(30°C)	(d)
Ethylene Glycol	9.88 ± 0.035	9.82 ± 0.006	(30oC)	(a)
		9.93	(30°C)	(d)
		9.88	(25°C)	(c)
		9.7	(30°C)	(b)

*Only those measured by thermodynamic method
(a) [Zhang et al., 1988]
(b) [Beyer, 1959]
(c) [Zhu et al., 1983]
(d) [Law et al., 1985]

Figure 3.6 shows the arrangement of the 25 ml velocimeter (after Law [1984]). It had three compartments separated by two quartz crystal transducers with resonance frequency of 3 MHz and was constructed of 304 stainless steel. The crystals were backed by degassed silicone oil (Dow Coming 710) and rubber absorbers with a surface at a 45° angle to the axis of the crystals, in order to greatly reduce reflections at the back face of the crystals. Three openings, one

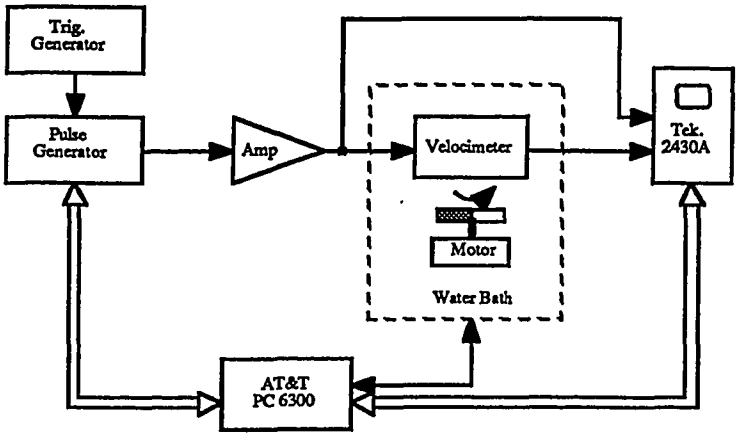

Figure 3.5 Block diagram of the 4 ml B/A measurement system.

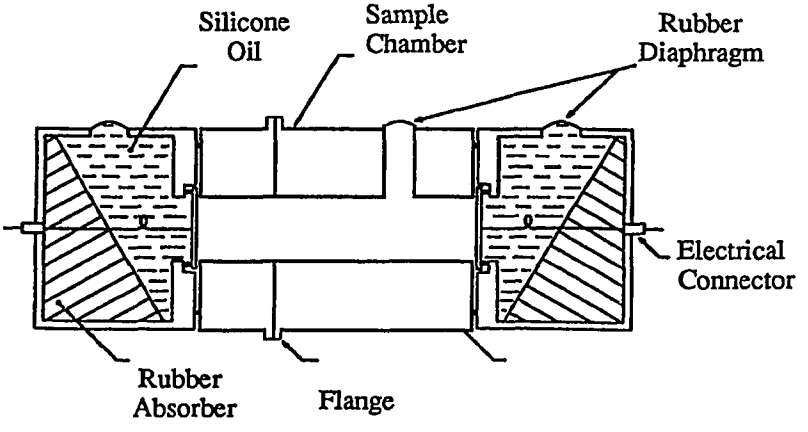

Figure 3.6 The 25 ml velocimeter design (after Law, 1984).

for each compartment, were provided to equilibrate the pressure among the three compartments and between the compartments and the pressure vessel in which the velocimeter is placed. Each opening was sealed with a Latex rubber diaphragm, made from a glove, in order to prevent the exchange of material between the two compartments. The rubber membrane sealed openings ensured the proper pressure build-up inside the sample compartment without developing a pressure gradient across the crystals, while the vessel was being pressurized.

The center compartment, the sample chamber, was 7.62 cm in length and 1.20 cm in diameter. It consisted of two pieces joined together by seven screws. This design facilitated the loading and unloading of samples.

The crystal transducers (Valpey-Fisher Corporation) were X-cut quartz disks 2.54 cm (1 inch) in diameter with a resonance frequency of 3 MHz. Both faces of the crystals were overtone polished, with complete gold-on-chrome plating on the ground side and a 1.27 cm in diameter gold-on-chrome plating axial spot on the other side. When assembled, the completely plated side of the crystals, the electrical ground side, were in electrical contact with the stainless sample chamber, and the other sides were compressed by recessed O-rings to enable a good electrical contact.

The 4 ml velocimeter featured a smaller sample volume, a large sample chamber opening for better elimination of small air bubbles in the sample, and a built-in stirring mechanism. As shown in Figure 3.7, it had three compartments machined from a single piece of 304 stainless steel. Separating the cylinder into three compartments were PZT 5A ceramic transducer elements instead of quartz crystals. The PZT elements provided a greater signal-to-noise ratio and lower Q values than did the quartz crystals. Transducers with smaller Q values contribute a lesser ringing effect and thus help contain both the transmitting signals and the complete received signals within the record length of one kilobyte. Degassed silicone oil and 45° angular cone rubber absorbers were employed as backing material.

The stirring mechanism consisted of a Teflon-coated miniature magnetic bar (2mm in diameter and 7mm in length) free to rotate in a track, and a motor-driven magnetic bar, shown in Fig. 3.7, outside

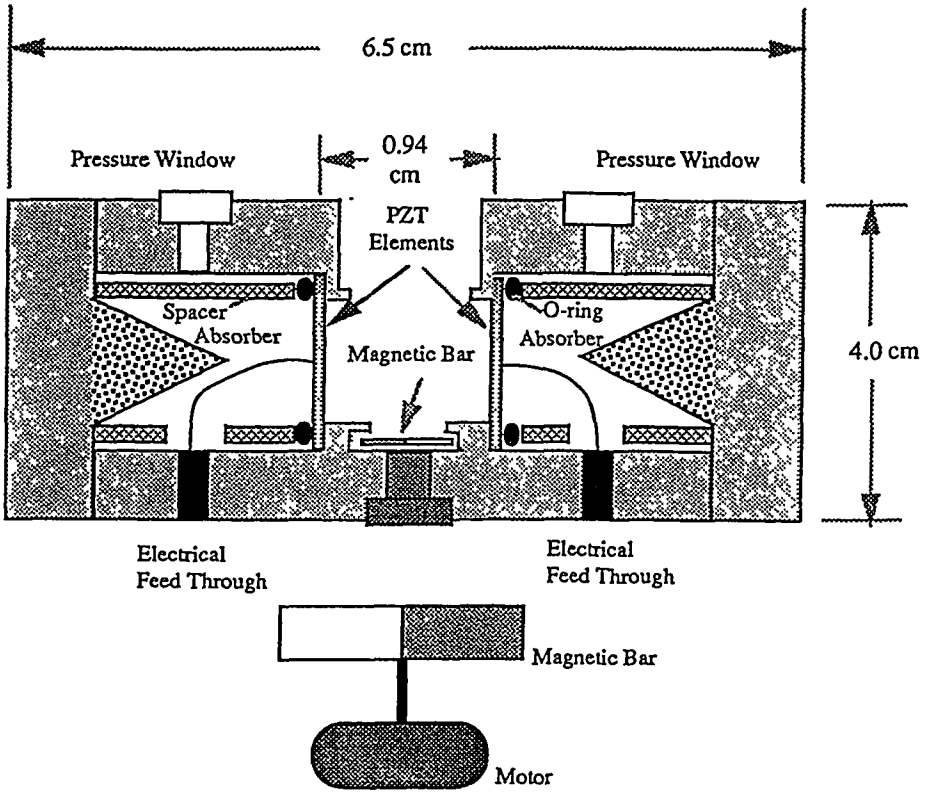

Figure 3.7 The 4 ml velocimeter design.

the pressure chamber. The miniature stirring bar could be taken out for replacement or cleaning by removing the screw that retained the stirring bar to the circular track. The stirring mechanism was designed to prevent, or at least slow down, the process of settling by some samples, such as the multilamellar vesicle liposomes and isolated hepatocyte suspensions.

The PZT elements, manufactured by Valpey-Fisher, were 2.54 cm in diameter and had a resonance frequency of 3 MHz. Both sides were overtone polished. One side of the element was completely plated with gold to serve as the electrical ground. The other side was plated with a 1.27 cm diameter gold-coated axial spot for the transmitter and 1.31 cm diameter gold-coated spot for the receiver. When assembled, the ground side of the element was in direct contact with the stainless steel pieces and the other side was compressed with an O-ring and a spacer to ensure a good electrical ground.

Temperature and Pressure Compensation of Velocimeter

In order to determine the velocity of the test sample accurately, it is important to know the separation distance between the two transducers with high accuracy. Since the length of the stainless steel column separating two transducers changes with temperature and pressure, the distance measured at room temperature and atmospheric pressure needs to be compensated for the changes that will take place at the elevated temperatures and pressures during experiments. In general, the temperature and the pressure correction should be in the form of

$$L = L_o(1 + e_L P + e_T(T - T_{rm})) \qquad (3.4)$$

where the L_o is the distance measured at room temperature and atmospheric pressure, e_L is the linear strain, e_T is the thermal expansion coefficient and T_{rm} is room temperature.

The bulk modulus was calculated from the data of elastic tension moduli and the Poisson's ratio. According to the theory [Maurer and

Withey, 1925], the bulk modulus

$$K = \frac{E}{3(1-2\upsilon)} \tag{3.5}$$

where E is the Young's modulus and υ is the Poisson ratio. The linear strain

$$e_L = \frac{e}{3} = \frac{P}{3K} \tag{3.6}$$

where e is the volumetric strain and P is the applied stress in pounds per square inch (psi). Combining the above two equations, we obtain

$$e_L = \frac{1-2\upsilon}{E} P \tag{3.7}$$

Substituting υ with 0.3 and E with 27.0 $\times 10^{-6}$ psi, we get

$$e_L = 1.5 \times 10^{-8} P \tag{3.8}$$

The thermal expansion coefficient provided by the manufacturer for 304 stainless steel is

$$e_T = 17.3 \times 10^{-6} \, 1/^{o}C \tag{3.9}$$

L_o was measured by micrometer to be

$L_o = 7.620 \pm 0.007$ (cm) for the 25 ml velocimeter
$L_o = 0.941 \pm 0.004$ (cm) for the 4 ml velocimeter

Thus, the distance between two transducers at the temperature T and the pressure P is

$$L = L_o(1 - 1.5 \times 10^{-8} P + 17.3 \times 10^{-6} (T-25.0)) \tag{3.10}$$

Hydraulic Pressure System

A hydraulic pressure system built by Law [1984], was used to create the pressure variation of the sample. Figure 3.8 is the schematic of the system which consisted of a hydraulic hand pump (Enerpac P-391), a pressure gauge (Heise CM-40385TC) and a pressure cell in which the velocimeter was sealed. The hydraulic lines were rubber-coated nylon hydraulic hoses and the hydraulic fluid was Enerpac hydraulic oil. The Heise pressure gauge has the range of 0 to 3000 psi and the full scale accuracy, as specified by the manufacturer, of $\pm 0.1\%$.

The pressure vessel was made of 304 stainless steel with a wall thickness of 0.64 cm. Two threaded end caps enclosed the pressure vessel. One of the end caps was fitted with a connector to the hydraulic system. The velocimeter was mounted to (and removable from) the other end cap. The latter end cap contained the electrical feed through connectors for the transmitter and receiver inside the velocimeter, as well as a fill-hole for bleeding air bubbles. To assemble, the pressure vessel was first filled with degassed water. Then the end cap, attached with the sample loaded velocimeter, was fastened to the vessel.

Separating the degassed water filling the pressure vessel and the oil filling the hydraulic system was a bellows (Servometer, Cedar Grove, NJ) whose function was to transmit pressure from the hydraulic system to the pressure vessel and to compensate the system for the volume change of the contents inside the pressure vessel due to the environmental temperature and pressure changes. The bellows was made of nickel with a 2.54 μm copper lamina. It had an effective area of 4.45 in^2, a spring rate of 80 lbs/in $\pm 30\%$, and a maximum allowable volume change of 20 ml. Care was taken to eliminate air bubbles inside the vessel when closing the pressure vessel, so that the bellows would not be extended beyond the maximum allowable volume change.

Computer and Interfaces

An AT&T 6300 computer was used to control the instruments and to process data. Most of the programs were written in Microsoft C version 5.0 and some were written in ASYST version 2.0. An HP-IB interface card (Hewlett-Packard version of IEEE 488 interface) was installed to provide a computer interface with the digital oscilloscope

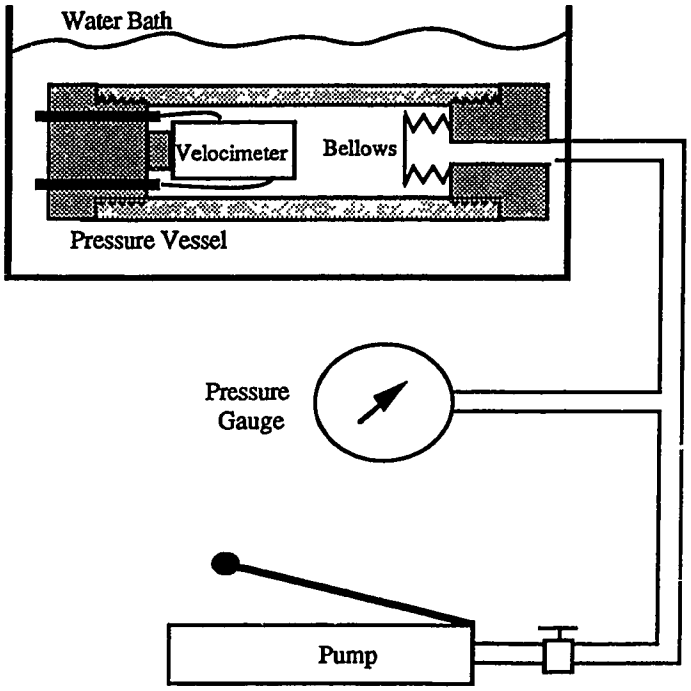

Figure 3.8 The pressure vessel design and the hydraulic pressure system.

and the pulse generator. The computer also controlled the water bath via an RS232 interface.

Digital Storage Oscilloscope

A Tektronix 2430A digital storage oscilloscope was used to acquire the transmitting and received pulses. The oscilloscope had an eight-bit analog-to-digital converter and the maximum transient sampling rate of 100 mega-samples per second. The bandwidth of the oscilloscope was 150 MHz and it had capabilities of signal averaging and direct memory access for fast waveform transmission. The sampling rate of 50 mega-samples per second was used.

Water Bath

A Neslab EX-500DD water bath was used to control the temperature of the system, including the sample. Its temperature stability was specified to be within $\pm 0.001^{o}C$. An RS232 interface inside the unit allowed the computer to initialize the water bath, set the desired temperature and read the temperature of the water bath.

3.1.2. Near field effects on velocity measurement --- a simulation study

The basic principle of velocity measurement using the velocimeter is based on the assumption of plane-wave propagation. The plane-wave assumption is only an approximation to the acoustic field generated by the disc transducer within the velocimeter. The error introduced by such an assumption is usually negligible for the far field region. However, when the receiver is placed in the near field, as is the case in the small volume velocimeter, this assumption can introduce significant error. For the velocity measurement procedure, there is concern about phase error. The significance of this error, and its correction, is taken up in this section. The acoustic field of the two-transducer arrangement, as shown in Fig. 3.9(a), is calculated using this linear diffraction theory, which is generally considered to be a more accurate description of the near field than is the plane-wave theory [Williams, 1951]. A comparison is made between the phases calculated

from two theories in order to assess the possible error in the velocity measurement procedure.

The acoustic transducer is modeled as a rigid circular piston mounted flush with the surface of an infinite rigid baffle and vibrating, in simple harmonic motion, with velocity u_o. With the plane of the piston source located at z=0, the acoustic field can be described by the Rayleigh integral [Pierce, 1981] as

$$p(x) = \frac{-j\omega\rho}{2\pi} \iint_D u_o(x_s,y_s) \frac{e^{jkR}}{R} dx_s dy_s \tag{3.11}$$

where $R^2 = z^2 + (x-x_s)^2 + (y-y_s)^2$, p is the acoustic pressure, ρ is the density, k is the wave number, and the integration is over the surface of the piston source denoted by subscript s. This integral can be evaluated numerically in a straightforward manner to obtain the pressure field at an arbitrary point in space x. However, because of the rapid change in the phase term exp(jkR), the summation increment needs to be very small to sustain the desired accuracy, and computation time increases accordingly. To achieve calculation in a reasonable computation time, the method of equidistant areas described by Swindell et al. [1982] and Ibbini [1988] is used. The method is very similar to the ring function method of Ohtsuki [1974]. The following is a brief description of the method.

Figure 3.9(a) shows the geometry used in the field calculation. To evaluate the Rayleigh integral, the observation point P is projected to P' on the source plane, z=0. A series of concentric rings about P' can be formed such that all points of each ring are in the same distance from point P. The integration is first over one of the strips (equidistance area) that is the intersections of the series of concentric rings and the disc, and then over all the annular strips so formed. The first integration is basically the multiplication of the integrand by the length of the arc strip, since every point in the strip is the same distance to P. By doing so, the double integral in the Rayleigh integral is reduced to a single integral. There are two cases to be considered for the integration boundary; the projected point P' is inside the disc ($r \leq a$) and the P' is

outside the disc (r>a). The former is slightly more complicated and requires that the disc area be divided into two regions (viz., $\sigma \leq$ a-r and $\sigma \geq$ a-r) as shown in Fig. 3.9(b). Finally, after some mathematical manipulation, the following expressions can be obtained:

For r>a

$$p(r,z) = K\int_{r-a}^{r+a} \frac{e^{-jk\sqrt{\sigma^2+z^2}}}{\sqrt{\sigma^2+z^2}} \tag{3.12}$$

where,

$$\Theta = \cos^{-1}\left(\frac{\sigma^2+r^2-a^2}{2\sigma r}\right)$$

and $K = -j\omega\rho/(2\pi)$.

For r≤a

$$p(r,z) = \int_{0}^{a-r} \frac{e^{-jk\sqrt{\sigma^2+z^2}}}{\sqrt{\sigma^2+z^2}} 2\pi\sigma\, d\sigma \tag{3.13}$$

with Θ defined as above. Riemann integration is employed to evaluate the integrals. The number of incremental areas needed depends upon the width of the annular strips. The narrower the strips, the more precise the computation, and the longer computation time required. Thus, the choice of the incremental strip width is a compromise associated with the trade-off between computation precision and computation time. The strip width of $\lambda/8$ was chosen, with λ being the the wavelength. The programs were written in C Language and run on a Tandy 4000 computer, with an 80386 processor and a Weitek 80387 coprocessor.

The simulation results were compared with the numerical analysis of Williams [1951], Zemanek [1971] and Seki et al. [1956] to

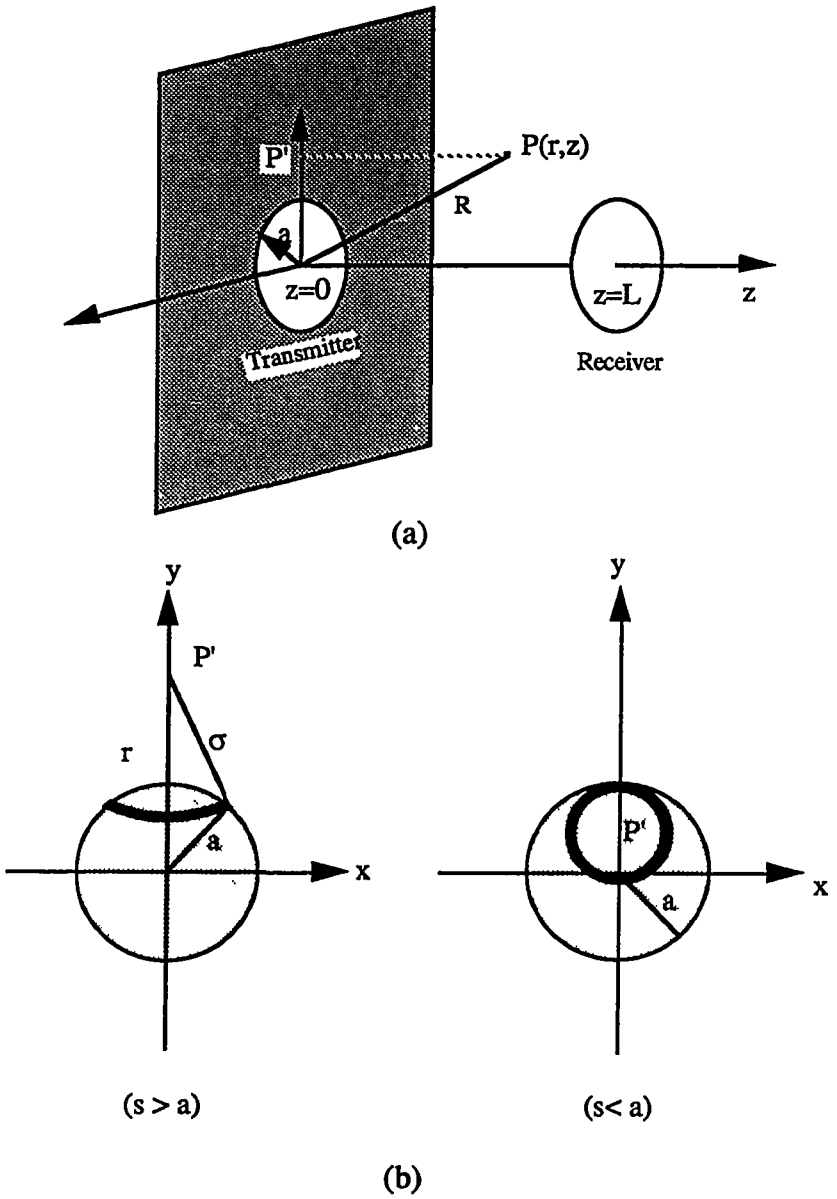

Figure 3.9 (a) The geometry used in the near field simulation. (b) The equidistance integration method for the evaluation of the Rayleigh integral.

test the validity of the methodology and were found to be in good agreement, as seen below.

To compute the received signal, the acoustic pressure field was averaged over the surface of the receiver and the averaged value was taken as the response pressure magnitude, p_{ave} and phase ϕ_{ave}. The input parameters are listed as follows:

Transmitter radius	$a_T = 0.64$ cm
Receiver radius	$a_R = 0.76$ cm
Frequency	$f = 3$ MHz
Speed of sound	$c = 1.509 \times 10^5$ cm/sec
Density of the medium	$\rho = 1.0$ gm/cm^3.

Figure 3.10 shows the averaged pressure magnitude $|p_{ave}|$ plotted against the transducer separation distance and compares the results with those of Williams [1951]. It can be seen that the two simulations are in a good agreement, and that the magnitude decreases with transducer separation, possibly due to phase cancellation and diffraction effects. The difference between the phases predicted by diffraction and plane-wave theories is shown in Fig. 3.11, which exhibits a maximum phase difference of about 88° at z=0.4cm and decreasing monotonically from this point with transducer separation distance. For the velocimeter case, interest is in the phase error produced when the separation distance is fixed, but media with different speed of sound are used. When the phase calculated from diffraction theory (-k'z) is plotted against the phase determined by the plane wave approximation (-kz), a linear relationship is obtained, as shown in Fig. 3.12, and is expressed as

$$(-k'z) = U(-kz) + V \tag{3.14}$$

where U and V are the slope and intercept, respectively, and can be determined from Fig. 3.12. At z = 0.94 cm, the separation distance between the two transducers, it is found that

$$(-k'z) = 1.0005 \times (-kz) - 0.7345 \tag{3.15}$$

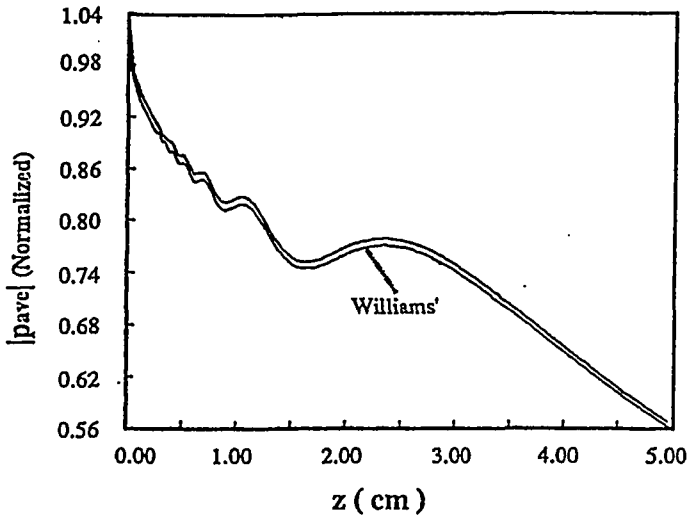

Figure 3.10 Comparison of Williams' simulation result and the result obtained in this study.

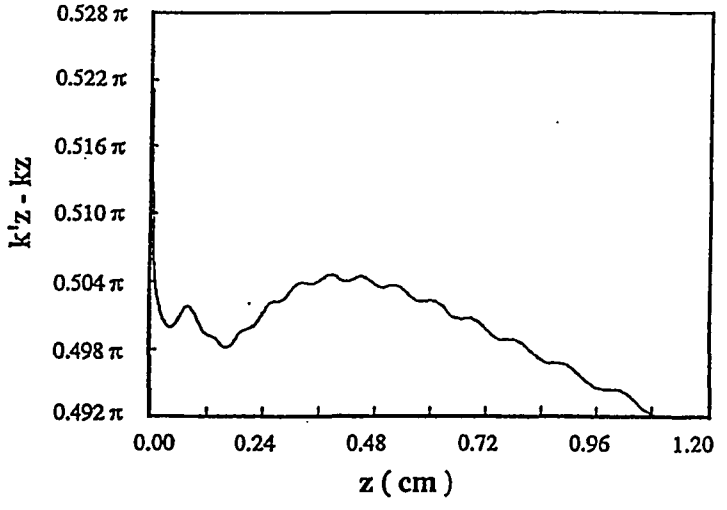

Figure 3.11 Difference between the phase calculated by the diffraction theory (-k'z) and that predicted by the plane-wave theory (-kz).

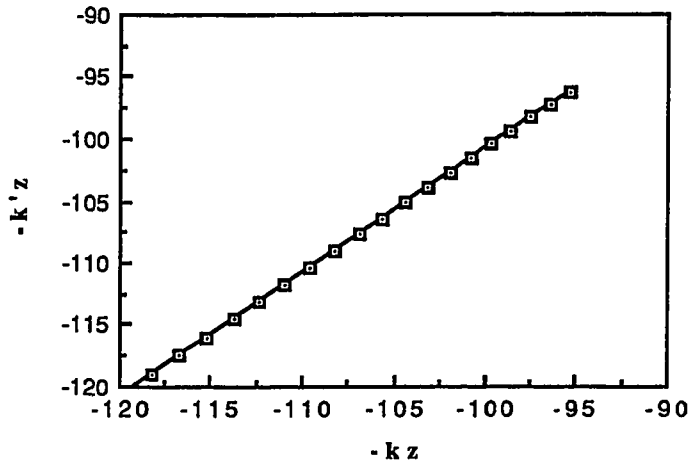

Figure 3.12 The linear relationship between the phases predicted by the diffraction theory and the plane-wave theory.

Equations 3.14 and 3.15 suggest that a simple relationship exists between the two phases and that their phase error can be corrected by the following procedure.

Dividing both sides of the above equation by -ω, we have,

$$\frac{z}{c'} = \frac{z}{c} + \frac{0.7345}{\omega} \tag{3.16}$$

where c' is the true velocity and c is the velocity predicted by plane wave theory. The first term, z/c', is the true time delay due to the propagation of an acoustic wave through the velocimeter. The second term, z/c, is the predicted time delay by the plane wave assumption, and the third term, 0.7345/ω, is the error in time delay prediction. Note that, given transducer separation z, the third term is not a function of the speed of sound in the medium, and thus can be experimentally determined with a medium with known speed of sound such as degassed water. Practically, this time delay error, due to near field effects, is grouped together with that due to the electronics and the total error is determined by calibration using degassed distilled water as the reference.

3.1.3 Signal Processing

The objective of signal processing was to extract the time delay between two acquired pulses. The transmitting pulse and the received pulse could be considered to be time-delayed copies of one another. The cross correlation method, which had the advantages of being accurate and insensitive to noise, was used to determine the delay.

Requirements for Sampling Rate

According to the Shannon sampling theorem [Roberts and Mullis, 1987], the minimum sampling rate required to preserve completely the information of an analog signal is twice the frequency corresponding to the highest frequency component of the signal to be sampled. The carrier frequency of the gated sinusoidal signal employed in the system was 3 MHz. Taking into account the higher frequency components

generated by gating the cw sinusoidal signal, and the harmonics generated by the nonlinear effect of acoustic wave propagation, the highest significant frequency component was estimated to be about 12 MHz, which is the fourth harmonic of the 3 MHz signal. Thus the requirement for the sampling rate was

$$\text{sampling rate} \geq 2 \times 12 \text{ MHz} = 24 \text{ MHz}$$

The sampling rate of 50 mega-samples per second was actually used for both the transmitting and received signals, and was considered to be sufficient.

Cross Correlation Method

This method of determining time delay by computing the cross correlation function has been widely used in radar and sonar target range determination [Chen, 1979] and in flow rate measurements [Ong and Beck, 1975; Embree, 1986]. The general principle of the method will be discussed in this section.

Let a(t) and b(t) be the transmitting and the received signals, respectively, and q(t) and r(t) be the white noise associated with the signals, respectively. The transmitting pulse and the received pulse can be represented by

$$\begin{aligned} x(t) &= a(t) + q(t) \\ y(t) &= b(t) + r(t) \end{aligned} \tag{3.17}$$

where $b(t) = Aa(t-t_o)$ is a delayed version of the transmitted signal a(t), A is a constant that accounts for the signal attenuation, and t_o is the time delay between a(t) and b(t). Further assuming both x(t) and y(t) are two stationary random processes, their cross correlation function is then defined as

$$R_{xy}(\tau) = E[x(t)\, y(t+\tau)] \tag{3.18}$$

where E denotes expectation.

$$R_{xy}(\tau) = E[\,(a(t) + q(t)) \cdot (b(t+\tau) + r(t+\tau))\,] = E[\,a(t)b(t+\tau) + q(t)\,b(t+\tau) + a(t)r(t+\tau) + q(t)r(t+\tau)\,] \tag{3.19}$$

Generally, the noise q(t) and r(t) have zero means, i.e., E[q(t)]=E[r(t)]=0, and are statistically independent of the signals a(t) and b(t). Then we have

$$R_{xy}(\tau) = E[a(t)\,b(t+\tau)] + E[a(t)]\cdot E[r(t+\tau)] + E[b(t+\tau)]\cdot E[q(t)] + E[q(t)]\cdot E[r(t+\tau)] = E[a(t)b(t+\tau)] \tag{3.20}$$

It can be seen that the cross correlation of two noisy pulses is equal to the cross correlation of two true signals, as if there was no noise presented. This desirable feature comes about because random noise is not correlated, and, thus is eliminated during the cross correlation operation.

Since b(t) is a delayed version of the transmitted signal, then

$$R_{xy}(\tau) = A\cdot E\,[\,a(t)\,a(t+\tau-t_o)] \tag{3.21}$$

and $R_{xy}(\tau)$ reaches a maximum when $\tau = t_o$, i.e., when a(t) superimposes with itself. In conclusion, the time delay between the transmitting and received pulses is where their cross correlation function reaches its maximum. Figures 3.13 and 3.14 show two pulses acquired experimentally and their cross correlation function.

Interpolation Procedures

For signals with a relatively low noise level, the uncertainty in determining the time delay can be approximated by the uncertainty in the peak detection of a correlation function, which is a ± 1 sampling interval, or ± 20 nsec in this case. The corresponding uncertainty in

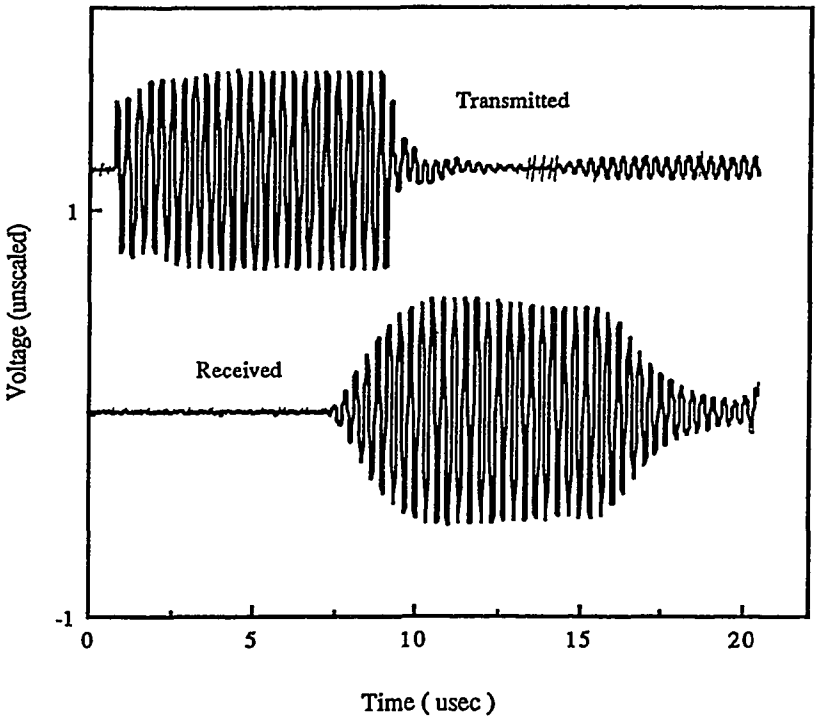

Figure 3.13 The acquired time domain signals. The distortions in waveforms are due to the printer resolution limit.

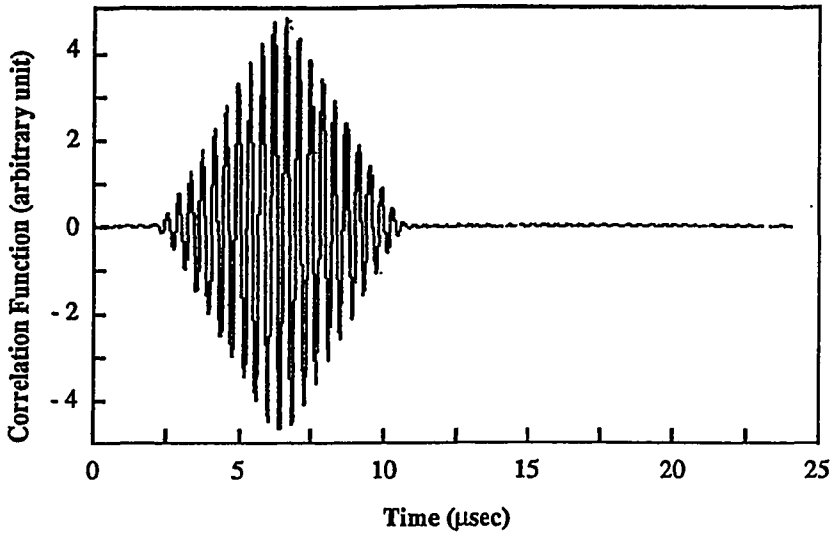

(a)

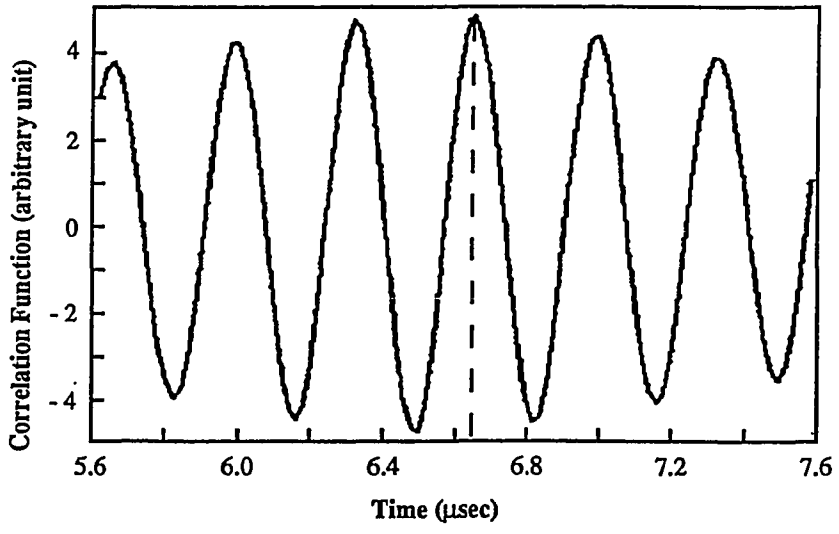

(b)

Figure 3.14 Cross-correlation function of two time-domain signals, such as those shown in the Fig. 3.13. The maximum of the function occurs at the time shift that is equal to the time delay between two signals. Figure 3.14(b) is a magnification of the peak portion of the waveform in Fig. 3.14(a)

velocity determination Δc, however, can be expressed as

$$\Delta c = \frac{\Delta x}{t} + \frac{\Delta t}{t}\frac{x}{t}$$

$$= c\frac{\Delta x}{x} + c^2\frac{\Delta t}{x} \qquad (3.22)$$

where x is the distance between two transducers, Δx is the uncertainty associated with measuring x, t is the time of flight, Δt is the uncertainty in determining t, and c is the sound velocity of the medium. For a medium with velocity 1.5×10^5 cm/sec and a transducer separation of 1 cm, the minimum uncertainty in velocity determination is

$$\Delta c \geq c^2 (\Delta t/x)$$
$$= 450 \text{ cm/sec}$$

which is unacceptable.

In order to determine with higher accuracy the peak of the correlation function, and consequently the time delay, two interpolation procedures were performed, viz., zero packing [Ludeman, 1986] and parabolic curve fitting for the correlation function peak.

Figure 3.15 illustrates the procedure of the zero packing. Let x(n) be a band-limited time domain sequence with 1 kilobyte of data and X(k) be its Discrete Fourier Transform (DFT). First, time domain signal x(n) is transformed to the frequency domain. Then, the DFT sequence X(k), which is also 1 kilobyte in length, is split in half at the center, and a new sequence X'(k) is constructed such that the first 512 elements are the copies of the first 512 elements from X(k) and the last 512 elements are the copies of the last 512 elements from X(k) with the remaining elements filled with 7 kilobytes of zeros. The sequence X'(k), which is now 8 kilobytes, is then transformed back to the time domain. The resulting sequence x'(n) would be the sequence with 8 data elements interpolated between each pair of original elements from x(n), as if the analog signal were sampled 8 times faster. Thus, the uncertainty in determining the peak of the correlation function would be $\pm(20/8)$ nsec or ± 2.5 nsec instead of 20 nsec. Therefore, the accuracy of the time-

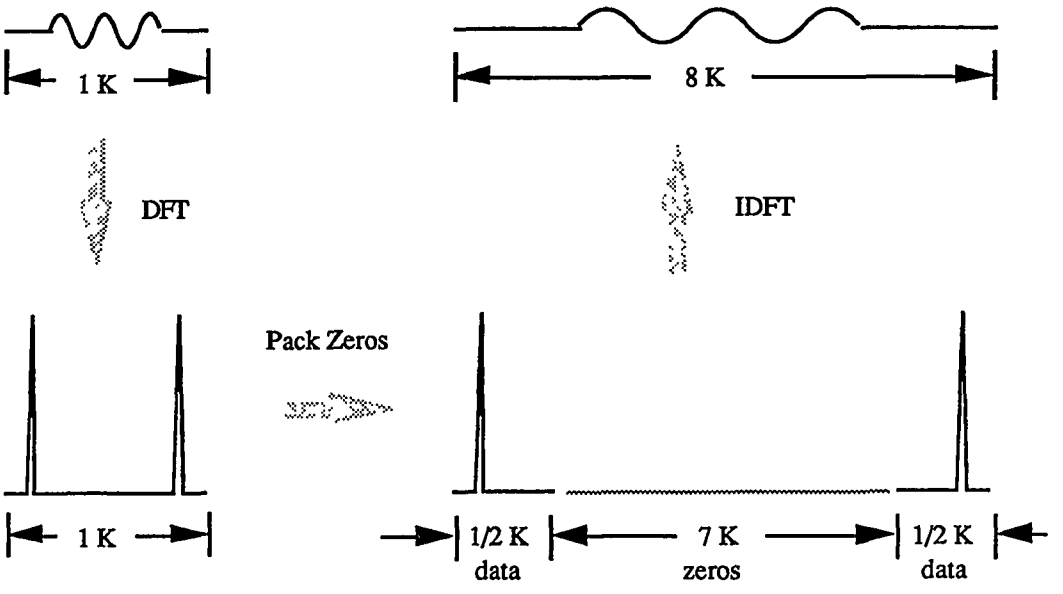

Figure 3.15 Illustration of the frequency-domain zero-packing procedure for the time-domain interpolation.

delay calculation is increased eight times, with, however, the sacrifice of additional computation time.

Further improvement can be achieved by fitting three data points near the peak to a parabolic curve to estimate the true peak location. Assume that the three discrete data are y_{n-1}, y_n and y_{n+1} corresponding to the (n-1)th, nth and (n+1)th elements in the closest vicinity of the peak, and that the parabolic curve has the form of

$$y = ax^2 + bx + c$$

with the constants a, b and c being the solutions of the following matrix equation:

$$\begin{bmatrix} (n-1)^2 & (n-1) & 1 \\ n^2 & n & 1 \\ (n+1)^2 & (n+1) & 1 \end{bmatrix} \begin{bmatrix} a \\ b \\ c \end{bmatrix} = \begin{bmatrix} y_{n-1} \\ y_n \\ y_{n+1} \end{bmatrix} \tag{3.23}$$

Solving the equation, we have

$$a = -\frac{2y_n - y_{n-1} - y_{n+1}}{2}$$

$$b = -\frac{-4y_n n + y_{n-1}(2n-1) + y_{n+1}(2n-1)}{2}$$

$$c = -\frac{2y_n(n^2-1) - y_{n-1} n(n+1) - y_{n+1} n(n-1)}{2} \tag{3.24}$$

with the maximum at

$$x_o = -\frac{b}{2a} = -\frac{-4y_n n + y_{n-1}(2n+1) + y_{n+1}(2n-1)}{2(2y_n - y_{n-1} - y_{n+1})} \tag{3.25}$$

3.1.4 Measurement procedures

We have discussed the systems employed for measuring the time for an acoustic pulse to travel through the sample, and the calculation of the velocity from the time of flight. The velocity data can be used to calculate the nonlinearity parameter B/A as discussed in Section 3.1.1. A typical experimental procedure using the measurement system is presented in this section.

The degassed sample was loaded into the velocimeter. Great care was taken to avoid introducing air bubbles into the sample chamber. The 25 ml velocimeter has to be tilted gently back and forth a number of times to eliminate the trapped air bubbles. Air bubbles were usually visible and could be eliminated easily for the 4 ml velocimeter since it has a wider opening. The velocimeter was then sealed with a Latex rubber membrane. The sealed velocimeter was rinsed with water and alcohol to wash away any excess sample material. A gentle vacuum was applied to the pressure vessel to remove the bubbles. The pressure vessel was then closed and submerged in the water bath. In order to monitor the extent to which temperature equilibrium was being reached, a program that measured the time delay every minute and displayed it continuously was used, since the velocity and, consequently, the time delay, were functions of temperature. The change in time delay would reach a plateau when temperature equilibrium was achieved, and data acquisition could then commence.

At the beginning of the measurement procedure, the pressure vessel was first pressurized to about 900 psi for the 25 ml velocimeter, and to about 1500 psi for the 4 ml unit, and maintained at that pressure until the heat, built up inside the vessel during the pressurization, dissipated. A program that measured the velocity was then triggered manually, and the pressure vessel was allowed to be depressurized. The velocity change was monitored before and after the depressurization, as shown in Fig. 3.3, and the B/A value was calculated.

The depressurization process took about one second; the heat exchange during this period of time is estimated. Assuming that the cylindrical sample holder inside the velocimeter has a volume V, a surface area S, containing water, and that the difference between the

radius of the cylinder and the radius of the transducer is Δx, the rate of heat flow through the surface area is given [Powell, 1963] as

$$\frac{dQ}{dt} = -\lambda\left(\frac{\Delta T}{\Delta x}\right)S \tag{3.26}$$

where λ is the thermal conductivity for water and T is temperature. The total heat loss by cooling the volume of water ΔT degree is given [Tipler, 1982; Furukawa and Douglas, 1963] as

$$Q = -\rho V C \Delta T \tag{3.27}$$

where ρ is the water density and C is the heat capacity of water. Thus, the ratio of the heat flow in the period of Δt to the total heat loss can be approximated by

$$\left|\frac{\Delta Q}{Q}\right| = \frac{\lambda\left(\frac{\Delta T}{\Delta x}\right)S\,\Delta t}{\rho V C \Delta T}$$

$$= \frac{\lambda S \Delta t}{\rho V C \Delta x} \tag{3.28}$$

Substituting the following parameters:

$V = 4\ cm^3$
$S = 12.5\ cm^2$
$\Delta x = 0.25\ cm$
$\lambda = 6.32 \times 10^{-3}\ W/cm\ ^oC$
$\rho = 1.0\ gm/cm^3$
$C = 4.18\ J/gm\ ^oC$
$\Delta t = 1\ sec$

$|\Delta Q/Q|$ is determined to be 2%, or about 2% of heat is exchanged between the sample and the environment in the depressurization process, a reasonably good approximation for an isentropic process.

3.2 Finite Amplitude Method

As discussed in Chapter 2, harmonic components are generated as finite amplitude acoustic waves propagate in media. The second harmonic component depends, among other factors, on the nonlinearity of the medium. The generation of harmonic components can be used to measure the nonlinearity parameter B/A. For a medium with a linear frequency dependence of absorption, the relationship can be written as [Law, 1984]

$$p_2(x) = \frac{\pi f(2+B/A)}{2\rho_o c_o^3} p_1^2(0)\, e^{-(\alpha_1 + \alpha_2/2)x}\, DIFF(x) \tag{3.29}$$

where x is the distance between the receiving transducer and the transmitting transducer, $p_1(0)$ is the acoustic pressure output of the transmitter at the fundamental frequency, f, $p_2(x)$ is the amplitude of the second harmonic acoustic pressure averaged over the surface of the receive transducer, DIFF(x) is the diffraction correction that is a function of the geometry of the medium as was discussed in Chapter 2, ρ_o is the equilibrium density of the medium, and c_o is the infinitesimal wave speed. α_1 and α_2 are the absorption coefficients of the medium at the fundamental and second harmonic frequencies, respectively.

During the course of this project, two measurement systems were employed for the finite amplitude method. The first system was modified from a previous version [Law, 1984; Dunn et al., 1981], which used a spectrum analyzer to measure the second harmonic pressure. The second system, instead of using a spectrum analyzer, employed a digital oscilloscope to digitize the waveforms and then compute the spectrum with a personal computer. Section 3.2.1 serves as a brief description of the apparatus of the first system and the procedure for determining the nonlinearity parameter. More detailed information is to be found in Law's dissertation [Law, 1984]. The second system is described in detail in Section 3.2.2.

3.2.1 Measurement system I

Figure 3.16 is a block diagram of the measurement system. A Wavetek model 3006 signal generator generated a continuous wave of 3 MHz to a pulser which converted the CW signal to gated sinusoidal pulses. The pulser, constructed in the laboratory, had the capability of adjusting the pulse width and the duty cycle. The sinusoid burst pulse was then amplified, filtered, and used to drive the transmitting transducer. The acoustic pulse, after traveling through the sample, was detected by the receiving transducer. The received signal was first passed through a 6 MHz high-pass filter and then to the HP Model 8557A spectrum analyzer. The high-pass filter was necessary to reduce the fundamental component to a level within the linear range of the analyzer, so that harmonics were not generated in the spectrum analyzer itself. The same spectrum analyzer was used to measure the driving voltage on the transmitting transducer. The pulse had an on time of 10 μsec and an off time of 1 msec.

Transducers

Both transmitting and receiving transducers were 1/2 in. in diameter, medium damped, immersion transducers obtained from K-B Aerotech. They were custom-made to resonate at 3 MHz and 5 MHz, respectively. Since the receiver had a 30% -3 dB bandwidth, the sensitivity was sufficient for measuring both 3 MHz and 6 MHz frequency components.

For calibration purposes, a 6 MHz transducer, with the same construction and from the same manufacturer, had been used as a 6 MHz acoustic source. Its use in calibration is described in the transducer calibration section.

A special transducer assembly was developed for the *in vivo* measurements [Zhang and Dunn, 1987; Ohtsuki et al, 1986]. As shown in Fig. 3.17, two transducers were mounted coaxially on a caliper which provided digital readout of the distance between the transducers. A stabilizing rod was used to prevent lateral displacement of one transducer relative to the other. Twelve screws positioned and aligned the two transducers for the maximum signal amplitude output.

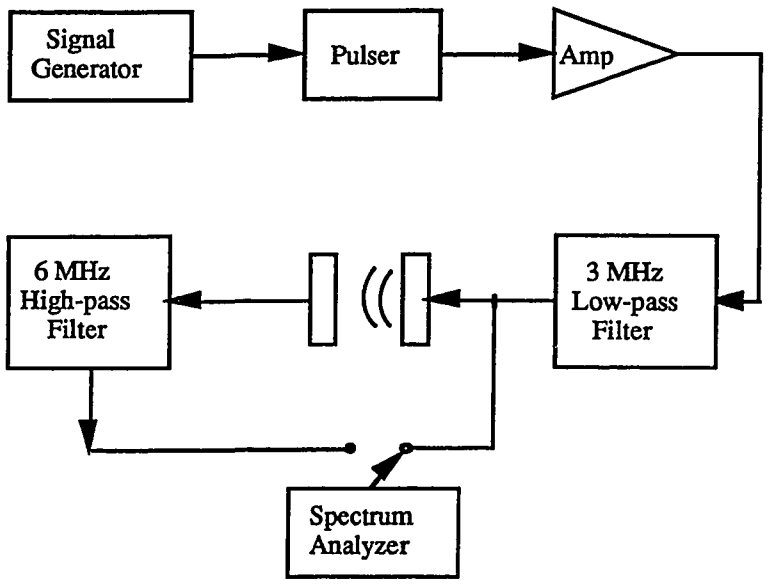

Figure 3.16 The block diagram of measurement system I of the finite amplitude method.

A special sample holder flexible in both the lateral and axial direction, illustrated in Fig. 3.18, was employed to hold the small amount of liquid sample and to aid in transducer alignment. Two sides of the sample holder were made of plexiglass, each having an opening the size of the transducers. The openings were lined with rubber O-rings and fit tightly onto the transducers. The remaining three sides were made of latex rubber membrane so that the transducers can move freely without interference from the sample holder.

Transducer Calibrations

Transducer calibration consisted of the following three procedures:

(1) determination of the effective acoustic aperture of the transducers,
(2) determination of the total pressure output and, consequently, the sensitivities for both the 3 MHz and 6 MHz transducers, and
(3) determination of the sensitivity of the 5 MHz transducer at both 3 MHz and 6 MHz.

The effective aperture of a transducer is usually slightly smaller than its geometric radius because of the edge effects of the piezoelectric disc. Here, effective radius refers to the radius of an ideal piston source which would produce a sound field distribution equal to that of the real transducer. An acceptable method for determining the effective radius [Khimumin, 1978] is to compare the respective theoretical and experimental values of the positions of the axial near the field extrema. The radius of the ideal piston giving an axial field distribution that best matches the positions of experimentally observed extrema is taken to be the effective radius of the transducer.

A miniature hydrophone (Model NP-1000, NTR Systems, Inc.) having a 0.5 mm diameter acoustically sensitive area was used to measure the axial extrema. The hydrophone was first moved into the far field to locate the acoustic axis of the transducer and then moved along the axis toward the transducer to locate the positions of the

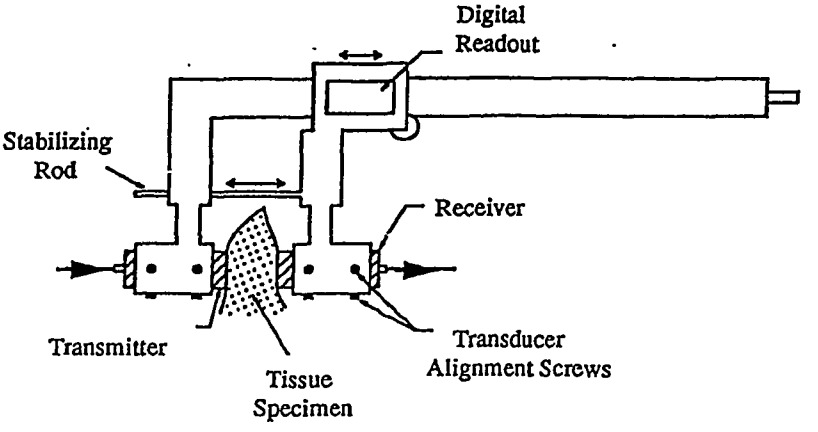

Figure 3.17 Transducer-caliper assembly employed in the *in vivo* B/A determination in liver.

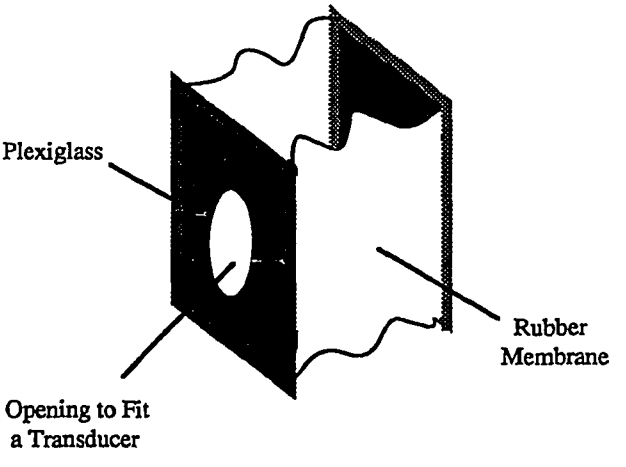

Figure 3.18 The sample holder designed for the transducer-caliper assembly for alignment adjusting and for small volume sample determination.

extrema. The measured location of extrema was then compared with the theoretical value [Kinsler et al, 1982],

$$x_m = \frac{a^2}{m\lambda} - \frac{m\lambda}{4} \tag{3.30}$$

where a is the transducer effective radius, x_m is the distance from the transducer to the m^{th} extremum, and λ is the wavelength in the medium. This procedure gave the effective radius for the 3 MHz transducers as 0.59 cm and that for the 6 MHz transducer as 0.63 cm. The fact that the effective radius of the 6 MHz transducer is closer to the geometrical radius could be due to its greater radius-to-wavelength ratio.

The transducer sensitivity was determined by dividing the output acoustic pressure by the driving voltage. The acoustic pressure can be estimated from radiation force measurements, using the plane-wave relationship between intensity and pressure, and the relationship between the radiation force and average acoustic intensity [Frizzell and Dunn, 1982], viz.,

$$I_{ave} = c_o \frac{F_r}{A}$$

$$I_{ave} = \frac{p_{ave}^2}{2\rho_o c_o} \tag{3.31}$$

where F_r is the radiation force, I_{ave} is the average acoustic intensity, p_{ave} is the acoustic pressure, A is the area of the effective aperture of the transducer, and ρ_o and c_o are the ambient density and speed of sound, respectively.

The radiation force was determined using a Mettler Model H15 balance with a sound absorbing target onto which the acoustic beam was projected. The target was made of sound absorbing rubber and shaped in a 45° cone. The radiation force target was suspended with a single steel wire, 0.01 in. in diameter, from the balance, and the acoustic beam was incident from below, onto the apex of the cone. The balance had an accuracy of 0.05 mg and a resolution of 0.1 mg.

Transducer sensitivity depends upon the intrinsic impedance of the medium with which the transducer is in direct contact. Thus, the above calibration procedure was conducted using test media with intrinsic impedance values ranging from 1.36×10^5 to 1.97×10^5 $gm/cm^2 \cdot sec$.

In order to measure the acoustic attenuation at 3 MHz and the second harmonic pressure at 6 MHz, the receiver needed to be calibrated at both frequencies. The calibration was performed with the secondary standards at two frequencies using the procedures described above. The receiver was placed about 2 cm from a calibrated source transducer. The driving voltage to the source transducer and responding voltage from the receiving transducer were monitored simultaneously, and the sensitivity was calculated by dividing the responding voltage from the receiver by the acoustic pressure corresponding to the driving voltage to the source transducer.

Measurement Procedure

As discussed at the beginning of this section, the second harmonic pressure $p_2(x)$ is proportional to the quantity (B/A+2) and to several other factors. Thus B/A can be determined only after these factors are evaluated. Two of these factors are the absorption coefficients of the sample at 3 MHz, the fundamental frequency, and at 6 MHz, the second harmonic. These absorption coefficients, α_1 and α_2, are approximated by the attenuations at the same frequencies by using

$$\alpha_i = -\frac{1}{x} \ln \frac{p_i(x)}{p_i(0)\, DIFF_i(x)} \qquad (i = 1, 2) \tag{3.32}$$

where x was the distance between transducers, p(0) and p(x) were the output pressure of the transmitter and the acoustic pressure at the position x from the transmitter, respectively, DIFF(x) was the diffraction correction factor, and the index i refers to the 3 MHz and 6 MHz frequencies. The speed of the sound, c_o, was determined by dividing the separation distance x by the time of flight measured by a Tektronix 2445 oscilloscope. In measuring the time of flight, the transmitting

signal was fed into one channel of the oscilloscope and the received signal into the other channel. The oscilloscope was operated in the delay mode and, by aligning the leading edges of the two signals, the delay time could be obtained directly from the screen digital readout. The time delay was calibrated against degassed, distilled water, for which the speed of sound is known, to determine the inherent delay of the system. The transducer separation distance x was measured by the digital caliper built into the transducer-caliper assembly. The uncertainty for the absolute measurement of the B/A value was estimated to be 8% [Law et al., 1985]. For the purpose of increasing the accuracy, the above measurement procedure was used in a relative fashion, as discussed in Section 4.1.1. of Chapter 4.

3.2.2 Measurement system II

A disadvantage of the measurement system described above is the relatively long data acquisition time (about 10 to 15 minutes) which prevents large numbers of data averaging and, in some cases, measurement of B/A changes in small time scale (see Section 4.1.3. of Chapter 4). A computerized system was designed to acquire the data automatically and to improve the B/A data acquisition rate, which is discussed in this section.

As shown in the block diagram in Fig. 3.19, the system consists of a pulse generator, a digital oscilloscope, an RF amplifier, the transducer-caliper assembly, and a computer. The components were described in previous sections. The Wavetek 271 pulse generator produces a sinusoidal burst of 15 cycles at 3 MHz, which, after amplification, drives the transmitter. The two channels of the Tektronix 2430A digital storage oscilloscope are used to acquire the transmitted and received pulses, which are transferred to the AT&T PC 6300 computer, via an IEEE 488 interface, as was described in Section 3.1.1.

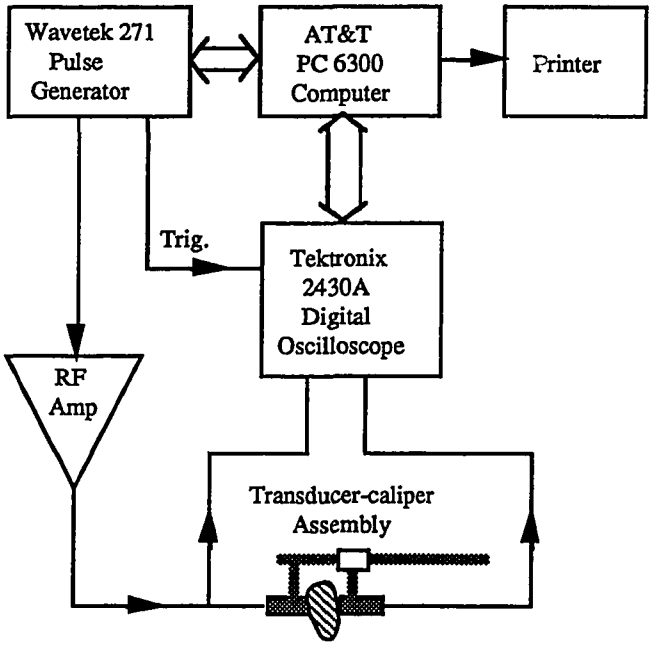

Figure 3.19 The block diagram for measurement system II of the finite amplitude method.

Spectrum Analysis Methods

After the waveforms have been digitized and stored, signal processing is employed to calculate the frequency components at 3 MHz and 6 MHz. In the method commonly used [Ludeman, 1986], the Hamming window sequence is applied to reduce the ripple in the frequency domain and then the Fourier transformation is performed to estimate the frequency components. There are more elaborate signal processing algorithms [Chen, 1988; Arun and Rao, 1988; Kung et al., 1983] for the harmonic estimation; one such method is known as the singular-value-decomposition-based approximation method [Kung et al., 1983] for the harmonic retrieval. Both methods were used. The simulation and the actual measurements showed that, for the level of signal-to-noise ratio encountered, the two methods were in a good agreement.

The Fourier transformation method is a much used spectrum analysis technique. However, there are two problems associated with direct application to the time domain signal shown in Fig. 3.13. First, the higher harmonic components calculated in the frequency domain may include contributions from waveform distortion due to the nonlinearity of the medium, which is desirable, as well as from the gating of the sinusoid wave, which is undesirable. Second, the spectrum may not have enough resolution for the peak to be detected accurately. The first problem is self-explanatory. The second difficulty is demonstrated in Fig. 3.20, which shows the direct Fourier transformation of the time-domain signal and its interpolated version. It is obvious that the peak is "cut off" due to the lack of sufficient resolution. The solutions to the above described problems were the interpolation method described in Section 3.1.3. To interpolate the spectrum, a section of the waveform, say 256 data points, was gated from the center of each pulse and applied with the Hamming window. Zero-elements were packed at the end of the resulting sequence to a total of 8 kilobytes. Thus, when the Fourier transform is calculated from such a time-domain signal (8 kilobytes), the contribution from the pulse edge is ignored and the spectrum is interpolated 8 elements between every two elements. Therefore, the peak can be determined with better resolution.

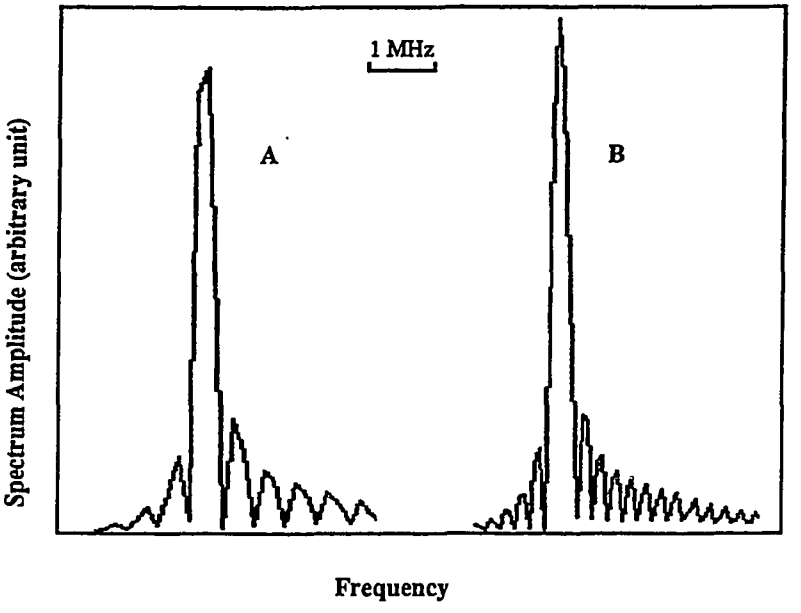

Figure 3.20 Direct Fourier transformation A and its interpolated version B. Spectrum A suffers from low resolution, and thus introduces an error in peak detection.

The basic principle of the singular value decomposition method is that, if the set of the harmonics can be seen as a base of the linear space in which a nonlinearly distorted signal is one of the vectors, then the evaluation of the harmonic components can be seen as solving a state-space equation in systems theory, which is a set of problems occurring in a wide range of applications which have been studied extensively [Chen, 1984].

To state it more concisely, suppose that x(t) is a signal which is a superposition of harmonics of frequencies, ω_o, $2\omega_o$, $3\omega_o$, ... and that only the first three frequency components, ω_o, $2\omega_o$ and $3\omega_o$, are significant, i.e.,

$$\begin{aligned} x(t) &= \sum_{k=1}^{\infty} c_k \cos(\omega_o k t + \theta_k) \\ &\cong \sum_{k=1}^{3} c_k \cos(\omega_o k t + \theta_k) \end{aligned} \tag{3.33}$$

where c_k and θ_k are constants. Then the digitized signal

$$\begin{aligned} x_n &= x(nT) \\ &= \sum_{k=1}^{3} c_k \cos(\omega_o k n T + \theta_k) \\ &= \sum_{k=1}^{3} c_k \cos(\omega_o T\, kn + \theta_k) \\ &= \sum_{k=1}^{3} \frac{1}{2} c_k [e^{j\omega_o T k n} e^{j\theta_k} + e^{-j\omega_o T k n} e^{-j\theta_k}] \\ &= \sum_{k=1}^{3} (\frac{1}{2} c_k e^{j\theta_k}) e^{j(\omega_o T n)k} + \sum_{k=1}^{3} (\frac{1}{2} c_k e^{-j\theta_k}) e^{-j(\omega_o T n)k} \end{aligned} \tag{3.34}$$

where T is the sampling interval. Substituting the following constants,

$$\alpha_1 = \frac{1}{2} c_1 e^{j\theta_1}$$

$$\alpha_2 = \frac{1}{2} c_2 e^{j\theta_2}$$

$$\alpha_3 = \frac{1}{2} c_3 e^{j\theta_3}$$

$$\alpha_4 = \frac{1}{2} c_1 e^{-j\theta_1}$$

$$\alpha_5 = \frac{1}{2} c_2 e^{-j\theta_2}$$

$$\alpha_6 = \frac{1}{2} c_3 e^{-j\theta_3} \qquad (3.35)$$

and

$$\omega_1 = 1 \cdot \omega_o T$$

$$\omega_2 = 2 \cdot \omega_o T$$

$$\omega_3 = 3 \cdot \omega_o T$$

$$\omega_4 = -1 \cdot \omega_o T$$

$$\omega_5 = -2 \cdot \omega_o T$$

$$\omega_6 = -3 \cdot \omega_o T \qquad (3.36)$$

we have

$$x_n = \sum_{k=1}^{6} \alpha_k e^{j\omega_k n} \qquad (3.37)$$

or, in state-space representation,

$$\mathbf{X} = \mathbf{A}\,\boldsymbol{\alpha} + \mathbf{n} \qquad (3.38)$$

where

$$\mathbf{X} = \begin{bmatrix} x_0 \\ x_1 \\ x_2 \\ x_3 \\ : \\ : \\ x_{N-1} \end{bmatrix} \tag{3.39}$$

$$\mathbf{A} = \begin{bmatrix} 1 & 1 & 1 & 1 & 1 & 1 \\ e^{j\omega_1} & e^{j\omega_2} & e^{j\omega_3} & e^{j\omega_4} & e^{j\omega_5} & e^{j\omega_6} \\ e^{2j\omega_1} & e^{2j\omega_2} & e^{2j\omega_3} & e^{2j\omega_4} & e^{2j\omega_5} & e^{2j\omega_6} \\ : & : & : & : & : & : \\ : & : & : & : & : & : \\ e^{(N-1)j\omega_1} & e^{(N-1)j\omega_2} & e^{(N-1)j\omega_3} & e^{(N-1)j\omega_4} & e^{(N-1)j\omega_5} & e^{(N-1)j\omega_6} \end{bmatrix} \tag{3.40}$$

and

$$\alpha = \begin{bmatrix} \alpha_1 \\ \alpha_2 \\ \alpha_3 \\ \alpha_4 \\ \alpha_5 \\ \alpha_6 \end{bmatrix} \tag{3.41}$$

and **n** is the noise vector. According to the least square approximation theory, the α that minimizes the square error, i.e.,

$$\min_{\alpha} \| \mathbf{x} - \mathbf{A}\mathbf{a} \| \tag{3.42}$$

is

$$\alpha = (\mathbf{A}^T\mathbf{A})^{-1}\mathbf{A}^T\mathbf{x} \tag{3.43}$$

where superscripts T and -1 denote the transverse and inverse operation of the matrix A.

Simulation Results

The two signal processing methods were tested and compared by simulation. The synthesized nonlinearly distorted waveforms and the experimentally acquired waveforms were used. This section reports the results of the simulation.

The nonlinearly distorted waveform was synthesized using the Fubini solution to the nonlinear wave equation [Beyer, 1974]. According to the solution, the nonlinearly distorted waveform was the superposition of harmonics, viz.,

$$\frac{p(x,t)}{p_o} = 2\sum_{n=1}^{\infty} \frac{J_n(\frac{nx}{L})}{\frac{nx}{L}} \sin(n\omega t - nkx) \tag{3.44}$$

where p(x,t) is the acoustic pressure at the distance x from the transmitting transducer, p_o is the magnitude of the the acoustic pressure at x=0, L is the discontinuity distance as discussed in Section 2.1.2., k is the wave number and J_n is the n^{th} order Bessel function. Using the parameters,

ρ_o = 1.0 gm/cm^3
c_o = 1.5 x 10^5 cm/sec
f = 3 MHz
p_o = 1 atm = 1.013 x 10^6 dyn/cm^2
B/A = 5.2

the shock parameter is calculated by Eq. (1.13) to be

$$L = 49.1 \text{ cm}$$

and, at x = 1.2 cm,

$$p(x,t)/p_o = 0.9992 \sin(\omega t - kx) + 1.222\times10^{-2} \sin(2\omega t - 2kx) + 2.240\times10^{-4} \sin(3\omega t - 3kx) + \ldots\ldots \quad (3.45)$$

With this synthesized waveform as the input to the programs implementing the spectrum analysis methods discussed above, the harmonics were recovered and compared with the expected coefficient as shown in Tables 3.2 and 3.3.

Table 3.2 Simulation Results for the Singular Value Decomposition Method

	Expected	Recovered			
SNR*		100 dB	60 dB	40 dB	20 dB
p_1**	9.9992×10^{-1}	9.9992×10^{-1}	9.9993×10^{-1}	1.0014	1.016
p_2	1.222×10^{-2}	1.222×10^{-2}	1.212×10^{-2}	1.199×10^{-2}	1.24×10^{-2}
p_3	2.240×10^{-4}	2.239×10^{-4}	2.142×10^{-4}	2.31×10^{-4}	6.26×10^{-3}

*Signal to Noise Ratio.
**p_1, p_2 and p_3 denote the fundamental, second harmonic and third harmonic amplitudes, respectively.

Table 3.3 Comparison Between the SVD and FT Methods

	Expected	SVD	FT
p_1*	9.9992×10^{-1}	9.9992×10^{-1}	9.9985×10^{-1}
p_2	1.222×10^{-2}	1.222×10^{-2}	1.2279×10^{-2}

*See footnote in Table 3.2

Table 3.2 shows that the singular value decomposition method works well for signal-to-noise ratios above 40 dB, and that significant errors are introduced when the SNR less than this level. Table 3.3 compares the singular value decomposition method (SVD) with the direct Fourier transformation method (FT), demonstrating the agreement in harmonic estimation, at least up to the second harmonic.

Table 3.4 Comparison of the Harmonics Estimated from an Acquired Waveform

	SVD	FT
p_1*	6.909×10^{-2}	6.916×10^{-2}
p_2	8.565×10^{-3}	8.553×10^{-3}

* See footnote in Table 3.2

Table 3.4 compares the two methods using an experimentally acquired waveform whose signal-to-noise ratio was estimated to be about 60 dB. It also shows good agreement between the two methods.

Due to its simplicity and the relatively large SNR of the data acquisition system, the Fourier transformation method was actually employed in measuring the harmonics for B/A determinations.

Measurement Procedure

The spectrum analysis procedures discussed above were used to measure the fundamental and second harmonic acoustic pressures. In order to improve its accuracy and circumvent the transducer calibration procedure, a comparative measurement procedure was designed which compared the acoustic pressures at the fundamental and second

harmonic frequencies with those from a standard solution of known B/A value, whose specific acoustic impedance was close to that of the sample.

Assuming that p_0, p_1 and p_2 are the transmitter output pressure, the fundamental acoustic pressure and the second harmonic pressure at some distance, x, from the transmitter, respectively, and that v_0, v_1 and v_2 are, respectively, the fundamental driving voltages of the transmitter, the fundamental and second harmonic voltage components in the received pulse, then the sensitivities of the transducers can be expressed as

$\eta_0 = p_0/v_0$, for the transmitter sensitivity at 3 MHz;
$\eta_1 = p_1/v_1$, for the receiver sensitivity at 3 MHz;
$\eta_2 = p_2/v_2$, for the receiver sensitivity at 6 MHz.

Assuming that η_0, η_1 and η_2 are independent of the acoustic impedance of the media with which the transducers come in contact, then it can be shown that (see Appendix),

$$\frac{(B/A+2)/(\rho_0 c_0^3)}{(B/A+2)^*/(\rho_0 c_0^3)^*} = \frac{v_2}{v_2^*}\left(\frac{v_1^*}{v_1}\right)^2 \frac{x^*\,\mathrm{DIFF}(x^*)}{x\,\mathrm{DIFF}(x)} \tag{3.46}$$

where the * denotes the value for the reference material. Additionally, let

$$K \equiv \frac{\rho_0 c_0^3\, v_2}{v_1^2\, x\,\mathrm{DIFF}(x)} \tag{3.47}$$

then,

$$\frac{(B/A+2)}{(B/A+2)^*} = \frac{K}{K^*} \tag{3.48}$$

By measuring the quantity K for the sample and for the reference material with known B/A value, the B/A value for the sample can be determined.

In reality, the transducer sensitivities η_0, η_1 and η_2 change slightly with the impedance of the medium; about 5% for an impedance change from 1.6 x 10^5 to 1.7 x 10^5 gm/cm^{2}sec. For the 10% NaCl solution reference with impedance 1.68 x 10^5 gm/cm^{2}sec, and the cat liver with impedance 1.64 x 10^5 gm/cm^{2}sec, the error introduced by making the above assumption is about 2%.

To test the measurement system and the procedure, a 10% NaCl solution was used as a reference, whose B/A value was determined to be 6.08 by the thermodynamic method, and a 23% BSA solution (impedance 1.67 x 10^5 gm/cm^{2}sec) was used as an unknown. The B/A of the 23% BSA solution was determined to be 6.12 by the above procedure, an error of 3% comparing with 6.31 determined by the thermodynamic method.

3.3 Experimental Procedures

3.3.1 Animal preparation

Random source cats of 6 to 9 lb. were anesthetized by injection i.p. with sodium pentobarbital (Nembutal, Abbott Laboratories) at the dose of 0.3 ml/lb body weight, for the experiment described in Section 4.1.1, and the overdose in Section 4.1.2. Male Sprague-Dawley SD rats were obtained from Harlan Sprague Dawley Inc., Indianapolis, Indiana, and were used when they are about 500 mg. They were anesthetized by Metofane inhalation anesthetic (Pitman-Moore, Inc., NJ). The anesthesia was confirmed by a lack of the pedal response, the reflex response from an animal when its foot was pinched. The abdomen was then incised, and liver was exteriorized or isolated for B/A measurements. After the measurements, cats were sacrificed by injecting T-61 euthanasia solution (Manufactured by Taylor Pharmacal Co., Decatur, IL, distributed by American Hoechst Corp. Somerville, NJ) i.v. at the dose of 0.14ml/lb body weight. The liver specimens obtained from the rats weighed about 15 grams. The left lobes weighed about 6 grams, the volume was about

6 ml, and the thickness ranged from 0.6 to 0.9 cm, sufficient for adequate transducer separation.

3.3.2 Tissue perfusion procedure

In vitro perfusion of the liver, first in the absence of calcium and then in the presence of collagenase, was first used by biochemists to obtain large yields of hepatocytes [Seglen, 1973, 1976]. This procedure was adapted in this study to provide a gentle method for the gradual dissociation of the intercellular adhesive interactions among hepatocytes. The procedure is briefly described in this section.

It is well documented, in a variety of species [Obrink et al., 1977; Seglen, 1973, 1976; Kawaguchi et al., 1981; Kuhlenschmidt et al., 1982], that upon loss of tissue calcium, hepatocytes lose intercellular adhesive contacts, begin to "round-up" or change from a cuboidal to a more spherical morphology, and remain attached to each other only by the tight junctions and gap junctions [Drochmans et al., 1975]. Following subsequent perfusion with collagenase, the cell contacts are digested, the cells become separated from each other and single hepatocyte suspensions can be isolated with only gentle mechanical agitation of the liver following removal of Glisson's capsule [Seglen, 1973, 1976]. Morphologically, at the electron microscope level, the unperfused liver tissue shows intact intercellular adhesion; the membranes from two hepatocytes remain in intimate contact and parallel to each other, as shown in Fig. 3.21 [Tanikawa, 1979]. The liver tissue perfused with Ca^{++}-free buffer is seen to contain spherically-shaped cells and partially dissociated cell-cell contacts which include gap and tight junctions, as shown in Fig. 3.22 (after Drochmans et al. [1975]). At the end of the perfusion procedure with collagenase buffer, only cell cords remain, as shown in Fig. 3.23. Further complete dissociation of these cell cords can be achieved by gentle mechanical treatments, such as massage or rolling the cell suspension in a round-bottom flask.

The perfusion arrangement is shown in Fig. 3.24. The pump (Masterflex, catalog number 7553-10, Cole-Parmer) delivered perfusates, at the rate of 76 ml/min for cats and 56 ml/min for rats, into the liver via a bubble trap, which prevents air bubbles from being

Figure 3.21 Intact hepatocyte intercellular adhesion. It shows parts of the two hepatocytes (one in lower right and the other in the upper left). The bile canaliculus is labeled BC. x 26,000 (Tanikawa, 1979)

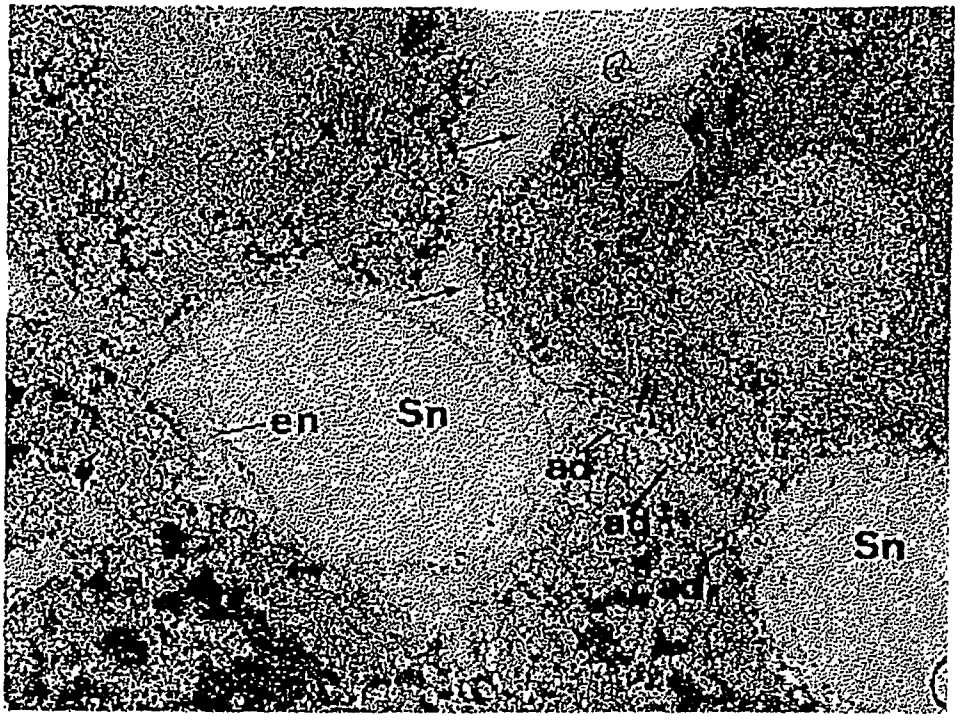

Figure 3.22 Electron micrograph showing the morphological change in the intercellular adhesion of two hepatocytes after Ca^{++}-free buffer perfusion. The segments of cell surfaces which normally remain in close contact are dismantled here (arrows) and lie in continuity with the lumen of the sinusoid. x 4,000 (Drochmans et al., 1975)

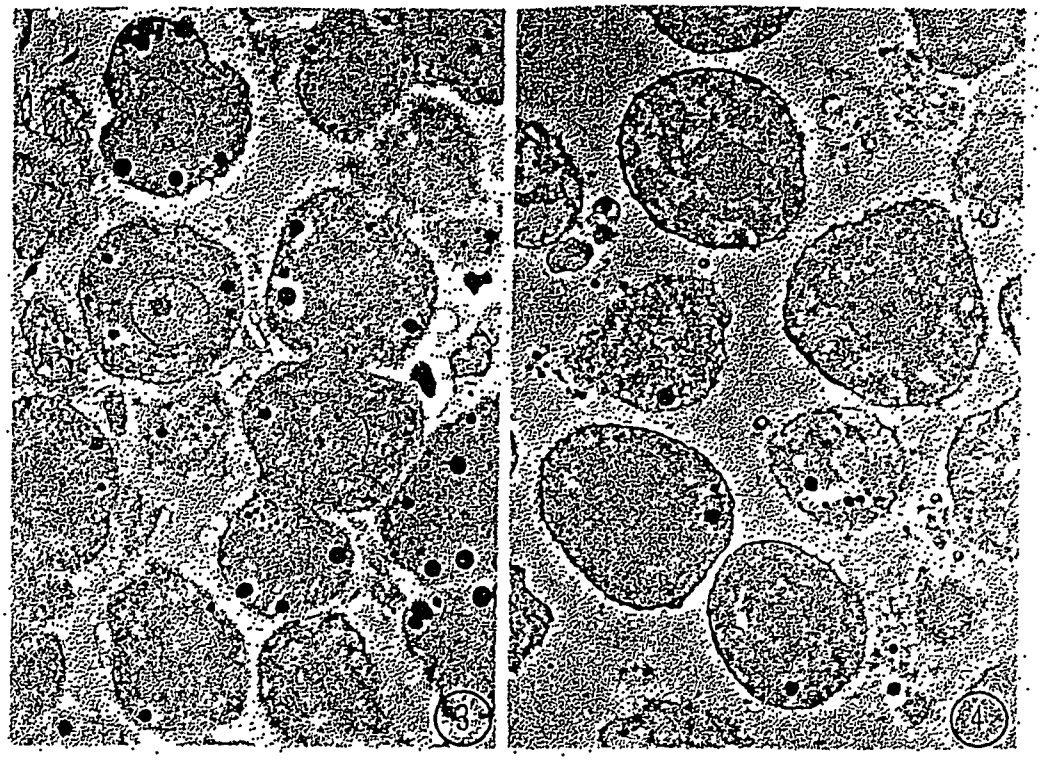

Figure 3.23 Phase-contrast micrographs showing the presence of cell cords at the end of the perfusion with collagenase buffer, on the left, and the free hepatocytes after gentle mechanical agitation, on the right. x 1,200 (Drochmans et al., 1975)

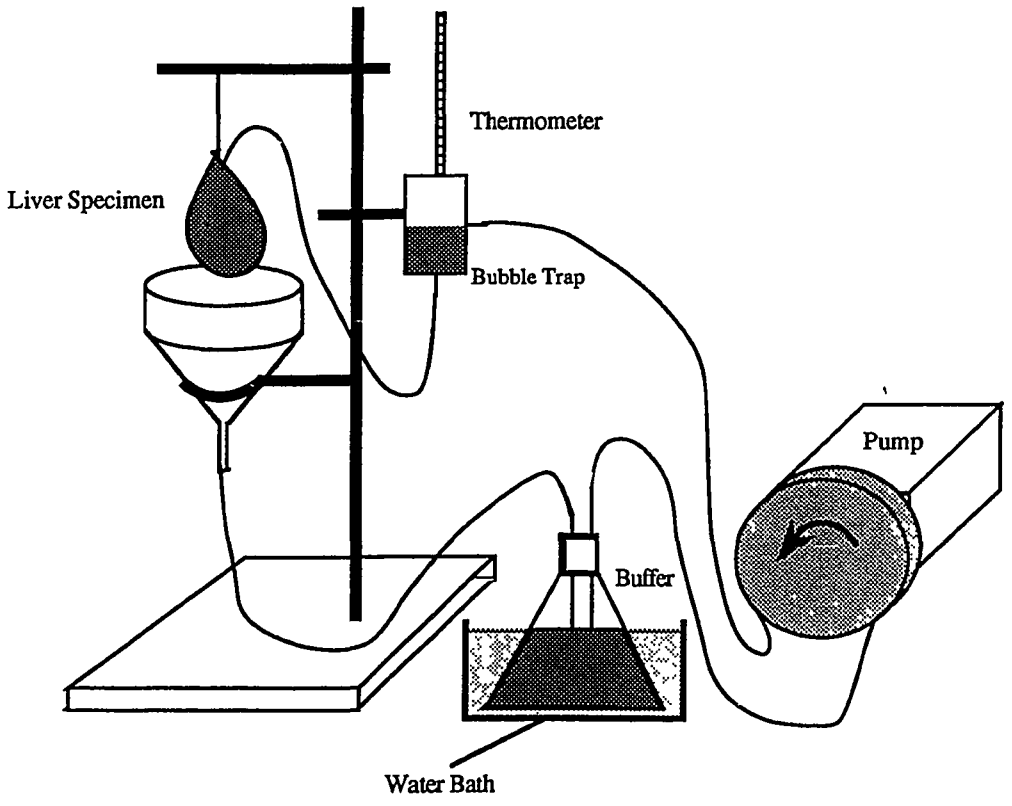

Figure 3.24 Schematic diagram of liver perfusion apparatus.

pumped into the liver. The perfusate was then returned to the reservoir and recirculated. A graduated cylinder serves as a convenient reservoir for monitoring the amount of perfusate intake into the liver.

Cats of 6 to 9 lb. were anesthetized at the overdose of 3.5 ml, and rats of about 500 mg by inhalation anesthetic, as described in Section 3.31. After the abdomen was opened and the left lobe was excised, a branch of the portal vein was cannulated. The cannula was ligated in place and the liver was suspended on a supporting stand as shown in Fig. 3.24. The perfusate was circulated through the portal vein recovered by a funnel which returned the perfusate back to the reservoir.

Three kinds of perfusates were used, viz., the physiological buffer, the Ca^{++}-free buffer, and the collagenase buffer. The physiological buffer was prepared using powdered cell culture medium (Eagle Medium-GIBCO Laboratories) containing 2 mM $CaCl_2$, pH 7.5. The Ca^{++}-free and the collagenase buffers were prepared using the following recipes:

Ca^{++}-free buffer:

8.3	g/l	NaCl
0.5	g/l	KCl
2.4	g/l	HEPES
4	mM	EDTA
pH	7.4.	

Collagenase buffer:

3.9	g/l	NaCl
0.5	g/l	KCl
0.7	g/l	$CaCl_2 \cdot H_2O$
24.0	g/l	HEPES
15.0	g/l	BSA (Cohn Fraction V, Sigma)
pH	7.6	

The Ca^{++}-free buffer was stored at refrigeration temperature (about 4°C to 5°C) and the collagenase buffer was stored frozen until used. Collagenase (Type IV, Sigma) was added to the collagenase buffer, at the

concentration of 40mg/50ml, at the time of use to prevent loss of activity during storage.

The perfusion procedure began with the physiological buffer, which was allowed to pass through the liver directly to waste, thereby flushing all blood from the organ, before switching over to recirculation. The perfusion of the physiological buffer was not expected to alter the structure of the liver tissue and thus provided a control state. After a period of time (usually 20 minutes to 60 minutes), perfusion with Ca^{++}-free buffer was initiated. Caution was exercised not to introduce air bubbles into the liver during the switch-over from one buffer to another. The perfusion of the Ca^{++}-free buffer lasted about 60 to 90 minutes before the perfusion with the collagenase buffer was initiated. The appearance of the liver during the perfusion was considered a good indicator of the extent to which structural alteration was taking place. At the end of the perfusion with the physiological buffer, the liver appeared dark brown and firm. By the time the perfusion with the Ca^{++}-free buffer was completed, the liver appeared pale, being a "washed-out" brown color. Towards the end of the perfusion with the collagenase buffer, the tissue displayed visible areas of tissue dissociation, and lobule definition was more clearly demonstrated beneath Glisson's capsule. The liver was friable and easily damaged when gently probed with a hemostat.

Since B/A values are temperature sensitive, the perfusion procedure was carried out at room temperature to minimize the temperature fluctuation in the specimen due to the heat exchange with the environment. The lowered temperature also slows down the tissue dissociation process.

3.3.3 Sample Sonication

A high intensity ultrasonic sonicator (Model 375, Heat System, NJ) was used to destroy hepatocyte cellular structures in examining their effects on the B/A (see Section 4.2.1). The sonicator was operated at 50% total output power and 80% duty cycle for one minute. Examinations of the hepatocyte samples under a light microscope (Nikon AFX-II, magnification 100), before and after the sonication, confirmed

destruction of the cellular structure. The presonicated sample appeared to have intact hepatocytes freely floating in the sample, occasionally with a few other cells attached, whereas the post-sonicated sample exhibited no intact cells and only small fragments of cell membranes.

3.3.4 Sample degassing

Small air bubbles within a sample were found to increase the B/A value significantly [Everbach, 1989]. Therefore, before each experiment, a liquid sample was degassed in a rotary evaporator capable of creating and sustaining a vacuum of about 760 mmHg. Depending upon the surface tension of the liquid, the degassing time varied from a half hour to two hours. Usually a large quantity of bubbles emerged from inside the liquid at the beginning of the degassing process. As the process continued, the number of bubbles decreased. Highly viscous samples with a large number of air bubbles present, such as sonicated hepatocyte suspensions in which the sonication process produces a large quantity of bubbles, required several cycles of on-off vacuum to remove the large air bubbles first, before it was subjected to prolonged degassing. An empirically derived criterion for determining the completeness of the degassing procedure was 1/2 hour after no further visible bubbles appeared in the liquid.

3.3.5 Hepatocyte suspension preparation

A hepatocyte suspension was obtained by gently messaging, in a small plastic bag, the liver perfused with the procedure described in Section 3.3.2. The suspension was first concentrated by sedimentation at unit gravity for 10 to 15 minutes to allow preferential settling of hepatocytes. The supernatant was removed by pipetting, and the concentrated hepatocyte suspension was then degassed as described in Section 3.3.4 for one and a half hours. Examinations under a light microscope (Nikon AFX-II, magnification 100) show intact cellular structure. The suspension was carefully transferred to the velocimeter using a transfer pipette, so that no air bubbles were introduced. The B/A determination followed. At the end of the measurement, the

hepatocyte suspension was transferred back to a test tube and added to the unused portion of the sample to compensate for the loss in sample handling. The suspension was then subjected to the sonication procedure described in Section 3.3.3 and another degassing procedure, before its B/A was determined again.

Weight to weight percentage concentration was determined by placing a preweighed sample in an oven at 120°C for 20 hours, after which the dehydrated sample was weighed again. The difference in weight is the amount of water evaporated.

The procedure used to concentrate the hepatocyte suspension was essential. Without it, when a diluted sample was placed inside the velocimeter chamber, the settling process moved some hepatocytes out of the acoustic field, as the sample chamber was oriented horizontally and the diameters of the transducers are smaller than that of the chamber. Therefore, the B/A value so determined would have been less than it should have been without settling.

3.3.6 Liposome suspension preparation

Liposomes, small lipid vesicles of diameters between 0.02 to 10 μm, consist of single or multiple bilayers of phospholipid molecules. They were employed as cell models for investigation of influences of the cellular structure on the B/A (Section 4.2.2). All the liposomes studied were prepared from a 4:1 (w/w) ratio of dipalmitoyl phosphatidyl choline (DPPC) and dipalmitoyl phosphatidyl glycerol (DPPG) phospholipid (Dehydrated, from Avanti Polar-Lipids, Inc., Birmingham, AL). The liposomes were suspended in HEPES buffered saline (10 mM HEPES, 139 mM NaCl, 6 mM KCl, pH.7.4). Large unilamellar vesicle (LUV) suspensions were prepared by the reverse phase evaporation method based on the work of Szoka and Papahadjopoulos [1978]. Multilamellar vesicle (MLV) suspensions were prepared by rehydrating the dried lipids in the HEPES buffer solution, vortically mixing the sample at that temperature for one to two minutes and cooling down to 25°C until use. Small unilamellar vesicle (SUV) suspensions were made by sonicating the MLV suspensions in a bath-type sonicator (Model G112P1T, Laboratory Supplies co., Inc., Hicksville, NY) at 45°C until the

suspensions became transparent. The suspension was sealed in nitrogen gas, to prevent lipids from oxidizing in the process of mixing and sonication. The SUVs so prepared had diameters between 20 and 50 nm, while the LUVs between 70 to 400 nm. The MLVs which, rather than being single bilayers, consisted of concentric spheres of bilayers. They exhibited broad size distribution in the range of 0.1 to 10 μm. The LUV liposomes are known to have a transition temperature at 42.5°C [Magin and Weinstein, 1984].

3.3.7 Protein denaturing sample preparation

Bovine serum albumin (BSA) was employed to investigate the effect of the secondary structure of the protein on its B/A (Section 4.3.1). The alteration of the secondary structure was produced by the denaturing agent sodium dodecyl sulfate (SDS) [Weber and Osborn, 1969]. SDS solutions with concentration ranging from 0% to 3.0% were prepared using 0.1 M phosphate buffer solution, and adjusted to pH 7.0. BSA (Sigma, St. Louis, MO) of 0.1g/100ml was then added to each sample. For control blanks, SDS solutions with the same concentrations as those above were prepared using the same procedure but without BSA. All the samples were degassed for 1.5 hours before being loaded into the velocimeter for B/A measurement.

Ribonuclease A (Sigma, St. Louis, MO) samples were also prepared for heat denaturation experiments (Section 4.3.1). The protein was dissolved in water, buffered by 1 M glycine and adjusted to pH 2.77 by HCl. Denaturation under these conditions was confirmed by measurement of the optical extinction coefficient at 287 nm by spectrophotometry (Beckman Model DU-50). The result is shown in Fig. 3.25 for protein concentrations of 0.04%, 0.1% and 0.2% and shows that the protein denatures at about 42°C and that the denaturation, as observed by the optical extinction coefficient, is independent of the protein concentration. The B/A was measured at the higher protein concentration of 3.9% in order to have available a greater signal level. The sample was degassed for 1.5 hours before the measurement.

3.3.8 Protease digestion sample preparation

BSA solutions in the presence of protease were prepared for the investigation of the influence of protein primary structure on the B/A (Section 4.32). The protease solution was made by dissolving 4.8 mg of protease in 0.5 ml of water, and the BSA solution by dissolving 100 mg of BSA in 20 ml of phosphate buffer solution (8.00g/L NaCl, 0.20g/L KCl, 0.20g/L KH_2PO_4, 0.15g/L Na_2HPO_4 and pH 7.35). The BSA solution was adjusted to pH 7.62 and degassed. The protease solution was not degassed due to its small amount. At the time of B/A measurement, the 0.5 ml of protease solution was the first transferred into the 4 ml velocimeter, which was then filled with the BSA solution. Finally, the sample chamber was sealed and the sample was mixed by revolving the velocimeter by hand. The final concentration of BSA was determined to be 43.1 mg/ml, and that for proteases was 1.33 mg/ml. The mixture under these conditions was known to undergo protein digestion [Spiro, 1965]. For control blanks, a BSA solution of 50 mg/ml and a glycine solution of 50 mg/ml were prepared in a phosphate buffer solution by the same procedure as above, without protease.

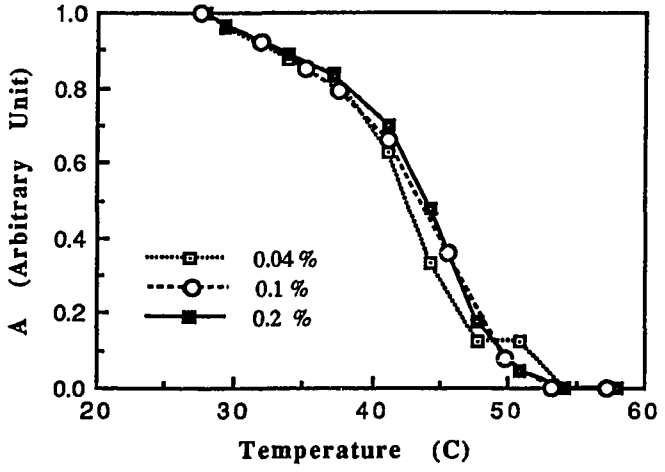

Figure 3.25 Normalized extinction coefficient at the optical wavelength of 287 nm during the heat denaturation of ribonuclease A.

CHAPTER 4

RESULTS AND DISCUSSIONS

As discussed in Section 1.3, the acoustic nonlinearity parameter B/A was found to be dependent on the chemical composition of a medium. It was hypothesized that, in addition to its compositional dependence, the B/A also depends on the structural factors of the medium. Presented in this chapter are results of experiments designed to investigate the structural dependence of the B/A at tissue, cellular and molecular levels of biological media. The chapter is organized into three sections: tissue, cellular and molecular levels. The evidence for such dependence of B/A is presented, and the relative contribution that each structural level contributes to the total B/A value is assessed.

4.1 Tissue Level

Two experiments were designed to assess the structural dependence of the B/A parameter at this level of tissue structure using cat and rat liver. The first experiment examined the difference in the B/A parameter in cat livers determined *in vivo* and *in vitro*. The second experiment examined the importance of intercellular adhesion on B/A. The biochemical technique used in the second experiment, to alter intercellular adhesion forces of cat and rat liver, is discussed in Section 4.1.2, prior to presenting the results in Section 4.1.3.

4.1.1. Effect of blood and blood flow

The objective of this study was to assess the influence on the B/A value due to the functioning vascular system. From the point of view of the origin of the acoustic nonlinearity, it is important to consider the contribution of this level of tissue organization on B/A. From a more practical point of view, it is considered important to know the relation of *in vitro* measurements to *in vivo* applications, since many of the B/A values reported were measured *in vitro* and yet the

major medical applications are *in vivo*. Herein, "*in vivo*" refers to that state in which the specimen is under deep anesthesia, its liver is exteriorized, and the blood flow is normal. Further, "*in vitro*" refers to that for which the animal is dead, blood circulation has been stopped and the blood has been allowed to drain out of the organ of interest.

Finite amplitude system I, described in Section 3.2.1, was used. The special transducer-caliper assembly described in Fig. 3.17 was used for transmitting and receiving the ultrasound signals which composed the *in vivo* measurement.

Random source cats of 6 to 9 lb were used and prepared according to the procedure described in Section 3.3.1. After the liver was exteriorized, the caliper assembly was positioned about the specimen to be examined. The body fluid on the liver surface served as the acoustic coupling fluid, i.e., the transducers were coupled directly to the liver surface. The velocity, attenuation, and ultrasonic second harmonic pressure amplitude were obtained without moving the transducers from their original positioning and the *in vivo* B/A value was calculated from these measurements.

The cat was sacrificed according to the procedure in Section 3.3.1. The blood in the liver was partially drained by a cut in the liver near the observation site. During all these operations, the relative position of the transducer assembly with respect to the liver specimen was maintained unchanged. Determination of the *in vitro* B/A value followed.

Table 4.1 The B/A values of cat liver

Cat #	*In vivo*	*In vitro*	Δ(B/A)
1	6.9	6.9	0
2	7.0	6.9	+0.1
3	6.5	6.4	+0.1
4	6.6	6.6	0
5	7.0	6.9	+0.1

Table 4.1 shows the results of *in vivo* and *in vitro* B/A values measured in five cats, as described above. It is seen that blood

circulation and blood content seem not to contribute to the tissue B/A within the experimental error which was estimated to be better than 8% [Law et al, 1985].

The finding also implies that the information of B/A parameter obtained from *in vitro* measurement can be utilized directly to the *in vivo* applications without introducing a significant amount of error [Zhang and Dunn, 1987].

4.1.2. Effect of intercellular adhesion

Cat and rat livers, whose intercellular adhesive forces could be altered by the removal of Ca^{++} and the perfusions of collagenase as described in Section 3.3.2, were used. Finite amplitude system II, together with the transducer-caliper assembly, as described in Section 3.2.1, was employed to monitor the relative B/A changes during the perfusion procedure. After an animal was prepared by the surgical procedure (see Section 3.3.1), the left lobe of the liver specimen was isolated and canulated. A site for observation was chosen relatively free of large blood vessels, but sufficiently thick that standing waves could not be established, and the transducers were attached for the measurement procedure. The distance between transducers was adjusted so that they pressed against the liver surface tight enough to prevent an air layer from occurring between transducers and the tissue surface, and yet loose enough not to obstruct the perfusate flow through the sinusoid spaces within the liver. The chosen observation site remained unchanged throughout the entire procedure so that the spatial variation of the B/A parameter would not influence the results.

Figure 4.1 shows typical B/A values obtained during an *in vitro* perfusion of a cat liver specimen. It is seen that during perfusion with physiological saline for 20 minutes, the B/A value does not vary significantly. However, the B/A value decreases significantly as Ca^{++} ions are removed from the liver, i.e., during perfusion with Ca^{++}-free buffer. When perfusion with the collagenase buffer begins 115 minutes after initiation of the procedure, the B/A value increases sharply and then decreases. The trend for B/A to decrease during the perfusions with the Ca^{++}-free and collagenase buffers are considered to be related

to the breakdown of intercellular adhesive contacts. The question of whether the decreases in B/A could be due to alterations in perfusate flow, turbulence or other mechanical factors was tested by considering different perfusion schedules. Figure 4.2 shows the perfusion with physiological saline extended to two hours with no significant B/A change, though the B/A value began decreasing after initiation of the perfusion with Ca^{++}-free buffer. This result demonstrates that the decrease in the B/A is not due to mechanical damage to the liver, but is a biologically relevant event, most likely due to the dissociation of cell-cell contacts.

In order to have more homogeneous conditions and better control over pathological states of those animal tissues employed in the experiment, large male Sprague-Dawley rats from Harlan Sprague Dawley Inc. were used instead of random source cats. The uses of these animals resulted in less animal to animal variations and more reproducible results.

Figures 4.3 and 4.4 show typical B/A parameter and speed of sound profiles obtained for a rat liver during the *in vitro* perfusion procedure. Although there is a trend for the B/A value to decrease, it also exhibits a significant amount of noise. The first step in processing these data was to reduce the noise by using the sliding average smoothing technique with a smooth width of 5 [Rafferty and Norling, 1986]. Figure 4.5 shows the smoothed version of these data of Fig. 4.3. No smoothing procedure was applied to the velocity data since they were relatively free of noise.

Figure 4.6 shows the results of the B/A (left column) and the speed of sound (right column) of six rat liver specimens. Although the rates of B/A decrease due to the introduction of the two buffers varied from animal to animal, the results demonstrate the consistent decrease in the B/A value as the intercellular adhesive force is destroyed. The magnitudes of the decreases in B/A are tabulated in Table 4.2. An average of 0.68 is obtained from the Δ(B/A) column, which accounts for 38% (38%=0.68/(7.0-5.2)) of the total B/A, taking the B/A for liver tissues as about 7.0 and that for water B/A as 5.2.

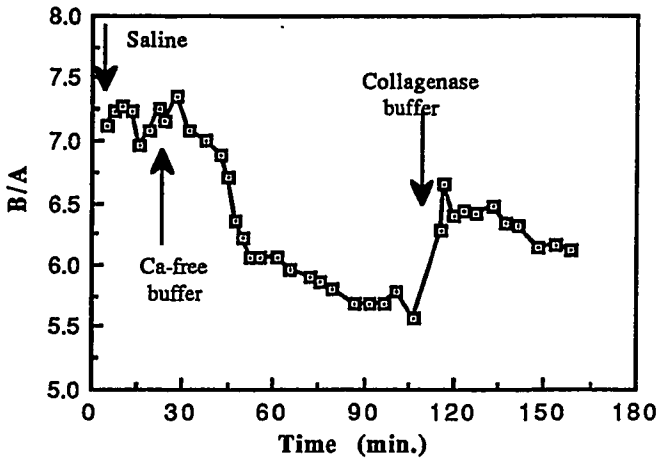

Figure 4.1 B/A values of a cat liver specimen as a function of time at the different stages of perfusion.

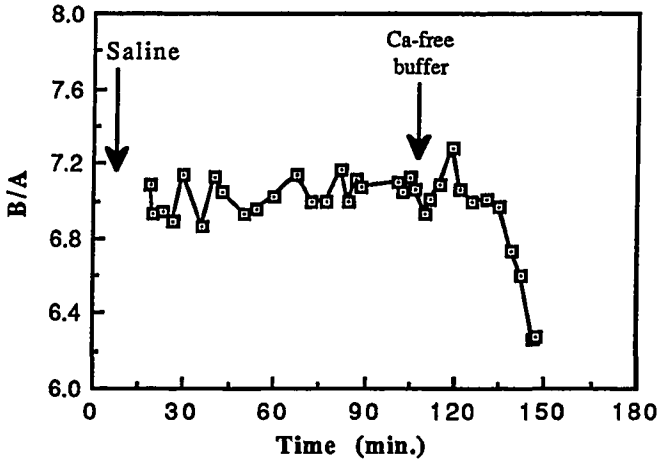

Figure 4.2 B/A vs. time for perfusion with saline.

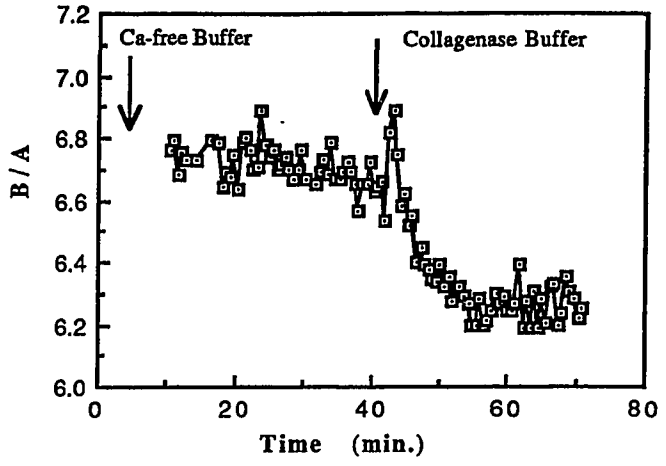

Figure 4.3 B/A data obtained in a rat liver specimen during the perfusion procedure.

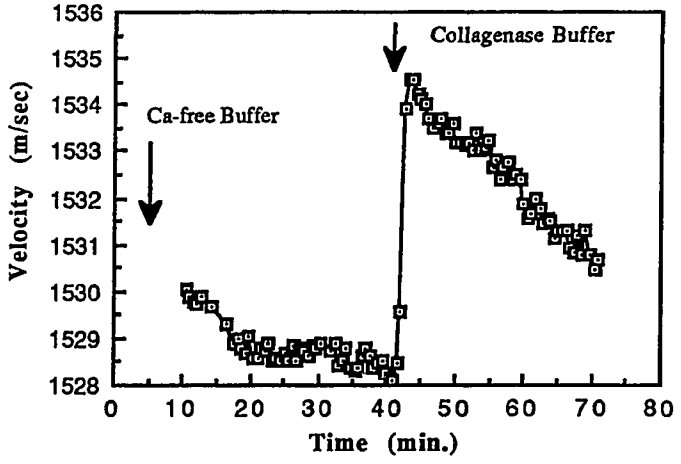

Figure 4.4 Speed of the sound measured at the same time as the B/A values of Fig. 4.3 were obtained, showing decrease of speed of sound during the perfusion process.

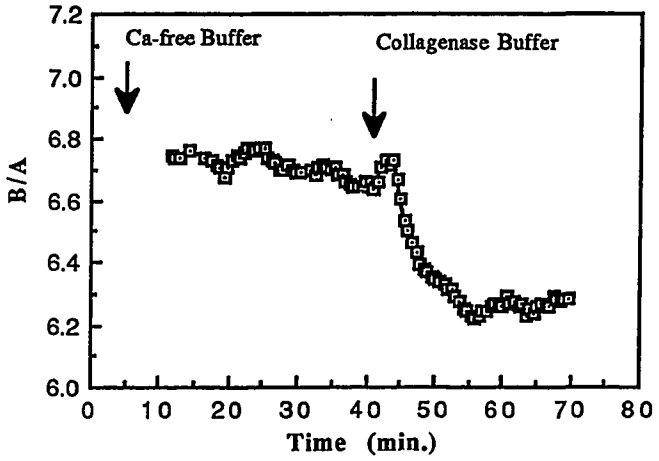

Figure 4.5 Smoothed version of Fig. 4.3 making the B/A decrease more apparent.

Table 4.2 Magnitude of B/A and Velocity Change

Rat #	-Δ(B/A)	Δc_d(m/sec)	-Δc (m/sec)
1	0.5	6	5.5
2	0.4	5	3.5
3	0.5	6	9.0
4	0.7	5	5.0
5	1.1	5	7.0
6	0.9	5	5.0

Figure 4.6 B/A and velocity data collected from 6 rat liver specimens, with the B/A profiles on the left column (labeled *a) and the velocity profiles on the right (labeled *b). The arrows indicate the onset of the perfusions.

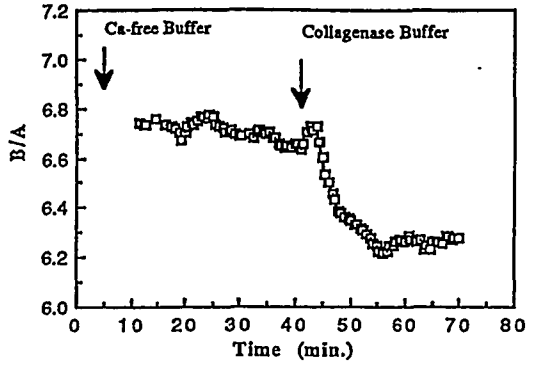

(1a)

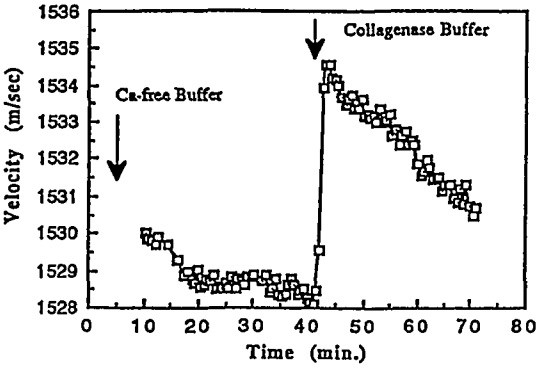

(1b)

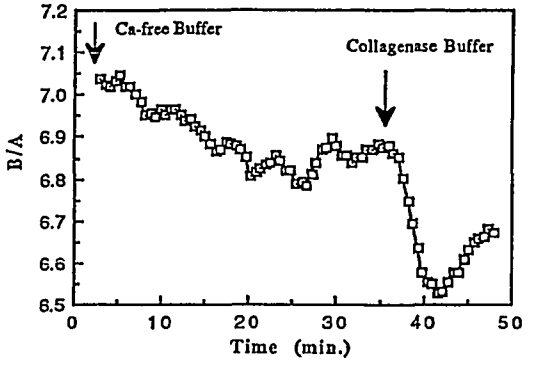

(2a)

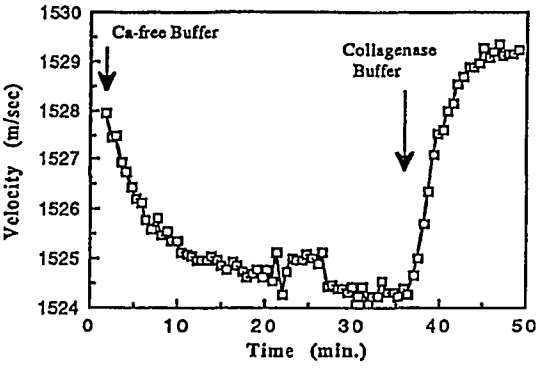

(2b)

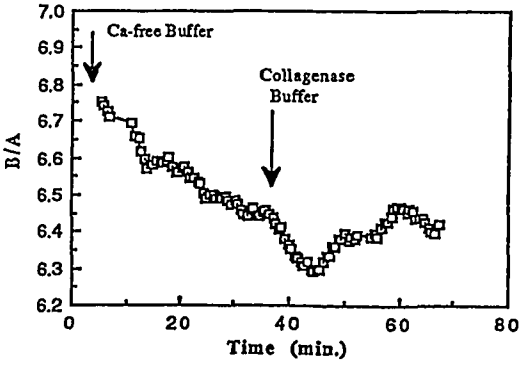

(3a)

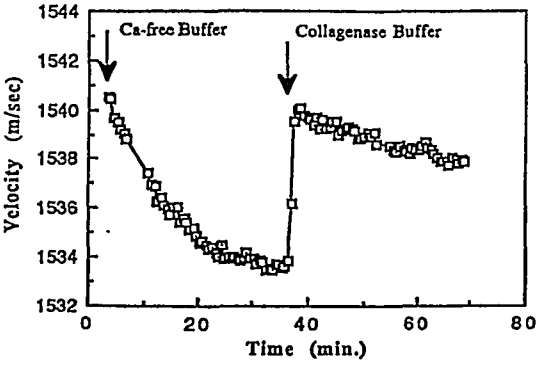

(3b)

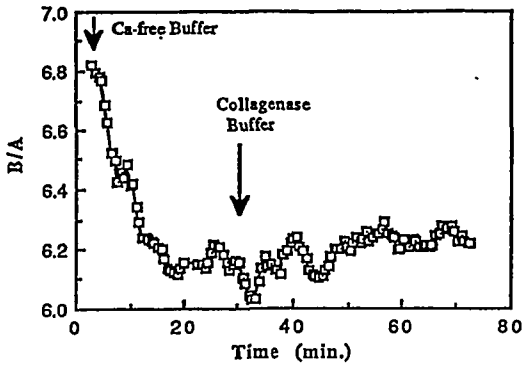

(4a)

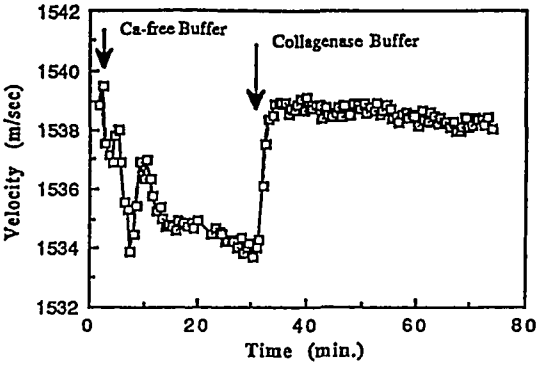

(4b)

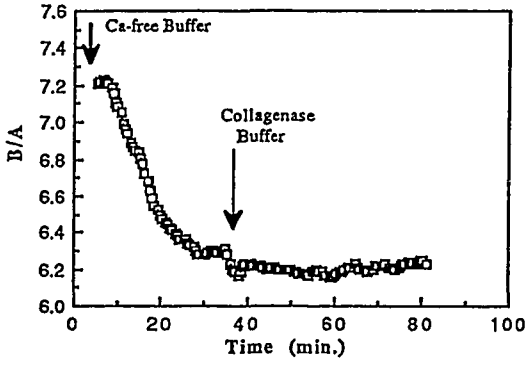

(5a)

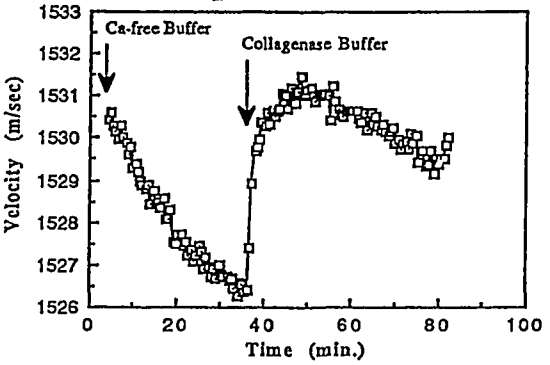

(5b)

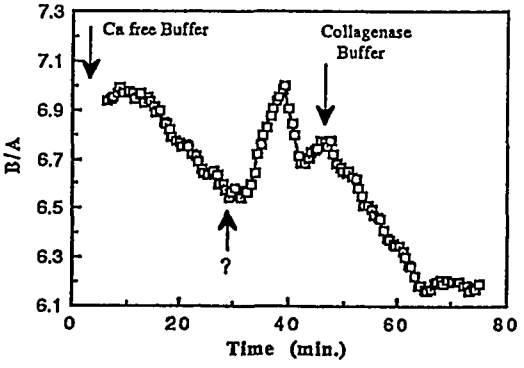

(6a)

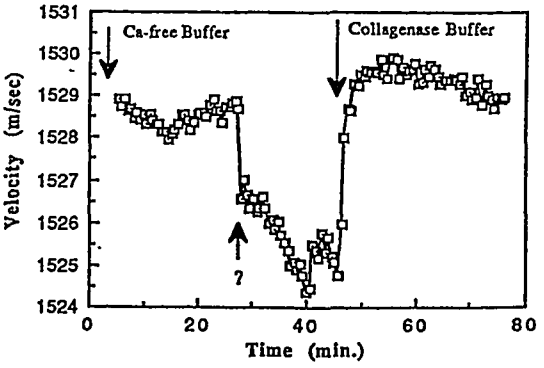

(6b)

The velocity of the rat liver decreases during perfusions with the Ca^{++}-free buffer and collagenase buffer. However, introduction of collagenase buffer causes the sharp increase in the velocity. The sharp increases are thought to be due to the proteinaceous content of the collagenase buffer, viz., 2.4% (w/w) HEPES and 1.5% (w/w) BSA which is known to be a velocity enhancement agent. The magnitude of the velocity discontinuity Δc_d caused by BSA and HEPES was estimated to be

$$\Delta c_d = 70\% \times (2.4\% + 1.5\%) \times h \simeq 8.3 \text{ (m/sec)}$$

where h is the slope of the velocity increase with the concentration of BSA, which is estimated to be 296 m/sec [Law, 1984], and 70% is the water content of the livers, which was replaced by the collagenase buffer upon its introduction. This estimate is comparable in magnitude to those in Table 4.2, supporting the above postulation that the sharp increases in velocity upon introduction of collagenase buffers are due to their HEPES and BSA content.

The cumulative velocity decreases during perfusions of both buffers, without taking into account the discontinuity, are also tabulated in Table 4.2.

The discontinuity in the velocity and the corresponding upward surge in the B/A value, marked by question marks in the vicinity of 30 minutes in Fig. 4.6, 6(a) and 6(b), were due to some unidentified sources. However, judging from the discontinuity of the velocity, they are most likely the artifacts due to some mechanical disturbance.

Without any volume constraint, a liver volume was observed to increase 1.5 ml to 2.0 ml from the initial volume of about 6 ml, due to the morphological changes taking place within the liver specimen as described in Section 3.3.2. The B/A changes measured under this circumstance reflect the structural change as well as the decrease in dry weight concentration. Constraints, such as the retaining transducers in the above experiments, partially prevented the portion of specimen volume between the transducers from enlargement. This volume increase has to be known before the net B/A decrease due to structural features can be estimated. No direct measurement was performed to assess the extent of the volume increase for the liver portion between

the two transducers, due to its technical difficulty. However, this volume change can be estimated by using an appropriate model.

Assuming that the liver swelling is homogeneous and isotropic, then a relative volume increase $\Delta V/V$ is proportional to the solid angle for the unconstrained portion of the liver tissue, i.e.,

$$\frac{\left(\frac{\Delta v}{v}\right)}{\left(\frac{\Delta V}{V}\right)} = \frac{\phi}{\Phi} \tag{4.1}$$

where $(\Delta V/V)$ and Φ are the relative volume increase for a completely unconstrained liver, which is 2ml/6ml, or 33% and 4π steradians, respectively; $(\Delta v/v)$ and ϕ are the relative volume increase for a partially constrained liver and the solid angle defined by the unconstrained portion, respectively. Considering the cylindrical volume between the two transducers with the diameter of 1.5 cm and the transducer separation of 0.6 cm, as shown in the illustration below, then v and ϕ can be calculated to be 1.06 cm^3 and 1.49π steradians, respectively, and according to Eq. (4.1), $(\Delta v/v)$ = 12%. Thus the concentration and the B/A decrease 12% because of the volume increase in the portion of the liver between the transducers. Subtracting this B/A decrease due to volume increase from the total B/A decrease of 38% estimated above, the net decrease is 26%.

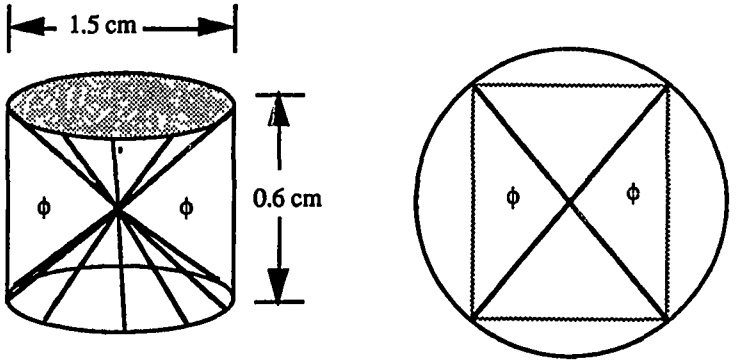

Illustration of the portion of liver between the transducers and solid angle ϕ.

4.2. Cellular Level

It was seen in the previous section that as the structure of the liver tissue was dissociated by perfusion with Ca^{++}-free and collagenase buffers, the B/A value of the liver decreased. These data suggest that the tissue level structure, viz., the cellular adhesion, contributes to the overall B/A value. At the end of the perfusion process, a collection of hepatocytes attached to each other, was obtained. With gentle massaging of the perfused tissue the cells are completely loosened from their anchorings, and a hepatocyte suspension is obtained. The question of whether hepatocyte cellular structure also contributes to the tissue B/A value, and the nature of this contribution to the total B/A value is unknown. Experiments were designed to investigate the dependence of the B/A parameter on the cellular level of structure, and these results are presented in the following sections.

4.2.1. Effect of hepatocyte cellular structure

This experiment was designed to assess the change in B/A due to hepatocyte cellular structure. Hepatocyte suspensions were prepared using the procedure described in Section 3.3.5. The B/A values were determined according to the procedure described in Section 3.1.

Figure 4.7 shows the results of B/A measurements in hepatocyte suspensions, before and after sonication as described in Section 3.3.3. The B/A values of the unsonicated samples are consistently greater than those obtained using sonicated hepatocytes, by about 0.08 to 0.15 B/A units. The major difference between the sonicated and unsonicated samples is the missing cellular structure from the sonicated hepatocytes. This result demonstrates that the B/A parameter decreases as the hepatocyte cell structure is destroyed.

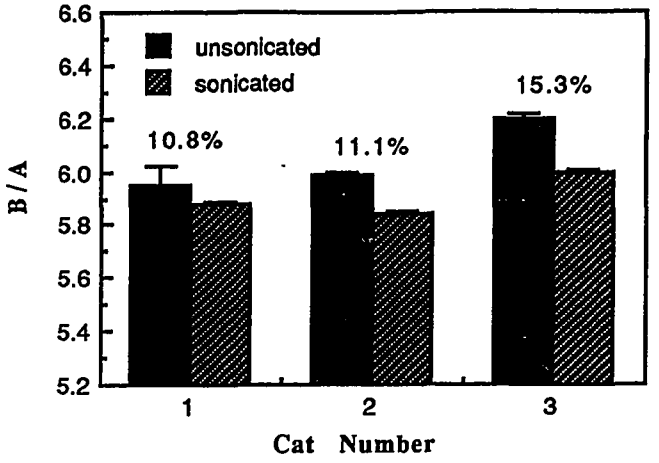

Figure 4.7 B/A values of cat hepatocyte suspensions with and without sonication treatment.

If the results in Fig. 4.7 are extrapolated to the dry weight concentration of 30%, i.e., similar to that which exists in intact livers, the average B/A decrease would be 0.36 units, which accounts for 20% of contribution to the total B/A of the liver tissues, 7.0 (20%=0.36/(7.0-5.2)).

4.2.2. Effect of liposome membrane structure

Liposomes, small lipid vesicles described and prepared according to the procedure in Section 3.3.6, provide a model for the biological cell membrane. As temperature is increased the membrane goes through a phase transition from an ordered crystalline-like state below the transition temperature to a fluid-like state above it. The B/A values were measured in liposome suspensions with three different structures [Zhang et al., 1988].

Figure 4.8 shows B/A measurements made at various temperatures in LUV liposome suspensions prepared at two different concentrations. Regardless of liposome concentration, B/A increases

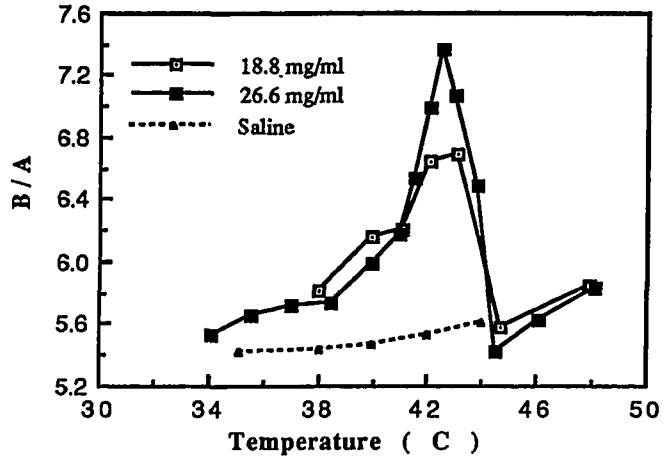

Figure 4.8 B/A in LUV liposome suspensions at two lipid concentrations. The dotted line represents the B/A of the saline solution in which the liposomes were suspended.

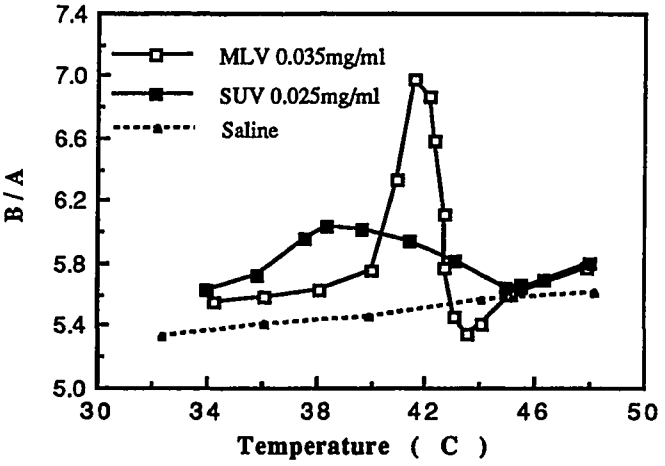

Figure 4.9 B/A in MLV and SUV liposome suspensions.

dramatically near the liposome's transition temperature at 42.5°C [Magin and Weinstein, 1984], and the higher the concentration, the higher the peak. Figure 4.9 shows B/A for MLV and SUV liposome suspensions. Despite variations in lipid concentration, a difference is seen between the B/A of SUV and MLV suspensions. B/A in SUV has a broader peak at lower temperature, while the MLV B/A has a narrower peak at higher temperature. Both peaks coincide with the SUV and MLV transition temperatures at 39°C and 41°C, respectively [Harkness and White, 1979]. Similar behavior has been observed for the acoustic absorption coefficient of liposome suspensions of these same compositions [Maynard et al., 1983]. The data also exhibit a region, just beyond the transition temperature, where the B/A value of the suspension is even lower than the buffered saline control, i.e., the suspending medium.

In order to determine the relative contribution of the lipid component to the B/A value of the suspension, it was considered that the B/A value of the liposome suspension can be represented as a linear combination of the B/A values of the lipid bilayer and of the buffered saline in which the liposomes are suspended, with the weight fractions of concentration as the coefficients. That is,

$$(B/A)_{suspension} = x_{lipid}\,(B/A)_{lipid} + x_{buffer}\,(B/A)_{buffer} \qquad (4.2)$$

where x_{lipid} and x_{buffer} are the weight fractions for lipid and suspending buffer, respectively, and $(B/A)_{suspension}$ and $(B/A)_{buffer}$ are the experimentally determined B/A values for the liposome suspension and the buffer. $(B/A)_{lipid}$ is the B/A contribution of hydrated lipid. This procedure is the same as a normalization to concentration. Figures 4.10 and 4.11 show replots of those data in Figs. 4.8 and 4.9, respectively, exhibiting the contribution due to the lipid component alone, viz., $(B/A)_{lipid}$. The mixture laws of Apfel [1983] and Sehgal et al. [1986a] were also used to calculate the lipid component $(B/A)_{lipid}$. Figure 4.12 shows a comparison of these three mixture laws applied to the MLV data, demonstrating the same conclusions irrespective of the mixture law used. The following observations can be made: (1) It is seen that in the regions below and above transition, B/A

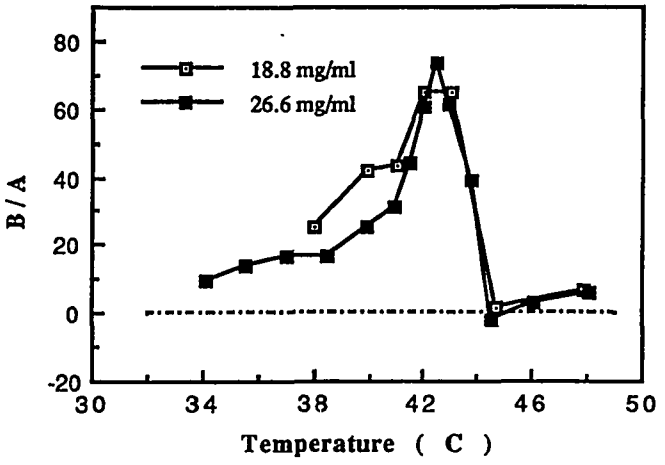

Figure 4.10 B/A contribution from the hydrated lipid bilayers, calculated from Fig. 4.8 using Eq. (4.1). The dotted line indicates the zero B/A value.

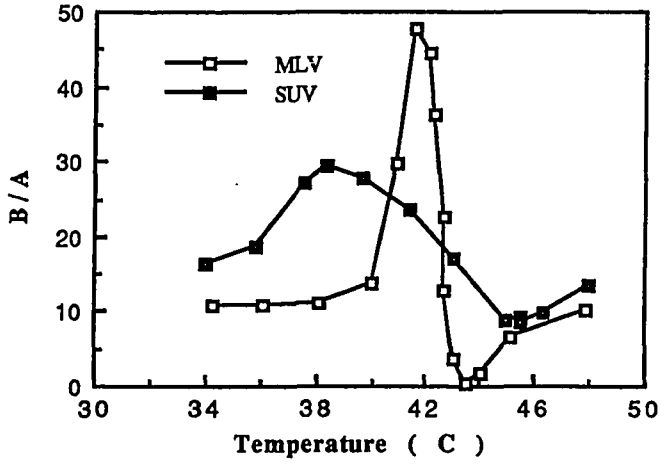

Figure 4.11 B/A of (hydrated) lipid bilayer in MLV and SUV, calculated from Fig. 4.9.

exhibits values of about 10 to 15, which is close to the B/A value obtained for fat [Law et al, 1985; Errabolu et al., 1987]. As both fat and phospholipids have similar molecular structures [Stryer, 1981], this result is expected. Furthermore, this result also supports the general categorization of biological molecules into groups with low and high B/A values, as discussed in Section 1.3. (2) In the transition region, the B/A value of the bilayer is approximately 10 times that measured for parenchymal tissues (see Tables 1.1 and 1.2). (3) Even if the concentration is normalized, SUV and MLVs still show differing B/A profiles, with this difference possibly being due to the difference in the way the phospholipids are organized to form vesicles, viz., differences in structure. (4) At least in the case of the LUV and MLVs, there exists a region, just beyond transition, at which lipid bilayers appear to exhibit zero nonlinearity.

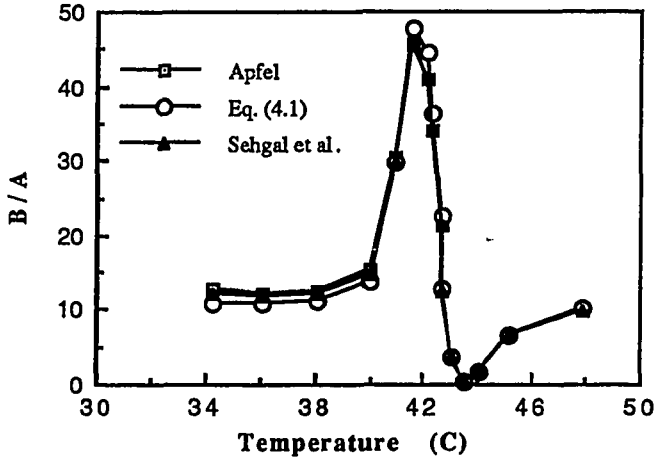

Figure 4.12 Comparison between three different mixture laws.

Structural relaxation has been suggested as a mechanism of ultrasonic absorption in these liposome suspensions [Strom-Jensen et al., 1984]. The unusually high B/A values near the liposome transition regions, and the unusually low B/A value in the region immediate beyond transition, seem also to suggest some kind of relaxation phenomenon, possibly the same relaxation mechanism.

4.3. Molecular Level

It has been demonstrated, so far, that the B/A value depends on both tissue and cellular level structural factors. This finding also prompts us with the question whether molecular level structure may also be a determinate factor. Protein is the most abundant group of molecules in mammalian tissues, besides water [Spector, 1956]. Experiments were designed to investigate the B/A dependence on structures of protein.

4.3.1. Effects of protein tertiary and secondary structures

The tertiary and secondary structures of protein were examined. BSA was employed, with alteration of the structures produced by the denaturing agent sodium dodecyl sulfate (SDS) [Weber and Osborn, 1969].

BSA solutions were prepared with SDS ranging from 0% to 3%, and control blanks were prepared with SDS only, as described in Section 3.3.7. The 4 ml system for the thermodynamic method was used for B/A measurement. Figure 4.13 shows the B/A values of the samples with and without BSA at the different SDS concentrations. Thus, the difference in B/A value between the two is most likely due to contribution of BSA itself and interaction between BSA and SDS and water. The B/A value of 5.7 in the BSA buffered saline alone, i.e., at the 0% SDS concentration, is in agreement with that obtained by other investigators [Law et al., 1985; Cobb, 1982]. Figure 4.14 shows the difference in B/A values following subtraction of the SDS buffer control for the different SDS concentrations. The difference decreases as the SDS concentration increases, and the change levels off at the SDS concentration of about 1%. This decrease of 0.08 B/A units represents 15% of the total B/A, 5.7. If it is assumed that this B/A value difference is due to the presence of BSA molecules in the buffer, then it is most likely that the state of the BSA molecules change at the higher SDS concentrations, and that the B/A parameter reflects such change. If it is hypothesized that the B/A value associated with the intact BSA protein is greater than that associated with the denatured molecule,

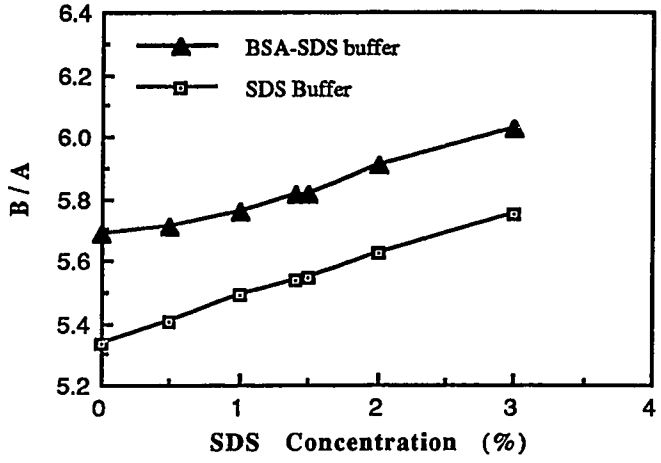

Figure 4.13 B/A values in SDS denaturing buffer with and without the presence of 10% (w/w) BSA protein, exhibiting protein contribution.

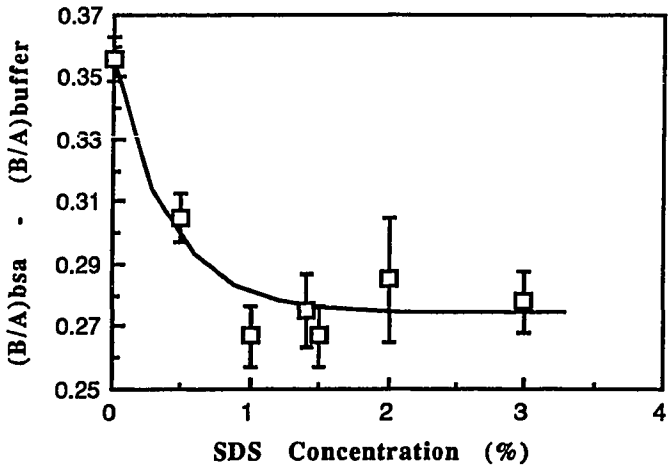

Figure 4.14 The difference in B/A values calculated from Fig. 4.13.

then the experimental result can be explained as follows. With no SDS molecules present in the solution, tertiary and secondary structures of all the BSA molecules are intact and the B/A value of the buffer solution is high. As more SDS is added, more BSA molecules are denatured and the B/A decreases. The B/A value finally decreases to the minimum value when sufficient SDS is present in the solution to denature all the BSA molecules. The experiment was repeated with the lower BSA concentration of 0.04g/100cc, and the results for the two concentrations are shown in Fig. 4.15. When the B/A values are normalized to the protein concentrations, the two curves are essentially superimposed upon each other, demonstrating that the B/A change is independent of the BSA concentration. This result also supports the above hypothesis that the B/A value associated with the native protein structure is greater than that with the denatured.

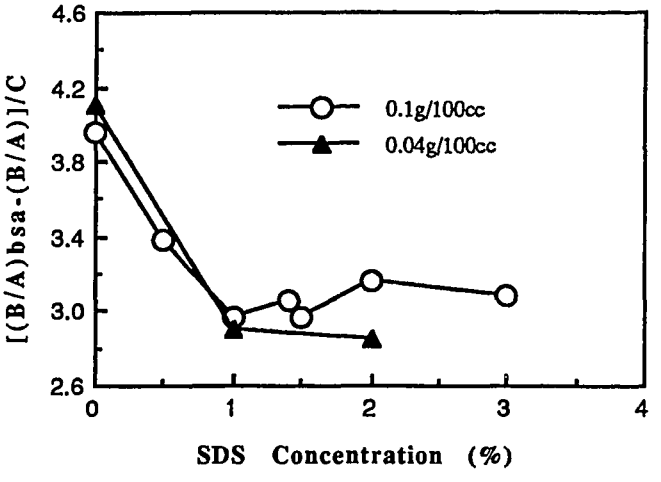

Figure 4.15 The B/A difference normalized to the BSA concentration.

If the above hypothesis is true, the conclusion that the B/A value decreases as the BSA protein is denatured should hold, irrespectively of how the protein is denatured. This hypothesis was

tested by measuring the B/A value in the process of heat denaturation of ribonuclease A.

Ribonuclease A is a protein of 14,200 molecular weight and is known to undergo reversible conformational transition between native and denatured status at about 40°C in pH 2.77 aqueous solution [Brandts and Hunt, 1967; Brandts, 1965]. The B/A was measured in a solution of 3.9% ribonuclease A, pH 2.77, prepared as in Section 3.3.7. The result is shown in Fig. 4.16, together with the B/A values of water. The net B/A change due to the ribonuclease A itself was obtained by the linear mixture law Eq. (4.1), and is shown in Fig. 4.17. It is seen that the B/A value due to ribonuclease A decreases as it is denatured, which supports the result obtained by SDS denaturation.

Errabolu et al. [1987] have also observed the lower B/A value associated with denatured protein. The authors investigated the dependence of the B/A parameter on the different constituents of fat tissues by decomposing the fat tissues into three components, viz., water, oily residue and solid residue, and pointed out that the solid residue, one of the dehydration products composed largely of denatured proteins, exhibits significantly lower B/A value.

One of the mechanisms suggested to explain different B/A values in aqueous solutions is the bound to free water ratio in the solution [Yoshizumi et al., 1987; Sehgal et al., 1986b]. Free water has been shown to have a high B/A value and bound water a low value [Yoshizumi et al., 1987]. The B/A value varies as the relative population of the free water and bound water changes. Qualitatively, the result in this section can be seen as indirect evidence supporting this hypothesis, since denaturation of protein alters the free and bound water ratio. The amount of bound water associated with a protein increases as the protein is denatured, because a denatured protein takes an extended linear form, and thus has greater surface area. Consequently, an aqueous solution of denatured protein has a greater amount of bound water, which exhibits a smaller B/A value, and a lesser amount of free water, which exhibits a greater B/A value, than that of native protein. Therefore, the effective B/A in the solution of denatured protein exhibits smaller values.

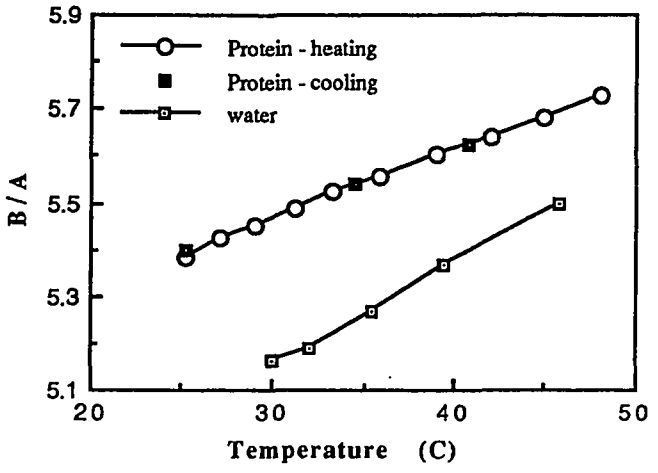

Figure 4.16 B/A in ribonuclease A solution as a function of temperature, during heating and cooling. B/A of water is also shown for comparison.

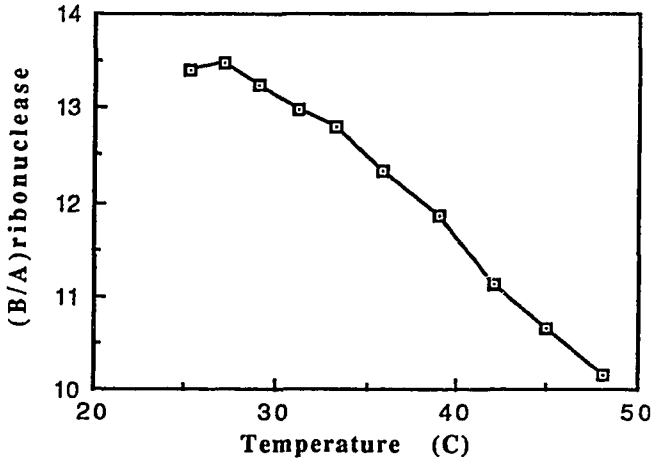

Figure 4.17 B/A contribution from ribonuclease showing decrease as the protein denatured.

It can also be observed from Fig. 4.17 that the B/A value for intact BSA protein calculated by using the mixture law of Eq. (4.1), about 13, is close to those of fats [Law et al., 1985; Errabolu et al., 1987] and phospholipids (see Section 4.2.2). This evidence supports the observation in Section 1.3 that as far as B/A value is concerned, proteins and fats are indistinguishable from one another.

4.3.2. Effect of protein primary structure

It can be seen from the previous section that the B/A decreases as BSA is denatured. Thus, the secondary structure of proteins influences their B/A value. To investigate whether primary structure also contribute to B/A and to compare its influence relative to secondary structure, a nonspecific protease (Boehringer Mannheim Biochemicals, IN) was used to digest BSA protein into its constituent amino acids. The underlying idea was to examine the B/A change when this level of protein structure was destroyed. When the nonspecific protease was added to the BSA solution, it catalyzes the hydrolysis of peptide bonds, resulting in the conversion of the protein into free amino acids. For a particular temperature, the higher concentration of the protease, the faster the rate of the digestion. The concentration of protease was chosen so that the entire process of digestion was completed in about 10 hours, long enough to collect sufficient B/A data.

The B/A values of BSA aqueous solutions, with and without the presence of protease, are shown in Fig. 4.18. There is no significant B/A change in the process of digestion, suggesting that the B/A parameter is not sensitive to this level of structure. Also shown in Fig. 4.18 is B/A values for the glycine solution, which exhibit no significant difference from the B/A values the intact or digested BSA solutions and the digested BSA solution. These data again support the contention that B/A is not influenced by protein primary structure. The speed of sound was also measured in these solutions and the results are shown in Fig. 4.19. Three observations can be made from Fig. 4.19. First, it reconfirms indirectly the existence of the digestion process, since the only preparation exhibiting the velocity change is the one with protease

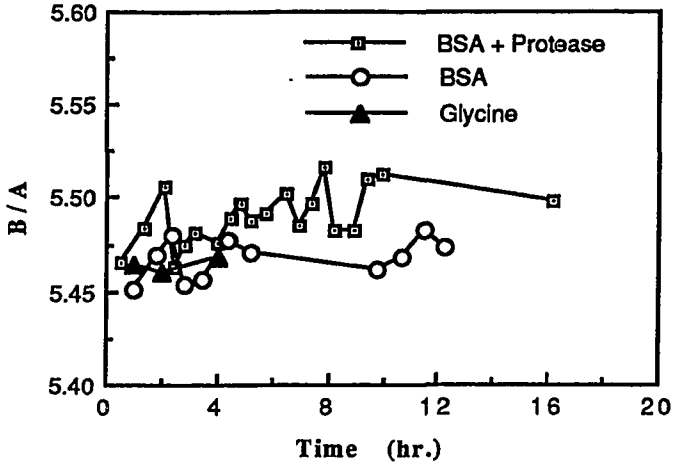

Figure 4.18 B/A in the BSA solution as a function of time, with and without the presence of nonspecific protease.

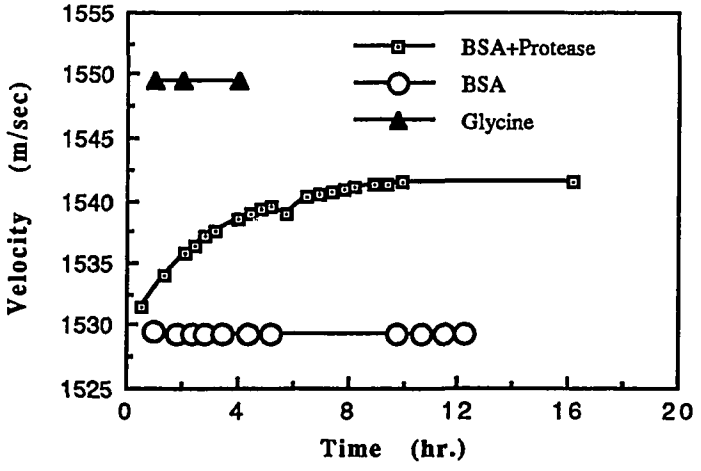

Figure 4.19 Speed of sound in the same digestion process.

added. Second, it demonstrates the increase of velocity as the protein is digested. Third, the velocities measured in glycine solution are greater than both the intact and the digested BSA solutions. This result agrees with the conclusion that the digested BSA, which is basically a collection of different amino acids, exhibits higher velocity than intact BSA. The large scattering of the data in Fig. 4.18 is due to the one-time measurement, and no attempt was made to average the B/A values, since the 0.5 hours per data point is the highest data collection rate the thermodynamic method can achieve.

CHAPTER 5

CONCLUSIONS AND FUTURE WORK

This chapter is divided into two parts: instrumentation and the B/A parameter. Each part presents the principal conclusions drawn in this dissertation, a discussion of the conclusions in a broader perspective, and suggestions for future research.

5.1. Experimental Instrumentation

A small volume measurement system, implementing the thermodynamic method, was developed for this research project. The system is capable of obtaining the nonlinearity parameter B/A from small samples (4ml), with an accuracy of better than 0.2%. The earlier developed [Law, 1984] finite amplitude measurement system was modified to investigate the structural dependence of the B/A parameter in tissues. The system now has the advantage of fast data acquisition capable of obtaining more than one B/A value per minute, which is necessary for determining B/A changes in a short time interval.

Improvement is suggested for further reduction of the required sample volume to less than one milliliter. Such a volume is believed to be small enough for the measurement of biochemical preparations of minute yields and for studying small tumors. However, it should be noted that the accuracy for the absolute measurement of the B/A parameter deteriorates rapidly as the sample volume decreases. It is, therefore, suggested that a dual channel interferometer be constructed [Sarvazyan and Chalikian, 1988] one channel for the reference medium, such as degassed water, and the other for the sample under study.

Further instrumentation development should also include the construction of a set of velocimeters for B/A measurement over a broad range of frequencies in order to study the effects of relaxation processes on the nonlinearity parameter. Both the theoretical prediction and experimental evidence strongly suggest the need for such studies as discussed in Section 5.2.

5.2. B/A parameter

The effect of structural change on the B/A parameter has been studied at the tissue, at the cellular, and at the molecular levels. At each level, experiments were designed to investigate the contribution to the B/A parameter, due to a particular structural factor, by perturbing the structure biochemically and keeping the remaining B/A influencing factors, such as the chemical composition, unchanged. Specimens employed and the structural factors investigated are considered to be sufficiently representative of those encountered in biomedical ultrasound application to enable relevant and general conclusions to be drawn.

Three general conclusions formulated from the study are: (1) the structural dependence of the B/A parameter exists at all the three levels of biological structure, viz., the tissue level, the cellular level and the molecular level; (2) the sensitivity of the B/A parameter to each level of structural change can be arranged in the descending order

intercellular adhesion > cellular structure > tertiary and secondary structures of protein > primary structure of protein

and (3) no significant difference in the B/A value was found to exist, at least for liver tissue, between the *in vivo* and *in vitro* states.

Earlier studies [Everbach, 1989; Sehgal et al., 1986a; Apfel, 1986; Law et al., 1985; Gong et al., 1984; Cobb, 1982] have shown that B/A is dependent upon the chemical composition of a specimen medium and that, by assuming that a tissue can be modeled as an ideal mixture of the three components water, fat and protein, the B/A value can predict the tissue composition of these three components [Everbach, 1989; Sehgal et al., 1986a; Apfel, 1986], as discussed in Section 1.3. The conclusions drawn from the results of the present study show that B/A is additionally dependent upon structural features of the medium. Thus chemical composition and structure, together, determine the B/A parameter of a medium. That is, the B/A value of a medium depends not only upon the relative amount of the various biomacromolecular

constituents, but also upon how those constituent molecules and their assemblages are organized.

Furthermore, the structural and compositional factors can be seen as the two variables that together determine the B/A parameter of the medium, as suggested by Fig. 5.1. Studies exhibiting the compositional dependence of B/A reveal only one aspect of the nonlinear parameter, and this is illustrated in Fig. 5.1 as one intersection of the plane, where the structural variables are constant, and the B/A surface. In such studies, the structural variables are maintained unchanged, and only the variation of the B/A parameter with chemical composition is investigated. Similarly, the study presented in this dissertation reveals the other aspect of the B/A parameter, viz., the B/A dependence on structural variables, with the chemical compositions maintained unchanged. This structural dependency can be represented in Fig. 5.1 as another intersection between the plane, where compositional variables are constant, and the B/A surface.

These considerations can be made quantitative by the following example, employing the result presented in Section 4.3.1, and the B/A values for intact BSA solutions, obtained by Law et al. [1985]. The compositional variable is the concentration of BSA, [BSA], and the structural variable is the reaction coordinate of the denaturation which can be represented by the SDS concentration, [SDS], in Fig. 4.19. As illustrated in Fig. 5.2, the origin of the compositional variable is at [BSA]=0, and that for the structural variable is at [SDS]=0, i.e., the intact protein state. For intact BSA, Law et al. showed that B/A of the aqueous solution depends nearly linearly upon the BSA concentration, which can be represented in Fig. 5.2 as a straight line in the [SDS]=0 plane, with a positive slope. Figure 4.19 shows that the B/A value decreases as BSA is denatured, which can be represented in Fig. 5.2 as a decay curve in the [BSA]=10% plane (the concentration of the BSA solution of Fig. 4.19). The B/A surface thus generated represents the complete dependence of the B/A parameter on both composition and structure of the medium. The two curves meet at B/A = 5.7, viz., the B/A value in the aqueous solution of 10% intact BSA, as discussed in Section 4.3.1.

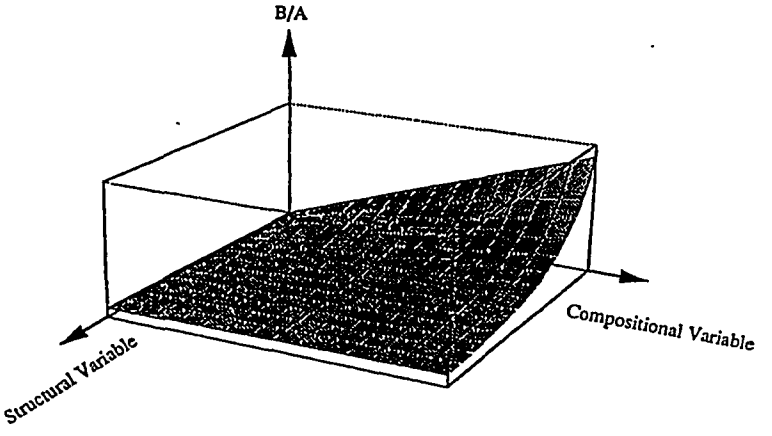

ure 5.1 A surface plot of a two-variable function representing the hypothetical dependence of B/A on both chemical composition and structure. The function linearly increases with compositional variable and exponentially decreases with structural variable.

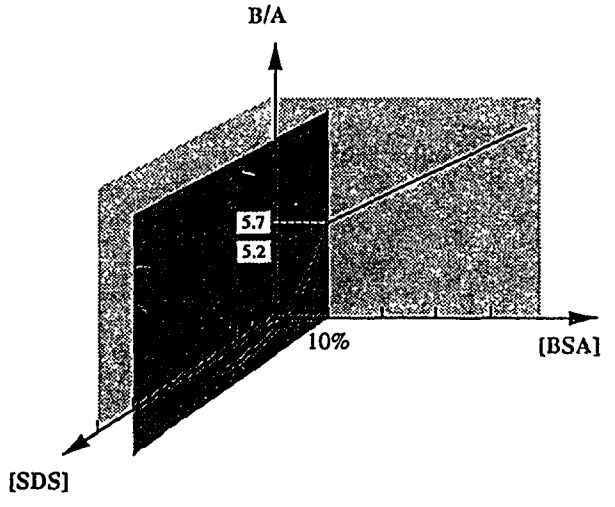

ure 5.2 A representation of the B/A dependence on BSA concentration and BSA molecular structure from two perspectives, constant structural variable ([SDS]=0) and constant composition variable ([BSA]=10%).

In the case of tissues, the representation is more complex because of the multiple compositional variables, such as the concentrations of water, fat, protein and other constituents, and the multiple structural variables. However, the rationale is applicable.

With the rationale proposed above, the relative contributions of compositional and structural factors to the total B/A value of a medium can be estimated. At the tissue level, the relative contribution is determined to be 39% due to structural and 61% due to compositional factors, respectively (see discussions in Section 4.1.3). The structural contribution of 39% is nearly the 40% obtained by Law et al. [1985] in beef liver homogenization experiments (also see discussion in Section 1.3). At the cellular level, the percentages are 20% due to structure and 80% due to dry weight in the hepatocyte suspension, normalizing to the dry weight concentration of 30% as in liver tissues (see Section 4.2.1). The relative contribution due to the macromolecular structure is 15% with the remaining 75% due to 10% (w/w) of macromolecules (see Section 4.3.1). These results are summarized in Table 5.1.

Table 5.1 Relative Contributions at Three Levels of Structures

Tissue	26%
Cellular	20%
Molecular	15%

It shows that the structural contribution at the tissue level to the total B/A is significantly more than at the cellular and molecular levels.

The above conclusions and discussions present the evidences and extent to which B/A may be dependent on structural factors, in addition to its compositional dependence, but more detailed experiments are needed to further understand such dependences and apply them to tissue characterization. It is suggested that future work be directed toward two general areas: (1) to improve the basic understanding of the B/A parameter in biological medium models, and (2) to extrapolate it to pathological tissues.

B/A dependence on molecular and the higher levels of structure seems to suggest that the interactions between solutes and water molecules are significant. One such interaction that has been suggested is water hydration [Sehgal et al., 1985; Yoshizumi et al., 1987]. It is noted that although bound and free water models can explain some of the experimental results, there is no direct evidence correlating the B/A data to the bound and free water ratio. Nuclear magnetic resonance relaxation time provides a means to measure the bound and free water ratio and can be employed for such a study.

It is further suggested that the effect of relaxation processes on the B/A parameter should be investigated. According to the theoretical model presented by Rudenko and Soluyan [1977], the Taylor's series expansion of the state equation describing the medium with relaxation mechanisms contains extra terms associated with the relaxation process. These relaxation terms could be significant when the acoustic frequencies are near the relaxation frequencies and can be identified with contributions to the quadratic term, i.e., the B-term, and to the linear term, i.e., the A-term. Thus, the effective B/A values near relaxation frequencies may be significantly different from those removed from the relaxation frequencies, or those in nonrelaxing media. It is believed that the unusually high B/A values of 50 to 70 exhibited near the liposome transition region are due to relaxation phenomena and that such relaxation effects may be very significant. Relaxation effects have been shown to contribute considerably to acoustic absorption [Slutsky et al., 1980; Wells, 1977; O'Brien and Dunn, 1972; Pauly and Schwan, 1971]. It has been shown that the nature of ultrasonic absorption in tissues can be explained by relaxation mechanisms occurring over a distribution of frequencies [Wells, 1977; Pauly and Schwan, 1971]. Whether this is the case for the nonlinearity parameter B/A has yet to be determined.

One of the reasons for wanting to have a better understanding of the B/A parameter in biological media is, as discussed in Chapter 1, to be able to use it for tissue characterization, either for differentiation among different human tissues or for the differentiation between pathological tissues and their normal counterparts. Perhaps the most challenging aspect of the work in the future will be to extrapolate the

basic understanding of the parameter to tissues and pathological models. Tissue composition and structure are two which are different, in the pathological state, and a major goal should be to characterize tissues and their altered pathologic or morphologic state by their B/A parameter values.

APPENDIX. DERIVATION OF EQUATION (3.46)

Using the notations in Section 3.2.2, Eq. (3.29) can be rewritten as

$$p_2 = \frac{\pi f(2+B/A)}{2\rho_o c_o^3} p_o^2 \, x \, e^{-(\alpha_1 + \alpha_2/2)x} \, DIFF(x) \tag{A.1}$$

For most biological media, $\alpha_2 \simeq 2\alpha_1$ [Law, 1984], thus,

$$p_2 \cong \frac{\pi f(2+B/A)}{2\rho_o c_o^3} p_o^2 \, x \, e^{-2\alpha_1 x} \, DIFF(x) \tag{A.2}$$

A similar equation can also be written for a reference medium as

$$p_2^* = \frac{\pi f(2+B/A)^*}{2(\rho_o c_o^3)^*} (p_o^2)^* \, x^* \, e^{-2\alpha_1^* x^*} \, DIFF(x^*) \tag{A.3}$$

where * denotes the reference medium. Dividing Eq. (A.2) by Eq. (A.3),

$$\frac{p_2}{p_2^*} = \frac{(2+B/A)}{(2+B/A)^*} \frac{(\rho_o c_o^3)^*}{\rho_o c_o^3} \frac{p_o^2}{(p_o^2)^*} \frac{x \, DIFF(x)}{x^* \, DIFF(x^*)} \, e^{-2(\alpha_1 x - \alpha_1^* x^*)} \tag{A.4}$$

can be obtained. Finally, assuming $e^{\alpha_1 x} = p_1/p_o$ and substituting the definitions of η_0, η_1 and η_2 in Section 3.2.2 into Eq. (A.4), Equation 3.46 can be obtained.

REFERENCES

Apfel, R. E. [1983]. Effective nonlinearity parameter for immiscible liquids mixtures. J. Acoust. Soc. Am. **74**, 1866-1868.

Apfel, R. E. [1986]. Prediction of tissue composition from ultrasonic measurements and mixture rules. J. Acoust. Soc. Am. **79**, 148-152.

Arun, K. S. and Rao, B. D. [1988]. An improved Toeplitz approximation method. International Conference on Acoustics, Speech, and Signal Processing, **4**, 2352.

Bacon, D. R. [1984a]. Finite amplitude distortion of the pulsed fields used in diagnostic ultrasound. Ultrasound in Med. & Biol. **10**, 189-195.

Bacon, D. R. [1984b]. The observation of distorted waveforms - nonlinear propagation or hydrophone overload? Ultrasound in Med. & Biol. **10**, 639-641.

Bacon, D. R. [1986]. Finite amplitude propagation in acoustic beams. Ph.D. dissertation, University of Bath, Bath, UK.

Bass, R. [1958]. Diffraction effects in the ultrasonic field of a piston source. J. Acoust. Soc. Am. **30**, 602-605.

Beyer, R. T. [1960]. Parameter of nonlinearity in fluids. J. Acoust. Soc. Am. **32**, 719-721.

Beyer, R. T. [1974]. Nonlinear acoustics. Naval Ship Systems Command Publication. 107.

Beyer, R. T. and Letcher, S. V. [1969]. Nonlinear acoustics. In Physical Ultrasonics. Academic Press, New York, Chapter 7, 202-230.

Blackstock, D. T. [1964]. Thermoviscous attenuation of plane, periodic, finite-amplitude sound waves. J. Acoust. Soc. Am. **36**, 534-542.

Blackstock, D. T. [1966]. Connection between the Fay and Fubini solutions for plane sound wave of finite amplitude. J. Acoust. Soc. Am. **39**, 1019-1026.

Blackstock, D. T. [1972]. Nonlinear acoustics (theoretical). In American Inst. Phy. Handbook, D. E. Gray, Ed. McGraw Hill, New York. Chapter 3n, 3-183.

Bjorno, L. [1986]. Characterization of biological media by means of their non-linearity, Ultrasonics **24**, 254-259.

Bjorno, L. and Lewin, P. A. [1982]. Nonlinear focusing effects in ultrasonic imaging. Proc. IEEE Ultrasonics Symposium, 659-662.

Brandts, J. F. [1965]. The nature of the complexities in the ribonuclease conformational transition and the implications regarding clathrating. J. Am. Chem. Soc., **87**, 2759.

Brandts, J. F. and Hunt, L. [1967]. The thermodynamics of protein denaturation. III. The denaturation of ribonuclease in water and in aqueous urea and aqueous ethanol mixtures. J. Am. Chem. Soc. **89**, 4826.

Cain, C. A. [1986]. Ultrasonic reflection mode imaging of the nonlinear parameter B/A: I. A theoretical basis. J. Acoust. Soc. Am. **80**, 28-32.

Carstensen, E. L., Law, W. K., McKay, N. D., and Muri, T. G. [1980]. Demonstration of nonlinear acoustical effects at biomedical frequencies and intensities. Ultrasound Med. & Biol. **6**, 359-368.

Carstensen, E. L., Becroft, S. A., Law, W. K., Barbee, D. B. [1981]. Finite amplitude effects on the thresholds for lesion production in tissue by unfocused ultrasound. J. Acoust. Soc. Am. **70**, 302-309.

Carstensen, E. L., McKay, N. D., Delecki, D. and Muir, T. G. [1982]. Absorption of finite amplitude ultrasound in tissues. Acustica, **51**, 116-123.

Chen, C. T. [1979]. One-dimensional digital signal processing. Marcel Dekker, Inc. New York. 356.

Chen, C. T. [1984]. Linear system theory and design. Holt, Rinehart and Winston, New York. 83.

Chen, C. H. [1988]. High-resolution spectral estimation algorithms. in Signal Processing Handbook. Edited by C. H. Chen, Chapter 5.

Cobb, W. N. [1982]. Measurement of the acoustic nonlinear parameter for biological media. Ph.D. dissertation, Yale University, New Haven, CT. 74 and 83.

Cobb, W. N. [1983]. Finite amplitude method for the determination of the acoustic nonlinearity parameter B/A. J. Acoust. Soc. Am. **73**, 1525-1531.

Coppens, A. B., Beyer, R. T., Seiden, M. B., Donohue, J., Guepin, F., Hodson, R. H. and Townsend, C. [1965]. Parameter of nonlinearity in fluids. II. J. Acoust. Soc. Am. **38**, 797-804.

Corry, P. M., Jabboury, K., Armour, E. P. and Kong, J. S. [1984]. Human cancer treatment with ultrasound. IEEE Trans. Son. Ultrason. **SU-31**, 444-456.

Dong, Y., Tong, J. and Sun, Y. [1987]. Relations between the acoustic nonlinearity parameter and sound speed and tissue composition. Proc. IEEE Ultrasonics Symposium, 931-934.

Drochmans, P., Wanson, J.-C., and Mosselmans, R. [1975]. Isolation and subfractionation on Ficoll gradients of adult rat hepatocytes. J. Cell Biol. **66**, 1-22.

Duck, F. A. [1984]. Finite-amplitude distortion and PVDF hydrophone response. Ultrasound in Med. & Biol. **10**, 643-644.

Duck, F. A. and Starritt, H. C. [1984]. Acoustic shock generation by ultrasonic imaging equipment. B. J. Radio. **57**, 231-240.

Dunn, F., Law, W. K., and Frizzell, L. A. [1981]. Nonlinear ultrasonic wave propagation in biological materials. Proc. IEEE Ultrasonics Symposium, 527-532.

Embree, P. M. [1986]. The accurate ultrasonic measurement of the volume flow of blood by time domain correlation. Ph.D. dissertation. University of Illinois at Urbana-Champaign. 22.

Endoh, N. and Dunn, F. [1986]. On a simple measurement method of the nonlinear acoustic parameter B/A of human tissue. Proc. Fall Mtg. Acoust. Soc. Japan (Acoust. Soc. Japan, Tokyo, 1986), 763-764, in Japanese.

Errabolu, R. L., Sehgal, C. M. and Greenleaf, J. F. [1987]. Dependence of ultrasonic nonlinearity parameter B/A on fat. Ultrasonic Imaging. **9**, 180-194.

Errabolu, R. L., Sehgal, C. M., Bahn, R. C. and Greenleaf, J. F. [1988]. Measurement of ultrasonic nonlinear parameter in excised fat tissues. Ultrasound Med. Biol. **14**, 137-146.

Evans, D. H., McDicken, W. H., Skidmore, R. and Woodcock, J. P. [1989]. Doppler ultrasound - physics, instrumentation and clinical applications. John Wiley & Sons, New York.

Everbach, E. C. [1989]. Tissue composition determination via measurement of the acoustic nonlinearity parameter. Ph.D. dissertation, Yale University, New Haven, CT.

Flachenecker, G. [1987]. Ultrasonic and focused shock-wave lithotrites: a revolution in treatment of bladder-, kidney-, and ureter-stones. Proc. IEEE Ultrasonics Symposium, 1001-1010.

Frizzell, L. A. and Dunn, F. [1982]. Biophysics of Ultrasound. Chapter 8, in Therapeutic Heat and Cold. J. F. Lehmann, Ed., Williams & Wilkins, Baltimore. 353.

Furukawa, G. T. and Douglas, T. B. [1963]. Heat capacity. In Section 4e, American Institute of Physics Handbook (Ed. D. E. Gary, 2nd ed.). 4-47, McGraw-Hill, New York.

Gong, X., Feng, R., Zhu, C. and Shi, T. [1984]. Ultrasonic investigation of the nonlinearity parameter B/A in biological media. J. Acoust. Soc. Am. **76**, 949-950.

Goss, S. A. and Fry, F. J. [1981]. Nonlinear acoustic behavior in focused ultrasonic fields: Observations of intensity dependent absorption in biological tissue. IEEE Trans. Son. Ultrason. **SU-28**, 21-26.

Harkness, J. E. and White, R. D. [1979]. An ultrasonic study of the thermotropic transition of dipalmitoyl phosphatidylcholine. Biochim. Biophys. Acta. **552**, 450-456.

Hartmann, B. [1979]. Potential energy effects on the sound speed in liquids. J. Acoust. Soc. Am. **65**, 1392-1396.

Heaps, H. S. [1962]. Waveform of finite amplitude derived from equation of hydrodynamics. J. Acoust. Soc. Am. **34**, 355-356.

Heremans, K., Ceuterick, F., and Rijkenberg, J. [1980]. High pressure pressure-jump apparatus. Rev. Sci. Instrum. **51**, 252.

Houshmand, H., McGough, R. J., Ebbini, E., Lee, H., and Cain, C. A. [1988]. Ultrasonic transmission mode imaging of nonlinear parameter B/A: A simulation study. Proc. IEEE Ultrasonics Symposium, 979-983.

Hynynen, K. [1988]. Present status of ultrasound hyperthermia. Proc. IEEE Ultrasonics Symposium. 941-946.

Ibbini, M. S. [1988]. Analysis and design of ultrasound phased arrays for hyperthermia cancer therapy. Ph.D. dissertation, University of Illinois at Urbana-Champaign. 41.

Ichida, N., Sato, T., and Linzer, M. [1983]. Imaging the nonlinear ultrasonic parameter of a medium. Ultrasonic Imaging **5**, 295-299.

Ichida, N., Sato, T., Miwa, H., and Murakami, K. [1984]. Real-time nonlinear parameter tomography using impulsive pumping waves. IEEE Trans. Son. Ultrason. **SU-31**, 635-640.

Ingenito, F. and Williams, Jr. A. O. [1971]. Calculation of second-harmonic generation in a piston beam. J. Acoust. Soc. Am. **49**, 319-328.

Kawaguchi, F., Kuhlenschmidt, M., Roseman, S., and Lee, Y. C. [1981]. Differential uptake of D-galactosyl- and D-glucosyl neoglycoproteins by isolated rat hepatocytes. J. Biol. Chem. **256**, 2230-2234.

Khimunin, A. S. [1978]. Ultrasonic propagation parameter measurements incorporating exact diffraction correction. Acustica. **39**, 87.

Kinsler, L. E., Frey, A. R., Coppens, A. B., and Sanders, J. V. [1982]. Fundamentals of Acoustics. John Wiley and Sons, New York, 3rd Edition. 177.

Knoche, W. and Wiese, G. [1974]. An improved apparatus for pressure-jump relaxation measurements. Chem. Instrum. **5**, 91-98.

Kuhlenschmidt, M. S., Schmell, E., Slife, C. W., Kuhlenschmidt, T. B., Sieber, F., Lee, Y. C., and Roseman, S. [1982]. Studies on intercellular adhesion of rat and chicken hepatocytes: Conditions affecting cell-cell specificity. J. Biol. Chem. **257**, 3157.

Kung, S. Y., Arun, K. S. and Rao, D. V. B. [1983]. State-space and singular-value decomposition-based approximation methods for the harmonic retrieval problem. J. Optical Soc. Am. **73**, 1799-1811.

Kuznetsov, V. P. [1971]. Equations of nonlinear acoustics. Soviet Physics - Acoustics. **16**, 467-470.

Law, W. K. [1984]. Measurement of the nonlinearity parameter B/A in biological materials using the finite amplitude and thermodynamic method. Ph.D. dissertation, University of Illinois at Urbana-Champaign.

Law, W. K., Frizzell, L. A., and Dunn, F. [1985]. Determination of the nonlinearity parameter B/A of biological media. Ultrasound Med. Biol. **11**, 307-318.

Law, W. K., Frizzell, L. A. and Dunn, F. [1983]. Comparison of thermodynamic and finite amplitude methods of B/A measurement in biological materials. J. Acoust. Soc. Am. **74**, 1295-1297.

Lewin, P. A. [1981]. Miniature piezoelectric polymer ultrasonic hydrophone probes. Ultrasonics. **19**, 213-216.

Ludeman, L. C. [1986]. Fundamentals of digital signal processing. Harper & Row, New York. 197, 294, and 295.

Magin, R. L. and Weinstein, J. N. [1984]. Liposome Technology, Vol. III, Chapter 10, 137, CRC Press.

Maurer, E. R. and Withey, M. O. [1925]. Strength of materials. John Wiley & Son, Inc., New York. 17.

Maynard, V. M., Magin, R. L., Strom-Jensen, P. R. and Dunn, F. [1983]. Ultrasonic absorption by liposomes. Proc. IEEE Ultrasonics Symposium. 806-809.

Moelwyn-Hughes, E. A. [1961]. Physical chemistry. Pergamon Press, New York. 321.

Muir, T. G. and Carstensen, E. L. [1980]. Prediction of nonlinear acoustic effects at biological frequencies and intensities. Ultrasound Med. Biol. **6**, 345-357.

Nakagawa, Y., Nakagawa, M., Honeyama, M., and Kikuchi, M. [1985]. New nonlinear parameter imaging CT system using a parametric acoustic array. in Acoustical Imaging. (Edited by A. J. Berkhout, J. Padder, and L. F. Vanderwall), Plenum Publishing Corp., New York, **4**, 595-604.

Narayana, K. L. and Swamy, K. M. [1981]. Acoustic nonlinear parameter (B/A) in n-pentane. Acustica **49**, 336-339.

O'Brien, Jr., W. O., and Dunn, F. [1972]. Ultrasonic absorption by biomacromolecules. In Interaction of ultrasound and biological tissues (Eds J. M. Reid and M. R. Sikov), 13-19. DHEW Publication (FDA) 73-8008.

Obrink, B., Kuhlenschmidt, M. S., and Roseman, S. [1977]. Adhesive specificity of juvenile rat and chicken liver cells and membranes. Proc. Nat'l. Acad. Sci. U.S.A. **74**, 1077-1081.

Ohtsuki, S. [1974]. Ring function method for calculating nearfield of sound source. Bulletin of the Tokyo Institute of Technology. **123**, 23-31.

Ohtsuki, S., Soetanto, K. and Okujima, M. [1986]. System for measurement of ultrasonic speed of a living tissue with a probe of small transducers. Proceedings 12th International Congress on Acoustics (Toronto, Canada). Vol. II, F1-2.

Ong, K. H. and Beck, M. S. [1975]. Slurry flow velocity, concentration and particle size measurement using flow noise and correlation techniques. Measurement and Control. **8**, 453-463.

Parker, K. J. [1985]. Observation of the nonlinear acoustic effects in B-scan imaging instrument. IEEE Trans. Sonics Ultrason. **SU-32**, 4-8.

Parker, K. J. and Friets, E. M. [1987]. On the measurement of shock waves. IEEE Trans. Ultrason. Ferroelec. Freq. Contr., **UFFC-34**, 454-460.

Pauly, H. and Schwan, H. P. [1971]. Mechanism of absorption of ultrasound in liver tissue. J. Acoust. Soc. Am. **50**, 692-699.

Pierce, A. D. [1981]. Acoustics: an introduction to its physical principles and applications. McGraw-Hill, New York. 214.

Powell, R. L. [1963]. Thermal conductivity. In Section 4g, American institute of physics handbook (Ed. D. E. Gary, 2nd. ed.). 4-76, McGraw-Hill, New York.

Rafferty, J. and Norling, R. [1986]. Cricket graph software manual. Cricket Software, Malvern, PA. 6-16.

Roberts, R. A. and Mullis, C. T. [1987]. Digital signal processing. Addison-Wesley, Massachusetts. 127.

Rudenko, O. V. and Soluyan, S. I. [1977]. Theoretical foundations of nonlinear acoustics. Translated by R. T. Beyer. Consultants Bureau, New York, NY.

Rugar, D. [1984]. Resolution beyond the diffraction limit in the acoustic microscope: a nonlinear effect. J. Appl. Phys. **56**, 1338-1346.

Sarvazyan, A. P. and Chalikian, T. V. [1988]. Development of a multichannel ultrasonic interferometer for the measurements under high pressure and its application to biomolecular studies. Proc. IEEE Ultrasonics Symposium, Vol. **2**, 937-940.

Seglen, P. O. [1973]. Preparation of rat liver cells, III. Enzymatic requirements for tissue dispersion. Exp. Cell Res. **82**, 391.

Seglen, P. O. [1976]. Preparation of isolated rat liver cells. Methods Cell Biol. **13**, 29-83.

Sehgal, C. M., Bahn, R. C., and Greenleaf, J. F. [1984]. Measurement of the acoustic nonlinearity parameter B/A in human tissues by a thermodynamic method. J. Acoust. Soc. Am. **76**, 1023-1029.

Sehgal, C. M., Brown, G. M., Bahn, R. C., and Greenleaf. J. F. [1986a]. Measurement and use of acoustic nonlinearity and sound speed to estimate composition of excised livers. Ultrasound Med. Biol. **12**, 865-874.

Sehgal, C. M., Porter, B. R. and Greenleaf, J. F. [1986b]. Ultrasonic nonlinear parameters and sound speed of alcohol-water mixtures. J. Acoust. Soc. Am. **79**, 566-570.

Sehgal, C. M., Porter, B. R. and Greenleaf, J. F. [1985]. Relationship between acoustic nonlinearity and the bound and the unbound states of water. Proc. IEEE Ultrasonics Symposium. 883-886.

Sehgal, C. M., Ravi Meher, E. L. and Greenleaf, J. F. [1986c]. Measurement of acoustic nonlinear parameters and sound speed in excised human livers. Proc. Institute of Acoustics. Vol. **8**, 63-69.

Seki, H., Granato, A. and Truell, R. [1956]. Diffraction effects in the ultrasonic field of a piston source and their importance in the accurate measurement of attenuation. J. Acoust. Soc. Am. **28**, 230-238.

Shoup, T. A. and Hart J. [1988]. Ultrasonic imaging systems. Proc. IEEE Ultrasonics Symposium. 863-971.

Slutsky, L. J., Madsen, L., White, R. D. and Harkness, J. [1980]. Kinetics of the exchange of protons between hydrogen phosphate ions and a histidyl residue. J. Phys. Chem. **84**, 1325-1329.

Spector, W. S. [1956]. Handbook of biological data. Saunders, Philadelphia.

Spiro, R. [1965]. The carbohydrate units of thyroglobulin. J. Biol. Chem., **240**, 1603-1610.

Starritt, H. C., Perkins, M. A., Duck, F. A., and Humphrey, V. F. [1985]. Evidence for ultrasonic finite-amplitude distortion in muscle using medical equipment. J. Acoust. Soc. Am. **77**, 302-306.

Strom-Jensen, P. R., Magin, R. L. and Dunn, F. [1984]. Ultrasonic evidence for structural relaxation in large unilamelar liposomes. Biochimica et Biophysica Acta **769**, 179-186.

Stryer, L. [1981]. Biochemistry. 2nd Edition. W. H. Freeman and Company, San Francisco.

Sun, Y., Dong, Y. and Zhao, H. [1985]. Study of the acoustic nonlinearity parameter in high attenuation biological media. Proc. IEEE Ultrasonics Symposium, 891-894.

Swindell, W. A., Roemer, R. and Clegg, S. [1982]. Temperature distribution caused by dynamic scanning of focused ultrasound transducers. Proc. IEEE Ultrasonic Symposium. 750-753.

Swindell, W. A. [1985]. The theoretical study of non-linear effects with focused ultrasound in tissues: an acoustic Bragg peak. Ultrasound Med. Biol. **11**, 121.

Szoka, F., Jr. and Papahadjopoulos, D. [1978]. Procedure for preparation of liposomes with large internal aqueous space and high capture by reverse-phase evaporation. Proc. Nat'l. Acad. Sci. USA. **75**, 4194-4198

Tanikawa, K. [1979]. Ultrastructural aspects of the liver and its disorders. 2nd. ed. Igaku-Shoin, Tokyo. 35.

Tipler, P. A. [1982]. Physics. 2nd. ed., 496, Worth Publishers, Inc., New York.

Tjotta, J. N. and Tjotta, S. [1981]. Nonlinear equations of acoutics, with application to parametric acoustic arrays. J. Acoust. Soc. Am. **69**, 1664-1652.

Vander, A. J., Sherman, J. H. and Luciano, D. S. [1980]. Human physiology. 3rd. ed. McGraw-Hill, New York. 211

Wade, G., Edt. [1976]. Acoustic imaging. Plenum, New York.

Weber, K. and Osborn, M. [1969]. The reliability of molecular weight determination by dodecyl sulfate-polyacrylamide gel electrophoresis. J. Biol. Chem. **244**, 4406.

Wells, P. N. T. [1977]. Biomedical ultrasonics. Academic Press, London and New York.

Westervelt, P. J. [1963]. Parametric acoustic array. J. Acoust. Soc. Am. **35**, 535-537.

Williams, Jr., A. O. [1951]. The piston source at high frequencies. J. Acoust. Soc. Am. **23**, 1-6.

Yoshizumi, K., Sato, T. and Ichida, N. [1987]. A physio-chemical evaluation of nonlinear parameter B/A for media predominantly composed of water. J. Acoust. Soc. Am. **82**, 302-305.

Zemanek, J. [1971]. Beam behavior within the nearfield of a vibrating piston. J. Acoust. Soc. Am. **49**, 181-191.

Zhang, J. and Dunn, F. [1987]. *In vivo* B/A determination in a mammalian organ. J. Acoust. Soc. Am. **81**, 1635-1637.

Zhang, J., Magin, R. L., Frizzell, L. A., and Dunn, F. [1988]. Dependence of the ultrasonic nonlinearity parameter B/A on cellular-level structure. Proc. IEEE Ultrasonics Symposium. Vol. 2, 975-978.

Zhu, Z., Roos, M. S., Cobb, W. L., and Jensen, K. [1983]. Determination of the acoustic nonlinearity parameter B/A from phase measurements. J. Acoust. Soc. Am. **74**, 1518-1521.

VITA

Jian Zhang was born in Fujian, China in 1961. He received his B.S. degree in physics from Xiamen University, China, in July 1982. Mr. Zhang began his graduate studies at the University of Illinois, Urbana-Champaign, in September 1983, and earned his M.S. degree in biophysics in May 1987. He joined the Bioacoustics Research Laboratory in September 1984 as a research assistant to Professor Floyd Dunn, working on problems of nonlinear ultrasonic propagation in biological media. At Illinois, his appointments included a research assistantship and a teaching assistantship in the Department of Electrical and Computer Engineering.